Hydraulics Research
Wallingford

DISPERSAL OF DREDGED MATERIAL

Long Term Predictive Models

M C Ockenden, MA
E A Delo, BSc, PhD, C Eng, MICE, MIWEM

Report SR 228
February 1990

Registered Office: Hydraulics Research Limited,
Wallingford, Oxfordshire OX10 8BA.
Telephone: 0491 35381. Telex: 848552

CONTRACT

This report describes work funded by the Department of the Environment under Research Contract PECD 7/7/224 for which the nominated officer was Mr C E Wright. It is published on behalf of the Department of the Environment, but any opinions expressed are not necessarily those of the funding Department. The work was carried out by Ms M C Ockenden in Dr E A Delo's section of the Tidal Engineering Department of Hydraulics Research, Wallingford, under the management of Mr M F C Thorn.

ABSTRACT

Sediments dredged from channels passing through industrial areas are often high in pollutants, particularly heavy metals. If these are being disposed of back into the marine environment, it is clearly of benefit to be able to predict the movement of dredged material onto which these pollutants are adsorbed.

This report describes the processes of long term dispersion, and reviews some field measurements of the dispersion of dumped dredged material. It also describes the development of a package of computer models which aims to create an economic means of predicting long term dispersion of dredged spoil.

Many factors affect the rate at which dredged material disperses from its disposal point, including type of material, its cohesivity and bulk density, water depth, tidal currents, bed roughness and slope. The major process in moving the material once it is on the bed appears to be the wave disturbance caused by storms.

Radioactive tracer studies at Mud Island, Brisbane, Australia, and the Tees Inner Disposal Site, UK, both support the idea that the initial footprint of mud may be represented by a normal distribution. The study at Mud Island also showed that material deposited on a slope could flow down the slope into deeper areas.

Three computer models were developed to predict long term dispersion, each model applicable for different circumstances. The model for transport of sandy material, LTDISP, combines the hydrodynamics from the existing TIDEFLOW-2D program and the wave climate from the existing HINDWAVE and OUTRAY programs. A probabilistic combination of the tides and currents over the period of interest (from a single tide up to several months or even years) gives vectors of net sediment transport of the background material. These vectors can be used to calculate mass changes on the bed. In addition the model calculates the average magnitude of the sediment transport vector, which is a measure of the dispersiveness.

The model for muddy dredged material allowed mixing of the mud with the background material. This pilot model is an extension of LTDISP, using the same sediment transport vectors. The mud cannot move from cell to cell, but it can be eroded by the tidal currents. The movement of sand is affected by the presence of the mud, and the erosion rate of the mud is affected by the presence of sand in the surface layer.

A third model was developed for flow of a viscous mud layer down a slope. The mud layer is assumed to have uniform density and viscosity. A no-slip condition is applied between the mud layer and the bed below. The difference between mud transport rates over opposite sides of each cell are used to determine a new mud distribution. The model does not include the effect of waves on the structure of the mud, and as such is most applicable to nondispersive sites.

The model for net sand transport was used in a study at Sizewell, UK. The effect of the waves on the sand transport was investigated, and the average

magnitude of the transport vectors indicated the degree of dispersion. If waves were not taken into account, the greatest dispersion was in the deeper central channel. If the model included tides and waves, the greatest dispersion was on the shallower banks. Overall, the effect of waves was to increase the sediment transport rates by about an order of magnitude.

The Tees Inner Disposal site was chosen as a site to test the pilot model for mixing of muddy dredged material. A TIDEFLOW model bed data file was set up, to include the disposal site. Current meter velocities and water levels measured at a point in the disposal area were used to generate velocities over the whole model area. LTDISP was used to predict net sediment transport vectors and bed mass changes. The net sediment transport rates were in a south-easterly direction, at approximately $0.001 kgm^{-1}s^{-1}$. The sediment transport vectors from LTDISP were used in the model for mixing of muddy dredged material. Continuous dumping of mud was simulated by allowing a dump of mud every timestep (each time step was one week). The amount dumped each time step was calculated from maintenance dredging figures from the Tees estuary. Other input parameters were calculated from laboratory and field data. The sand mass changes showed a build-up of sand around the centre of the mud dump, and a net loss of mud from the sides of the mud dump in the direction of the principal currents. The mud was accumulating slowly, at around $4kgm^{-2}$ per week. The percentage of sand in the muddy patch was around 20% (80% mud) at the centre of the patch, increasing outwards to 100%. This agrees roughly with field measurements of particle size in the Tees Inner Disposal Site, which showed samples with 20 - 80% of the material less than 90 microns, although the average percentage is around 30%.

CONTENTS

FIGURES

FIGURES (Continued)

APPENDICES

1. INTRODUCTION

Each year sees an increase in the size and draught of shipping vessels throughout the world. With this comes the need for more dredging, as many ports require a regular programme of dredging to maintain navigable depths in the port and entrance channels. Since dredging operations are expensive, there is increasing pressure to maximise dredging efficiency.

The disposal of dredged material is also of environmental interest. Sediments dredged from channels passing through industrial areas are often high in pollutants, particularly heavy metals. If these are being disposed of back into the marine environment, it is clearly of benefit to be able to predict the movement of dredged material onto which these pollutants are adsorbed.

There are therefore two main factors governing the suitability of a disposal site. Firstly, the movement of material back into the dredged area must be slow enough for the disposal method to be cost effective. Secondly, the environmental effects must be acceptable.

Researchers in the past, (see Ref 1 and Ref 2), have established that, of the material falling from a hopper dredger, at least 98% of it lands on the bed, with only a very small percentage (<2%) remaining in suspension. This study is concerned with the material which lands on the bed, and how it moves in relation to the background material. Other models have been developed under this contract (see Ref 3 and Ref 4) which predict the short term fate of the material which is left in suspension.

This report describes the work which was carried out on the modelling of the long term dispersal of dredged material. Section 2 discusses the physical processes affecting dispersion. Some field work which covered aspects of long term dispersion is reviewed in Section 3. Section 4 describes the computer models which were developed for predicting long term dispersion, and some applications of the models are described in Section 5.

2. DISCUSSION OF PHYSICAL PROCESSES AFFECTING DISPERSAL

Many factors affect the manner and rate at which dredged material disperses from its disposal point. One of these is the method of disposal (for instance, side-cast dredging generally results in material redepositing over a much larger area than dumping from a hopper dredger). In addition, the hydrodynamics at the disposal site are an important factor in determining whether the site will be a containment site or a dispersive site.

The size, shape and orientation of the initial footprint of dredged material from a disposal operation depend on many things. These include the type of material, its cohesivity, its bulk density at the time of disposal, the water depth, the current speed and direction at the time of disposal, and the roughness and slope of the bed on which the material lands. These will also affect the subsequent movement of the dredged material. Johanson and Boehmer (Ref 5) suggest that, as a first approximation, the initial footprint of material on the bed can be described as a normal distribution, with a standard deviation which depends on the above parameters. Thus, for a circular

distribution of mass on the bed, the initial distribution can be described by

$$m(r) = \int_{-r}^{r} \frac{M}{(2\pi)^{0.5}\sigma} \exp\ (-z^2/2\sigma^2)\ dz \qquad (1)$$

where

M = total mass in distribution

m(r) = mass of mud within radius r of centre of distribution

σ = standard deviation of the distribution (99.7% of a normal distribution is within 3σ of the mean)

This distribution of the initial mass is supported by the field work done previously by HR in 1978 in the tidal reaches of the Brisbane River, Australia. In this case, although the distribution is elongated in the direction of the principal tidal currents, the mass within any given radius from the centre approximates to a normal distribution, with standard deviation 470m (see Section 3).

Both Bohlen (Ref 6) and WES (Ref 7) suggest that once the material is on the bed, the major process in moving the material is the disturbance caused by storms. It is therefore important, especially for a model which aims to make long term predictions, to include the effect of waves, which may be greatly enhanced during storms.

If the tidal residual currents are large enough to transport the background material covering the whole bed, this sediment transport will be enhanced by waves. In the case of mud, the waves may cause fluidisation of the mud - a breakdown of the structure of the mud without necessarily changing its density. Once fluidised, the mud may flow down slopes under the influence of gravity or a water surface slope.

Water flowing over the mud may cause erosion of a settled mud or entrainment of a fluid mud. If mud is eroded from an area of dredged material, it will be diluted so much by the overlying water that it is unlikely ever to appear back on the bed in significant quantities in the area of interest.

3. REVIEW OF LONG TERM DISPERSAL FIELD MEASUREMENTS

3.1 Brisbane, Australia

In 1977, HR conducted a study involving a mathematical model and field investigation of sediment transport processes in the tidal reaches of the Brisbane River. Part of this study was to look at the efficiency of the spoil ground at Mud Island (Ref 8).

This involved dumping several cargoes of dredged spoil, labelled with radioactive tracer, at various stages of the tide. The initial deposition pattern of the tracer material (and hence also the deposited spoil) was measured using a towed radiation detector. Subsequent measurements were made over a period of 12 months. Vertical cores of the bed were taken to determine the thickness and burial of the layer. Surface bed samples were taken along the shipping channel to determine the amount of material entering the channel. Disposal of maintenance dredge spoil at this site was suspended for the duration of the study. Analysis of dredging records and bathymetry charts enabled some conclusions to be drawn about the fate of material previously dumped at the site.

Dumping at the site began in 1966. Prior to this, there seems to have been little change in the bathymetry at the site, suggesting that there is

little natural net erosion or accretion over the spoil ground. Over the period 1971-1976, with continuous dumping, there was a loss in mean water depth (and hence loss in spoil capacity) at the site of approximately 1m. Dredging figures for the period indicate that if none of the material which was dumped at the site had moved outside the spoil ground, this would have resulted in a greater loss in mean water depth than this. This suggests that significant amounts of the deposited material must have moved outside the disposal area.

Before the radioactive tracer study, a bathymetric survey showed a channel about 12m deep extending through the disposal site, with a deep hole, about 18m deep, 1800m to the south of the centre of the site (Fig 1). Another survey made towards the end of the study in June 1979 shows similar contours within the disposal area, but the deep hole has shallowed to about 15.4m (Fig 2). It is thought that material dumped on the edge of the disposal site could flow down the relatively steep slope into the hole.

Figure 3 shows the distribution of the tracer-injected sediment 2 days after disposal. This shows the sediment aligned in a north-south direction (the direction of the principal tidal currents), about 2800m long and 1000m wide, centred close to the middle of the disposal area. The distribution of mass relative to its distance from the centre of the spoil ground is shown in Figure 4, showing that most of the material is still fairly close to the centre of the spoil ground. This information has been plotted as cumulative mass against distance from the centre of the spoil ground in Figure 5, showing that approximately 75% of the material is within 500m of the centre. Also on this graph is the curve which represents a normal distribution with a standard

deviation of 470m, showing that a normal distribution would be quite a good fit here.

Figure 6 shows the distribution of the sediment 371 days after disposal. The sediment has spread out further at the northern tip, and although the whole distribution is still roughly the same length and width, the concentration of sediment has spread further away from the centre. This can be seen on Figure 7, which shows the proportions of sediment at given distances from the centre. The proportions of sediment are proportions of the total amount of sediment calculated after 2 days, so this figure may be directly compared with Figure 4 to see where the sediment has gone. There is now much more sediment further away from the centre of the disposal site. Looking at the new distribution alongside the original bathymetry indicates that the sediment has moved towards the deeper areas, particularly into the deep hole to the south and down the slope on the north side of the disposal area.

In Figure 7 the total amount of sediment is only about 55% of that after 2 days, so the remaining 45% must have spread outside the monitored area or have been lost into suspension.

The standard deviation of the distribution in Figure 7 (after 371 days) is 974m, which is approximately 500m greater than the distribution in Figure 4 (after 2 days). This is a measure of the spread of the distribution, so on average a particle of sediment has moved around 500m in 369 days. This gives a mean velocity of approximately 2 $10^{-5}ms^{-1}$ over this period. The bed slope in the area varies from 1 in 1000 on the western side of the disposal ground up to 1 in 100 on the sides of some of the deep holes. It is quite likely that the sediment does not move all the time,

but that the effect of the waves is to change the structure at the surface of the mud, thus encouraging it to move, probably as a viscous layer.

During the study, no attempt was made to measure the wave climate at the spoil ground. It is thought that severe weather conditions could generate orbital velocities which would agitate the bed material. In this particular case the material appears to move away from the navigation channel into deeper water, so this agitation was seen as beneficial, though this might not be the case elsewhere.

3.2 Tees Bay, UK

In September 1988, as part of this contract, HR planned a radioactive tracer study at the Tees inner disposal ground, which lies about 8km northeast of the mouth of the River Tees (Fig 8). The object of the study was to label cargoes of dredged spoil with a radioactive tracer, and to monitor movement of the tracer (and hence the spoil) both immediately after disposal and subsequently. Details of this study are given in Appendix 1.

Some severe operational problems were encountered, with the rough sea-bed causing damage and loss of equipment. In addition, inclement weather prevented some survey work. As a result, less information was gathered than hoped, and this was restricted to one survey 3 to 4 days after disposal of the tracer-injected sediment.

The distribution of the deposits and the times of disposal relative to high water are shown in Figure 9. This shows that the position of the initial deposit depends strongly on the current speed and direction at the time of deposit. The cumulative proportion of

tracer against distance from the disposal point is plotted in Figure 10. Although the initial footprint is made up of three individual dumps, the overall distribution can still be suitably represented by a normal distribution. Figure 10 also shows a fitted normal distribution, with mean 60m south east of the disposal point and standard deviation 300m.

4. DESCRIPTION OF LONG TERM DISPERSION MODELS

4.1 Existing software modules

The models for predicting long term dispersion were developed to use the output from many software programs or routines currently being used at HR. The hydrodynamics for the models are generated by Tideflow-2D. This is a depth integrated model, based on well established tidal flow equations for conservation of mass and momentum. Details of Tideflow-2D are given in Appendix 2.

The wave conditions at the site are specified in the form of a scatterplot of significant wave height against zero-crossing period. Often there is very little reliable wave data for a site, and it is better to predict a wave climate from wind data, which is generally more reliable. The HINDWAVE model has been developed to do this, and is described in detail in Appendix 3.

Once the wave climate for the area has been generated, a set of wave conditions for a particular point can be generated from the program OUTRAY. This model is a back-tracking ray refraction model, which calculates the wave conditions that would be refracted to a

particular nearshore point from an offshore boundary. Details of OUTRAY are given in Appendix 4.

All output files from the long term dispersion models are in the standard Tideway format, which means they can be read, analysed and graphed as vector and contour plots using the existing graphics software for Tideway files.

4.2 Model for transport of sandy background material

The model LTDISP has been developed to predict the transport of sandy material over the site of interest over a period of several months or even years. It uses the same grid of cells and the same model bathymetry as the TIDEFLOW model. It uses results from the TIDEFLOW-2D, HINDWAVE and OUTRAY programs, and combines them in a probabilistic way to calculate a probability distribution of bottom orbital velocities.

These results are used to compute an Eulerian residual sediment transport vector at every point in the model. It is an Eulerian residual because it is based on the time varying velocity at a fixed point, as opposed to the Lagrangian residual which is based on the velocity of a particle moving with the water body. The change in bed mass at each point in the model is calculated from the vectors for a given time period.

For the purposes of calculating the net transport vector, the program treats each cell of the model totally independently. The following description applies to each point in turn.

From the TIDEFLOW results the program extracts lunar hourly velocities for springs and neaps at that particular point. These velocities are combined with the tidal heights (input as a file) to produce a probability distribution of velocities at each hour of the tide.

The HsTz scatter diagram of wave conditions is combined with the mean water depth at the particular point to calculate a probability distribution of bottom orbital velocities.

For each hour of the tide, the probability distributions of tidal currents and wave induced bottom orbital velocities are combined. The sediment transport is calculated for each set of conditions according to a modified van Rijn formula, with a wave enhancement term.

The van Rijn sediment transport formula (Ref 9) is for currents only and has the form

$$q_t = q_b + q_s = A\ U\ (U - U_{cr})^{n-1} \qquad (U > U_{cr}) \qquad (2)$$

$$q_t = 0 \qquad (U \leqslant U_{cr})$$

where

q_t = total sediment transport
q_b = bed load
q_s = suspended load
A,n = constants
U = current speed
U_{cr} = critical U for sediment transport

Eqn 2 has been adapted by Mr R L Soulsby at HR to a wave-plus-current formula by using a similar line of argument to Grass (Ref 10), to become

$$q_{t+} = A\,U\,[(U^2 + BV^2)^{0.5} - U_{cr}]^{n-1} \quad (U > U_{cr}) \quad (3)$$

$$q_{t+} = 0 \quad (U \leq U_{cr})$$

where

B = constant

V = r.m.s. wave orbital velocity

The constant, A, and the critical velocity, U_{cr}, depend on the sediment particle size and therefore give different sediment transport rates for different sediments.

The sediment transport calculated from this formula is weighted according to the probability of the set of conditions in the combined wave-current probability distribution, and the direction of the transport vector is given by the direction of the hourly velocity vector.

The hourly sediment transport vectors are summed to give the net sediment transport vector (Eulerian residual), whose u- and v-components are stored in output files, and the magnitudes of the hourly sediment transport vectors are averaged to give an average magnitude, which is stored in a third output file.

In the second stage of LTDISP, the net sediment transport vectors are used to calculate the change in bed mass in each cell. The initial mass on the bed is zero everywhere, but the program assumes that there is an infinite depth of the sediment, so at subsequent times the mass may be positive or negative.

Since the change in bed mass is calculated from the difference in mass of sediment entering over one side of the cell and leaving over the opposite side, it is

very sensitive to small changes in the vectors. To reduce this sensitivity, the mass changes in each cell are smoothed by taking a weighted average from the mass changes in the surrounding cells. The smoothed result is given by:

$$\begin{aligned} \text{Mchange}(i) = \quad & (\text{SMTH1} * Av_{1*1}) \\ & + (\text{SMTH9} * Av_{3*3}) \\ & + (\text{SMTH25} * Av_{5*5}) \end{aligned} \qquad (4)$$

where

Mchange(i) = mass change in cell i

SMTH1, SMTH9, SMTH25 = weighting coefficients for grids of 1 cell, 9 cells (3*3), 25 cells (5*5) respectively

Av_{1*1}, Av_{3*3}, Av_{5*5} = average value of mass change in grid of cells 1*1 (ie the cell itself) 3*3, 5*5, centred on the cell i.

This model can be used to show general patterns of erosion and accretion over a sandy area, and is useful in cases where some change is made to the original bathymetry, to show how the sediment transport patterns may change. It is also a useful tool for determining the dispersiveness of a site. Details of the inputs required and file formats are given in Appendix 5.

4.3 Model for mixing of muddy dredged material

In general, dredged material is dumped at sites where the bed is either a similar muddy material or a sandy one, but not usually where the bed is fixed, such as on rock. For this reason, it was considered important to model the mixing process which occurs if there is any movement of the background material.

LTD3 is a model which simulates this mixing. It is an extension of the background transport program LTDISP. The program uses the u- and v-components of sand transport vectors, as calculated in LTDISP, and the average magnitude of the transport vector 1. For each cell, at a chosen time interval, the program records the mass of sand, the mass of mud and the proportion of sand in a surface layer of chosen depth. The proportion of sand (or mud) in this surface layer affects the sand transport rates and the mud erosion rates. These three quantities are recorded in tideway format files. These files can be plotted out as contour diagrams at any time later, using the standard Tideway programs for contouring. Details of file formats are given in Appendix 6.

Sand transport vectors for each cell are reconstructed from the net transport vectors and the average magnitude to give two vectors, positive and negative in the direction of the net vector. The average magnitude of these vectors should be equal to that calculated in Phase 1 and the difference of the vectors should be equal to the net vector. Thus, for a point where the net transport vector is $\alpha\tilde{n}$, and the average magnitude is β, the reconstructed vectors would be

$$(\beta + 0.5)\alpha\tilde{n}$$
and
$$-(\beta - 0.5)\alpha\tilde{n} \qquad (5)$$

The vectors are resolved into u and v-components, and used independently in the calculations. For a tidal flow where the ebb and flood are in opposite directions, with very little flow in any other direction, this reconstruction of the vectors is satisfactory.

The sand transport into and out of any cell may be affected by the material in the surrounding cells, up to four cells away in any direction. The choice of four cells was more than enough to be reasonably sure that any sand (even fine sand) picked up at one cell would have been deposited, or exchanged with other bed material, closer than four cells away. Usually, one or two cells (assuming minimum cell size of 50m) would be sufficient. This was calculated from the amount of time a particle of sand at the surface would take to settle to the bottom (an upper bound on the time taken for a particle in suspension to exchange with the bed material). The actual way in which material from one cell contributes to the sand transport in neighbouring cells depends on many things, but an estimate may be made by assuming a sand concentration profile in the water column and calculating how this sand would deposit in a uniform current over the next few cells. Weighting coefficients may then be assigned (which should add up to 1.0) for how each cell contributes to the sand transport through the next four cells in each direction. The contributions may often only come from one or two cells in each direction. These weighting coefficients are the same over the whole model.

Mud may be dumped during any time step (a time step of approximately one week is reasonable if the model is to be used for long-term predictions). Continual dumping can be simulated by having a dump during each time step. The size (total mass and spread), position of the centre and time of each dump is specified in the file of input data. Each dump covers a circular area, and corresponds to a gaussian distribution, with a specified standard deviation. A correction is made to ensure that the discretisation of the distribution does not result in a larger total dump than specified.

At the end of each time step the mass of sand lost or gained from each cell is calculated from the difference in sand transport over opposite sides of the cell. The sand transport over any line (cell side) is a weighted sum of the contributions from the four preceding cells. The contribution from each cell depends on the proportion of sand in that cell, and is weighted according to the weighting coefficients described earlier. Thus for a cell (i, j) , with i increasing in a west to east direction, the sand transport rate out of that cell over the eastern side would be:

$$S(i,j)_{out\ E} = (P_s(i,j)*CONT1 + P_s(i-1,j)*CONT2 + P_s(i-2,j)*CONT3 + P_s(i-3,j)*CONT4) * R(i,j)_{out\ E} \quad (6)$$

where

$S(i,j)_{out\ E}$ = sand transport rate out of cell i, j on eastern side

$P_s(i,j)$ = proportion of sand in surface layer of cell i, j

CONT1, (CONT2, CONT3, CONT4) = weighting coefficients for how the cell next to the sand transport line (and 2 cells, 3 cells, 4 cells away) affect the sand transport

$R(i,j)_{out\ E}$ = sand transport rate out of cell i, j on eastern side, calculated from reconstructed vector, assuming 100% sand.

Once the sand mass changes in each cell have been calculated, the results are smoothed according to a weighted average of the surrounding cells, as in LTDISP (see Section 4.2).

The mass of mud is also calculated at the end of each time step. This depends on the mass lost into suspension and the amount dumped. In LTD3, the mud is

not allowed to move from one cell to another once it has landed on the bed. It may be eroded by the waves and currents, but this mud is lost into suspension and not seen on the bed again. The rate of this loss into suspension is the same over the whole model for cells containing entirely mud, and should be based on field or laboratory determination of mud properties. Since each cell may also contain some sand, the rate is linearly reduced with decreasing proportion of mud in the surface layer, ie

$$M_E(i,j) = R\ \Delta t\ P_m(i,j) \qquad (7)$$

where

$M_E(i,j)$ = the mass eroded from cell (i, j) during one time step (kgm^{-2})

R = constant rate of erosion (kgm^{-2} per tide)

Δt = length of time step (tides)

$P_m(i,j)$ = proportion of mud in surface layer of cell $(i,j) = 1 - P_s(i,j)$

Both the changes in mud mass and sand mass are used to calculate the proportion of sand in the surface layer. Only the proportions of mud and sand in this layer are recorded. Although total mass of sand and mud is recorded, no record of the mixing is retained once the material is below the top layer. The subroutine which calculates this mixing is given in Appendix 6.

4.4 Model for flow of viscous mud layer down a slope

Field studies, such as the HR Brisbane study, indicate that a footprint of dredged material on the bed may spread out over a period of time. It is unlikely that this spreading is due to erosion and deposition, as once material has been eroded it is diluted too much

in the overlying suspension. The rate of spreading can be very slow, much too slow to be described by the movement of fluid mud. A third model has been developed to predict the movement of a fairly dense mud (>200kgm^{-3}), moving down a slope as a viscous layer. The model is based on theory developed by Mr R L Soulsby at HR.

In this model, the density and the viscosity of the layer are assumed to be constant (this is not unreasonable if the layer is quite thin). The actual values of the density and viscosity affect the rate of flow, so values used in the model should be based on rheological measurements. Examining the forces on an element of mud in a layer of thickness h, yields the force balance

$$(\rho_B - \rho)\ g\ \sin\theta + d\tau/dz = 0 \qquad (8)$$

where

ρ_B = bulk density of the mud
ρ = bulk density of the overlying water
g = acceleration due to gravity
θ = slope of bed on which mud layer is lying
$\tau(z)$ = stress profile in mud layer.

If there is zero stress at the top of the mud (z=h) then the stress profile is

$$\tau(z) = (\rho_B - \rho)\ g\ \sin\theta\ (h - z) \qquad (9)$$

For viscous flow, with constant viscosity

$$\tau(z) = \mu dU/dz \qquad (10)$$

where

μ = dynamic viscosity of the mud (Nsm^{-2})
$U(z)$ = velocity profile in the bed

Combining equations 9 and 10 and integrating gives a velocity profile. If a boundary condition of no slip at the mud-sand boundary (z=0) is applied, then the velocity profile is

$$U(z) = (\rho_B - \rho)\ g\ \sin\theta\ (hz - 0.5z^2)\ /\ \mu \qquad (11)$$

The transport rate of mud down the slope, Q ($kgm^{-1}s^{-1}$), is then given by

$$Q = \int_0^h \rho_B\ U(z)\ dz \qquad (12)$$

ie

$$Q = \rho_B\ (\rho_B - \rho)\ g\ \sin\theta\ h^3\ /\ 3\mu \qquad (13)$$

At the start of the program, a circular pancake of mud of uniform thickness is spread on the bed. The movement of mud from each cell is determined from equation 13, by calculating the difference in rates of transport over opposite sides of each cell. This gives a mud mass lost or gained during the time step. These masses are smoothed using the same method as LTDISP (Section 4.2). The thickness of mud in each cell is stored in a Tideway format file at a chosen interval. Details of file formats are given in Appendix 7.

This model could be used to predict what might happen at a non-dispersive site, with little or no movement of the background material, particularly if waves were not thought to be an important factor at that particular site.

4.5 Limitations of the models

The long term dispersion models LTDISP and LTD3 are models of potential transport: they assume that if the combined waves and currents are strong enough to cause sand transport, the material will be picked up instantaneously, and that there is always material there to be picked up. Because of this the models are most suitable for generally sandy areas of seabed.

The programs do not model the longshore currents which will be produced in the surf zone by the waves. Therefore the predicted sediment transport for any point above approximately -5m CD is not likely to be accurate.

The program LTDISP calculates the Eulerian residual net sediment transport vectors. These will generally be different from the true Lagrangian residuals in a model where the velocity field varies spatially. The difference between these has been investigated for some idealised cases of flow conditions, and these are described in Appendix 8. For certain conditions it is shown that the two would not produce significantly different bed mass changes.

The model for flow of a viscous mud layer is restricted at present to mud layers of uniform density and constant dynamic viscosity. At present the program does not include wave effects on the structure of the material.

5. APPLICATION OF MODELS

5.1 Sizewell, UK

In parallel with the development of the long term dispersion model, HR conducted a study for Kier Construction Limited at Sizewell, on the East Anglian coast of Britain (Ref 11). Part of this study involved looking at the background movement of sandy material up and down the coast over a summer season of about six months, and the dispersiveness of a site which was being considered for temporary storage of dredged material.

The newly developed model, LTDISP, was used alongside some existing sediment transport models to look at sediment transport in this area. The results from LTDISP were compared with SANDFLOW, a model which carries the sediment dynamically in suspension, and allows for the finite time and distance required to pick up the sediment. SANDFLOW only runs for the set of tidal conditions as calculated by TIDEFLOW-2D, and does not include wave effects. The advantage of LTDISP is therefore its ability to make predictions over a period of time for combined currents and waves.

A previous study (Ref 12) involved setting up a TIDEFLOW model of the area, and the more recent study of sediment transport was based on the hydrodynamics which were produced in the earlier study.

Figure 11 shows the area around Sizewell, with the area covered by the model, which was the same for LTDISP as in the earlier study. A 50m gridded model had been set up, aligned parallel to the National Grid, 4.5km long by 2km wide. The model was bounded on its west side by the coast. The open boundaries on

the east and north had prescribed velocities, while the south edge of the model had a prescribed elevation.

The bathymetry at the site consists of a fairly uniform slope from the coast on the western side of the model down to at channel at about -10m OD, and then rising back up to about -6m OD on Sizewell bank on the eastern side of the model. In the southern quarter of the model there are some ridges running from NE to SW. The bathymetry is shown in Figure 12. The marked wave points are the points for which the models HINDWAVE and OUTRAY predicted waves conditions.

The model floods from the north, with the maximum flood velocity reaching about $0.8ms^{-1}$ on a spring tide. The spring tide currents for three marked points are shown in Figure 13. There is little deviation of the flow at these three points from the north-south direction. Figure 14 shows the corresponding neap tide currents. In general, a higher peak velocity is reached on the flood than on the ebb.

The wave climate for the model was generated from nearby wind data. The HINDWAVE model was used to generate the offshore wave climate. The data produced, like the input data, is in the form of a time series, so the model does take into account the storm duration.

The OUTRAY model was then used to bring the waves towards the shore, taking into account the effects of refraction and shoaling. The resulting scatter diagram for wave point 3, which was used for this study, is shown in Figure 15.

For comparison with SANDFLOW, LTDISP was run with a single spring tide and no waves, and then to assess the effect of waves, LTDISP was run with a full range of tides and waves.

The LTDISP net sediment transport vectors for a mean spring tide with no waves are shown in Figure 16. The dominance of the flood tide is shown by the net sediment vectors with all points indicating a net southerly sediment transport. The largest vectors indicate a peak net sediment transport of approximately $0.1 kgm^{-1}s^{-1}$ which occurs in the central deeper region of the model. Net sediment transport decreases in the shallower waters towards the coast and the Sizewell Bank.

The LTDISP average tide net sediment transport vectors for a six month period of tides and waves are shown in Figure 17. In spite of lower tidal velocities over the sand banks on the eastern side of the model, the effect of the waves there is to increase the net sediment transport to a value similar to that in the deeper water in the centre of the model. The maximum vectors occur on the banks in the southern area of the model and reach $0.5 kgm^{-1}s^{-1}$.

The degree of dispersion of the model area can be represented in terms of the average size of the LTDISP sediment transport vectors as shown in Figure 18 (single spring tide) and Figure 19 (tides and waves). These do not indicate areas of erosion or deposition as that depends on the difference between adjacent points of the net sediment transport. Rather, they indicate the average rate of sediment transport at each point, or a measure of the dispersiveness. A single point could, for example, have a large average rate of sediment transport yet have a zero net

sediment transport due to the reversing directional aspects of tidal sediment transport.

The effect of the waves on the shallower banks is very evident from a comparison of Figures 18 and 19. For a spring tide, (Fig 18) the deeper central channel of the model had the greatest average sediment transport (ie greatest dispersiveness), of approximately $0.1 kgm^{-1}s^{-1}$ to $0.15 kgm^{-1}s^{-1}$. With waves and tides (Fig 19) the reverse was the case, with the greatest dispersiveness on the shallower bank on the eastern side, although the magnitude of the average sediment transport had increased by an order of magnitude over the whole model. In the central channel, the average magnitude of the sediment transport vector for tides and waves was up to $0.5 kgm^{-1}s^{-1}$, with 1.0 - $1.5 kgm^{-1}s^{-1}$ on the shallower banks. This shows the important effect of waves in the sediment transport, particularly in shallower areas.

The bed mass changes calculated by LTDISP during a single spring tide with no waves for the existing bathymetry based on the van Rijn sediment transport formula are shown in Figure 20. This may be directly comparable with Figure 21 which depicts the bed mass changes from SANDFLOW. The general trend, that the major bed mass changes are in the southern part of the model, is also predicted by the LTDISP model (Fig 20). However, other small areas of net deposition are shown throughout the whole of the northern four-fifths of the model, although their magnitudes are less than $5 kgm^{-2}$.

The LTDISP bed mass changes for an average tide based on six months of tides and waves for the existing bathymetry are given in Figure 22. The relative differences between this and Figure 20 indicates the effect of waves on the sediment transport.

5.2 Tees Bay, UK

The Tees Inner Disposal site was chosen as a site for the pilot model for mixing of muddy dredged material. A TIDEFLOW model bed data file was set up, covering an area 4km by 4km, including the disposal site. The bathymetry of the area is shown in Figure 23. The bed slopes down away from the coast, fairly uniformly, from -27m CD in the west corner to about -39m CD in the east. The grid of the model is aligned with the principal direction of flood and ebb velocities (125° from N), and the north-east and south-west sides of the model are designated as no-flow boundaries. This is a reasonable approximation as the flow is predominantly bi-directional. The model floods from the north-west.

At this particular site, high and low water are out of phase with periods of minimum velocity. This is shown in Figure 24, which shows current meter velocities and water levels measured at a point in the disposal area in 1987. This data was used to generate velocities over the whole model area, by assuming the same discharge through each line of cells north-east to south-west, and calculating the discharge, Q, through each individual cell as a function of the flow depth, d, at that cell, ie

$$Q \alpha d^{1.5} \qquad (14)$$

LTDISP was then used to predict sediment transport patterns. The net sediment transport vectors are shown in Figure 25, showing net sediment transport rates in a south-easterly direction, at approximately $0.001 kgm^{-1}s^{-1}$. The resulting pattern of bed mass changes is shown in Figure 26. This indicates patches of net sediment erosion and accretion after 4 weeks;

the net mass changes are very small, reaching a maximum change of about 1.0kgm^{-2} after 4 weeks.

The sediment transport vectors from LTDISP were then used in the model for mixing of muddy dredged material. Continuous dumping of mud was simulated by allowing a dump of mud every timestep (each time step was one week). The amount dumped each time step was calculated from maintenance dredging figures from the Tees estuary. These indicate that an average quantity of 1.8 million cubic metres (in situ) of material is dredged from the estuary each year and disposed of at the Tees Inner Disposal Site. Assuming an in situ density of 400kgm^{-3}, this gives a total of 15 million kg per week.

The erosion rate of mud was calculated according to the equation

$$dm/dt = m_e(\tau-\tau_c) \quad \text{for } \tau \geqslant \tau_c \qquad (15)$$
$$dm/dt = 0 \quad \text{for } \tau < \tau_c$$

where
dm/dt = rate of loss of mud per unit area (kgm^{-2}s^{-1})
m_e erosion constant (kgN^{-1}s^{-1})
τ = applied bed shear stress (Nm^{-2})
τ_c = critical shear stress for erosion (Nm^{-2}).

The erosion constant was determined in laboratory tests (Ref 13) to be around 0.0009kgN^{-1}s^{-1}. The current meter velocities were used to calculate bed shear stresses. The velocities were scaled for neap tides according to the ratio of the mean spring and neap tidal ranges, and for intermediate tides the velocities were calculated by linear interpolation between springs and neaps. Taking the critical threshold for erosion to be 0.1Nm^{-2} an average excess shear stress was calculated over the whole

spring-neap-spring cycle. This was approximately $0.025 Nm^{-2}$. An average value of the erosion rate was therefore around $1 kgm^{-2}$ per tide (12.33 hours). This is for 100% mud; for a mixture of mud and sand the erosion rate in the mixing model is reduced linearly according to the percentage of sand.

These values were used as input in the mixing model. Figure 27 shows the pattern of bed mass changes for the background material after 4 weeks. This can be compared with Figure 26, which shows the bed changes without the addition of the mud. Around the centre point of the dump there is now an accumulation of sand, and to the sides of the dump in the direction of the principal currents there is a net loss of sand. This is because although sand is being transported on to the patch of mud, the mud is then reducing the sand transport out of this area in both the ebb and flood directions.

The distribution and build-up of mud over the four weeks is shown in Figure 28. This shows a circular distribution of mud, building up gradually in the centre. After the first dump, the mass at the centre of the dump increases at around $4 kgm^{-2}$ per week. After four weeks, at the centre of the dump the mass of mud per unit area is less than $30 kgm^{-2}$, equivalent to around 10cm.

The proportion of mud in the surface layer of the bed is shown in Figure 29. This distribution is after four weeks, but in fact, for the input conditions used in this case, once these proportions are reached, they do not change. This shows a small area of about 80% mud at the centre of the dump, decreasing outwards, reaching zero at the edges of the muddy patch. The remaining proportion in each case is sand.

These proportions of sand and mud are not too different from those measured in the field. Field surveys of the disposal site in 1987, 1988 and 1989 collected bed samples which were analysed for particle size (Ref 14). These show the percentage of material less than 90 microns to be in the range 20 - 80% in the disposal area, although the average percentage is around 30%. Unlike the mixing model, there appear to be no distinct peaks, but in the model all the dumping is centred on one point whereas in the actual disposal area the dumping will not be restricted to one point.

These preliminary results indicate how the model may be used. It should be stressed that the model has not been calibrated and that further field measurements of the long term dispersion of dredged material are recommended to do this.

6. CONCLUSIONS AND RECOMMENDATIONS

6.1 Conclusions

1. Many factors affect the rate at which dredged material disperses from its disposal point, including type of material, its cohesivity and bulk density, water depth, tidal currents, bed roughness and slope. The major process in moving the material once it is on the bed appears to be the wave disturbance caused by storms.

2. Field work at Mud Island, Brisbane, looking at long term dispersion of dredged material supports the idea that the initial footprint of mud may be represented by a normal distribution (Fig 5). The study showed that material deposited on a slope could flow down the slope into deeper areas. The initial distribution in a radioactive

tracer study at the Tees inner disposal site (Appendix 1) could also be represented by a normal distribution (Fig 10). Subsequent measurements of the distribution in the Tees study were unfortunately thwarted by bad weather and damage to equipment, so only the initial measurements were able to be used.

3. A package of computer models was developed to predict long term dispersion, each model applicable for different circumstances. The model for transport of sandy background material combines the hydrodynamics from the existing TIDEFLOW-2D program and the wave climate from the existing HINDWAVE and OUTRAY programs. A probabilistic combination of the tides and currents over the period of interest (from a single tide up to several months or even years) gives vectors of net sediment transport of the background material. These vectors can be used to calculate mass changes on the bed. In addition the model calculates the average magnitude of the sediment transport vector, which is a measure of the dispersiveness.

4. The model for muddy dredged material allows mixing of the mud with the background material. It is an extension of LTDISP, using the same sediment transport vectors. The mud cannot move from cell to cell, but it can be eroded by the tidal currents. The movement of sand is affected by the presence of the mud, and the erosion rate of the mud is affected by the presence of sand in the surface layer.

5. A third model has been developed for flow of a viscous mud layer down a slope. The mud layer is assumed to have uniform density and viscosity. A

no-slip condition is applied between the mud layer and the bed below. The difference between mud transport rates over opposite sides of each cell are used to determine a new mud distribution. The model does not include the effect of waves on the structure of the mud, and as such is most applicable to non-dispersive sites.

6. The model for sand net transport was used in a study at Sizewell, UK. The effect of the waves on the sand transport was investigated, and the average magnitude of the transport vectors indicated the degree of dispersion. If waves were not taken into account, the greatest dispersion (as indicated by the average magnitude of the hourly transport vectors) was in the deeper parts of the model, in the central channel (Fig 18). For tides and waves, the greatest dispersion was on the shallower banks (Fig 19). Overall, the effect of waves was to increase the sediment transport rates by about an order of magnitude.

7. The Tees Inner Disposal site was used to test the mixing muddy dredged material. LTDISP was first used to predict net sediment transport vectors and bed mass changes. The net sediment transport rates were in a southeasterly direction, at approximately $0.001 kgm^{-1}s^{-1}$ (Fig 25). Continuous dumping of mud was simulated by allowing a dump of mud every timestep. The sand mass changes showed a build-up of sand around the centre of the mud dump, and a net loss of mud from the sides of the mud dump in the direction of the principal currents (Fig 27). The mud was accumulating slowly, at around $4kgm^{-2}$ per week (Fig 28). The percentage of mud in the muddy

patch was around 80% (20% sand) at the centre of the patch, decreasing outwards to zero (Fig 29). This agrees roughly with field measurements of particle size in the Tees Inner Disposal Site, with samples in which 20 - 80% of the material was less than 90 microns, although the mean percentage was around 30%.

6.2 Recommendations

It is recommended that the model for flow of a viscous mud layer down a slope should be extended to include a density profile in the layer, and non-uniform viscosity. The effect of waves on the structure of the layer should ideally also be included.

The mixing algorithm in the model for mixing muddy dredged material does not keep track of the relative proportions of mud and sand below the active surface layer. This algorithm should ideally be refined, and then movement of the mud down slopes also allowed. In order to understand better how sand affects the movement of mud down a slope, further laboratory tests are recommended.

At present, there is little field data against which to calibrate the long term dispersion models, as the field study at the Tees Inner Disposal Site unfortunately only resulted in information about the short-term distribution of dredged material. Further work measuring the long term dispersal of dredged material in the field is recommended to calibrate and verify these models.

7. REFERENCES

1. Gordon R B, "Dispersion of dredge spoil dumped in near-shore waters." Estuarine and Coastal Marine Science, Vol 2, pp 349-358. 1974.

2. Delo E A, Burt T N, "Dispersal of dredged material: Tees field study September 1987". Hydraulics Research, Wallingford, England. Report SR 112, June 1987.

3. Delo E A, Ockenden M C, Burt T N, "Dispersal of dredged material: Mathematical model of plume." Hydraulics Research, Wallingford, England. Report SR 133, June 1987.

4. Diserens A P, Delo E A, "Dispersal of dredged material: Application of short term model for cohesive sediments". Hydraulics Research, Wallingford, England. Report SR 210, May 1989.

5. Johanson E E, Boehmer W R, "Examination of predictive models for dredged material dispersion in open water." First International Symposium on Dredging Technology, Kent, England. September 1975.

6. Bohlen W F, "A comparison between dredge induced sediment resuspension and that produced by natural storm events." Proc. 18th Coastal Engineering Conference, 1980.

7. US Army Engineer Waterways Experimental Station, "Field study of the effects of storms on the stability and fate of dredged material in subaqueous disposal areas." WES, Vicksburg, Miss., USA. Technical Report D-77-22.

8. Hydraulics Research, "Port of Brisbane Siltation Study - Eleventh report: The efficiency of the Mud Island Spoil Ground - a study using radioactive tracers". Hydraulics Research, Wallingford, England. Report EX 977, March 1981.

9. van Rijn, L.C. "Sediment Transport, Part III: Bed forms and alluvial roughness." Journal of Hydraulic Engineering, Vol.110, No.12, pp1733-1754. 1985.

10. Grass, A.J. "Sediment transport by waves and currents." SERC London Centre for Marine Technology, Report No. FL29, 26pp. 1981.

11. Hydraulics Research, "Sizewell 'B' Power Station: Temporary disposal of dredged material". Hydraulics Research, Wallingford, England. Report EX 2011, December 1989.

12. Hydraulics Research, "Sizewell Power Station: Midfield cooling water plume model." Hydraulics Research, Wallingford, England. Report EX 1882 June 1989.

13. Ockenden M C, Delo E A, "Dispersal of dredged material: River Tees mud properties". Hydraulics Research, Wallingford, England. Report SR 205, March 1989.

14. Diserens A P, Delo E A, "Dredged material and heavy metals in tidal waters: Site monitoring and analysis". Hydraulics Research, Wallingford, England. Report SR 235, March 1990.

FIGURES.

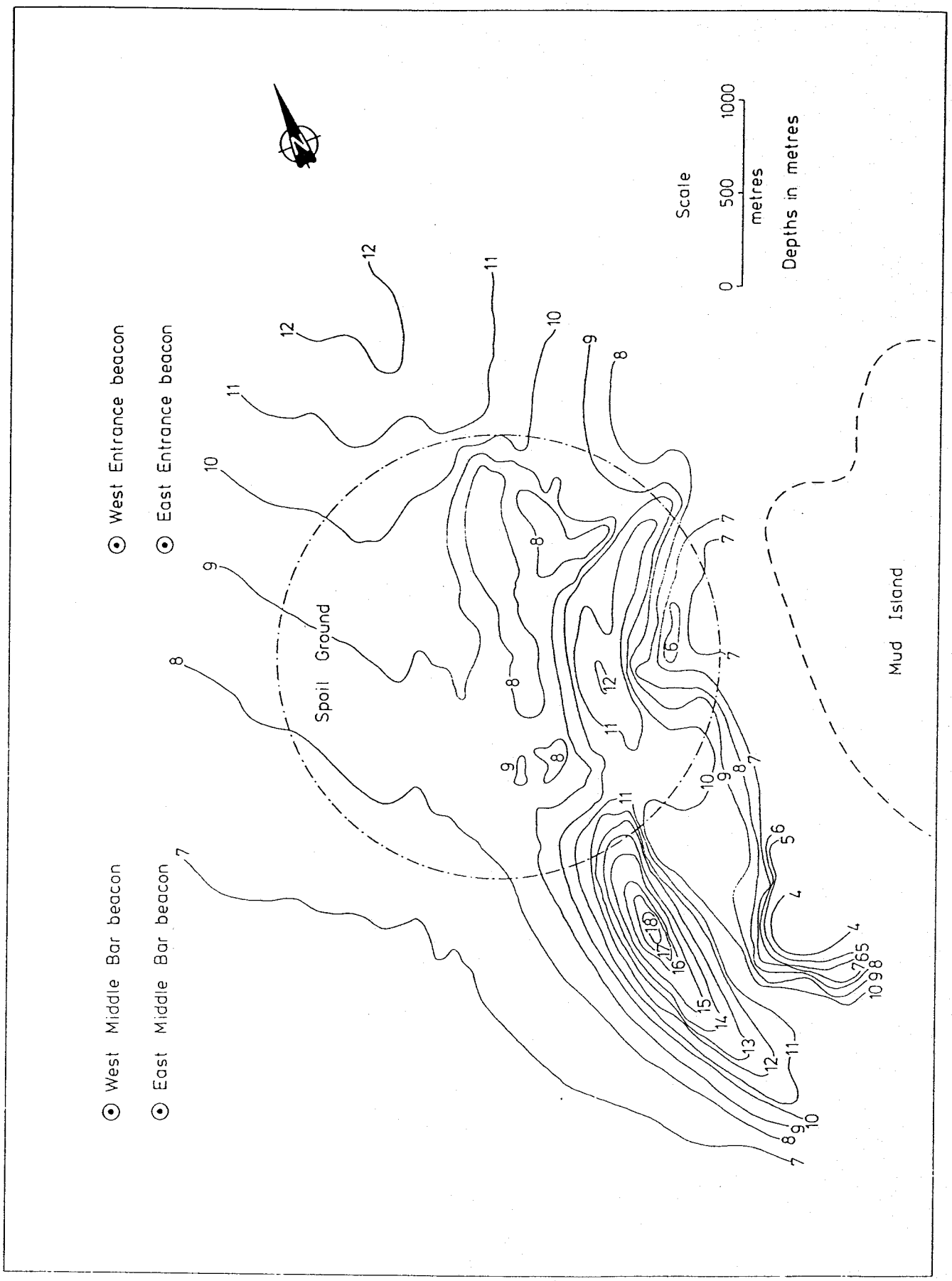

Fig 1 Bathymetry of the Mud Island disposal site, Brisbane River, 1976/77

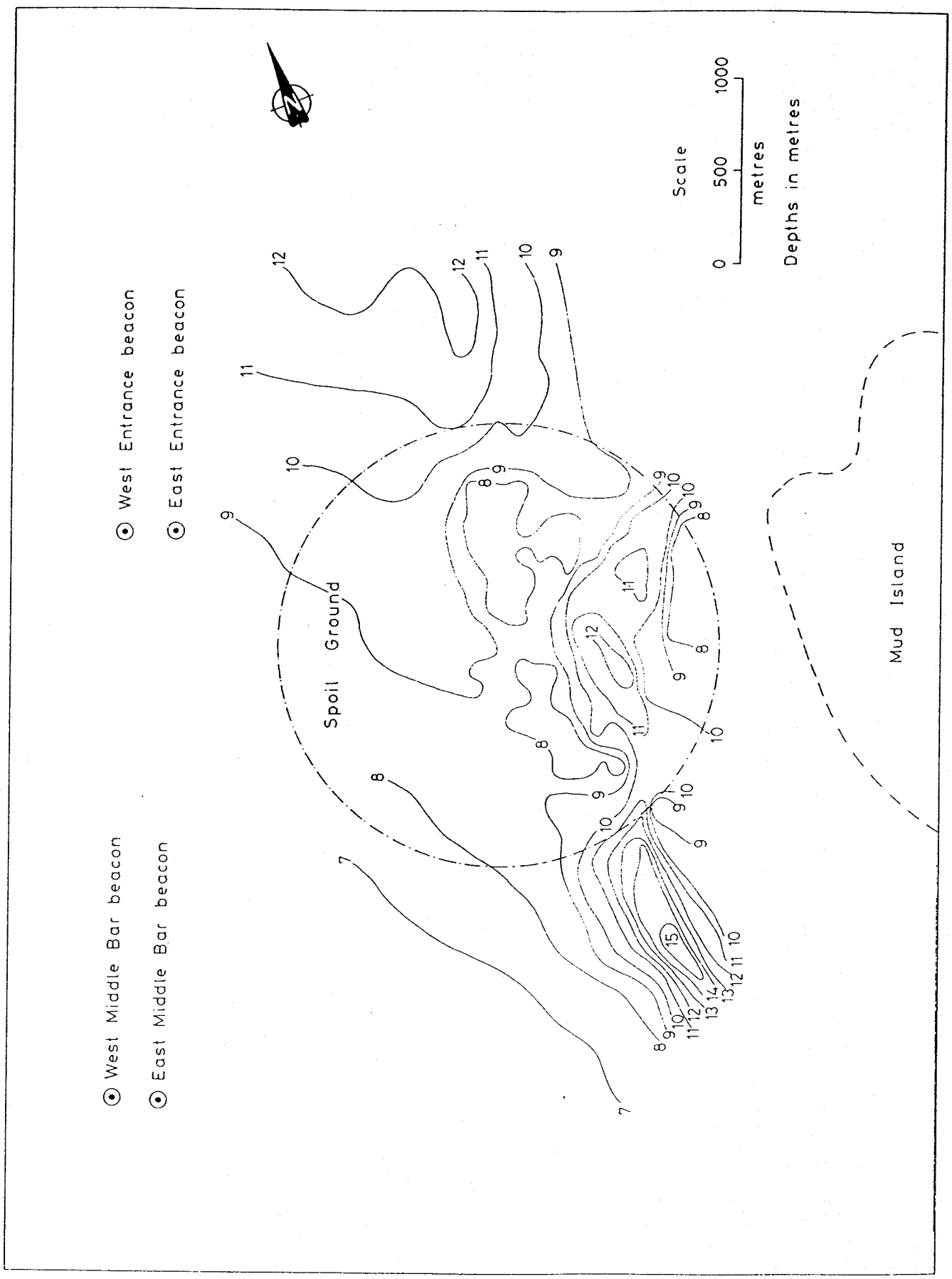

Fig 2 Bathymetry of the Mud Island disposal site, Brisbane River, June 1979

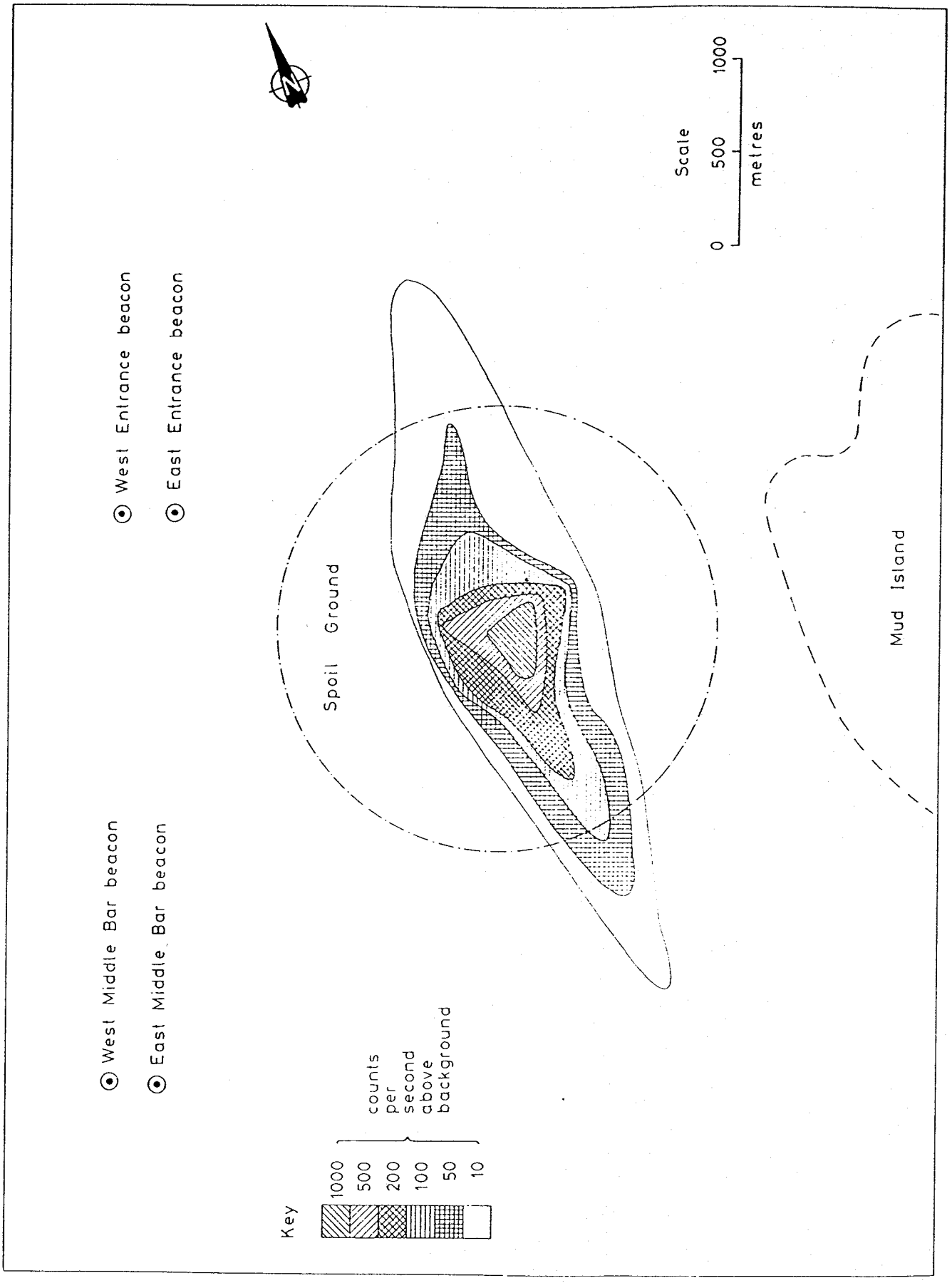

Fig 3 Mud Island: Distribution of tracer-injected sediment, 2 days after disposal

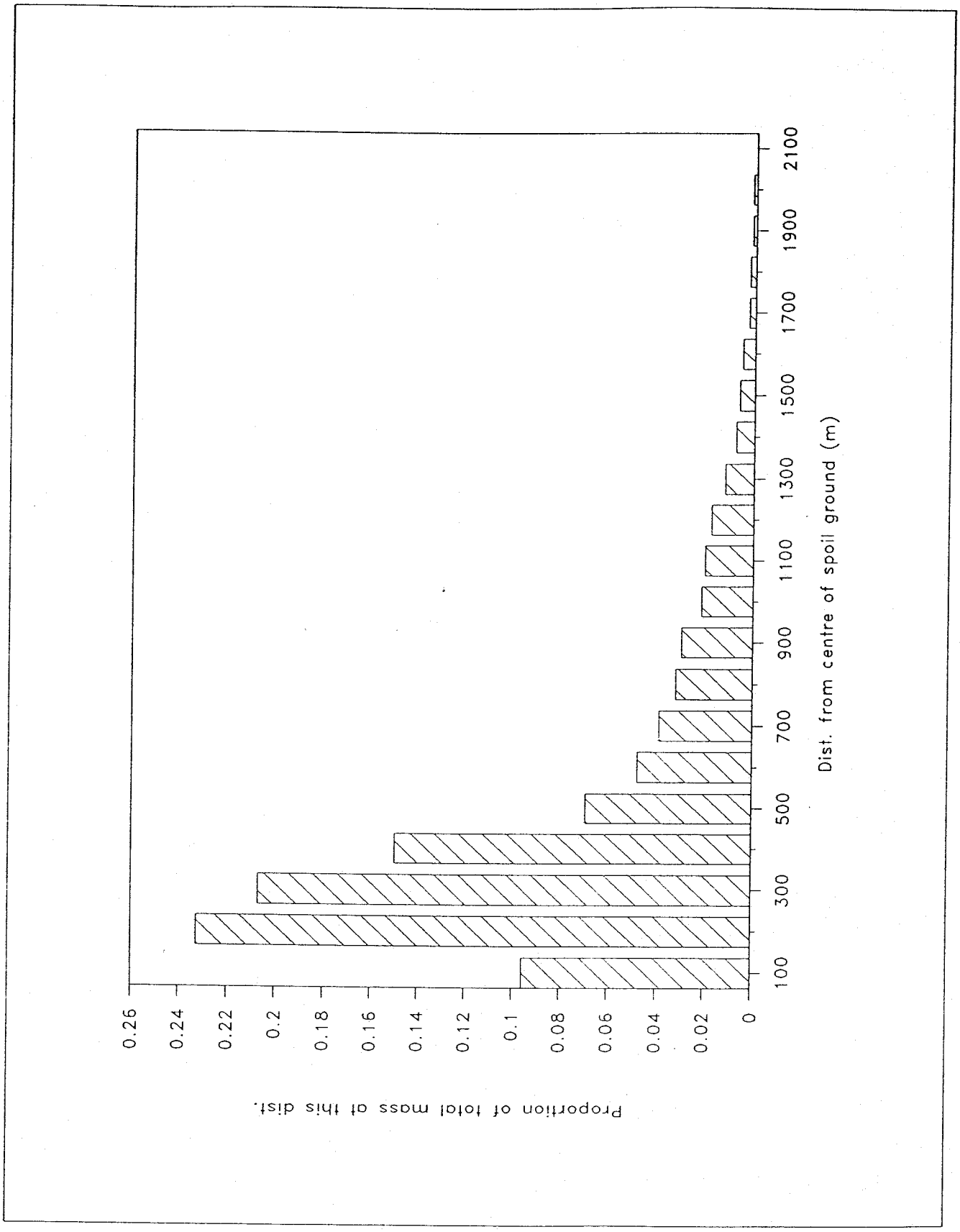

Fig 4 Distribution of sediment mass relative to distance from centre of disposal site, 2 days after disposal

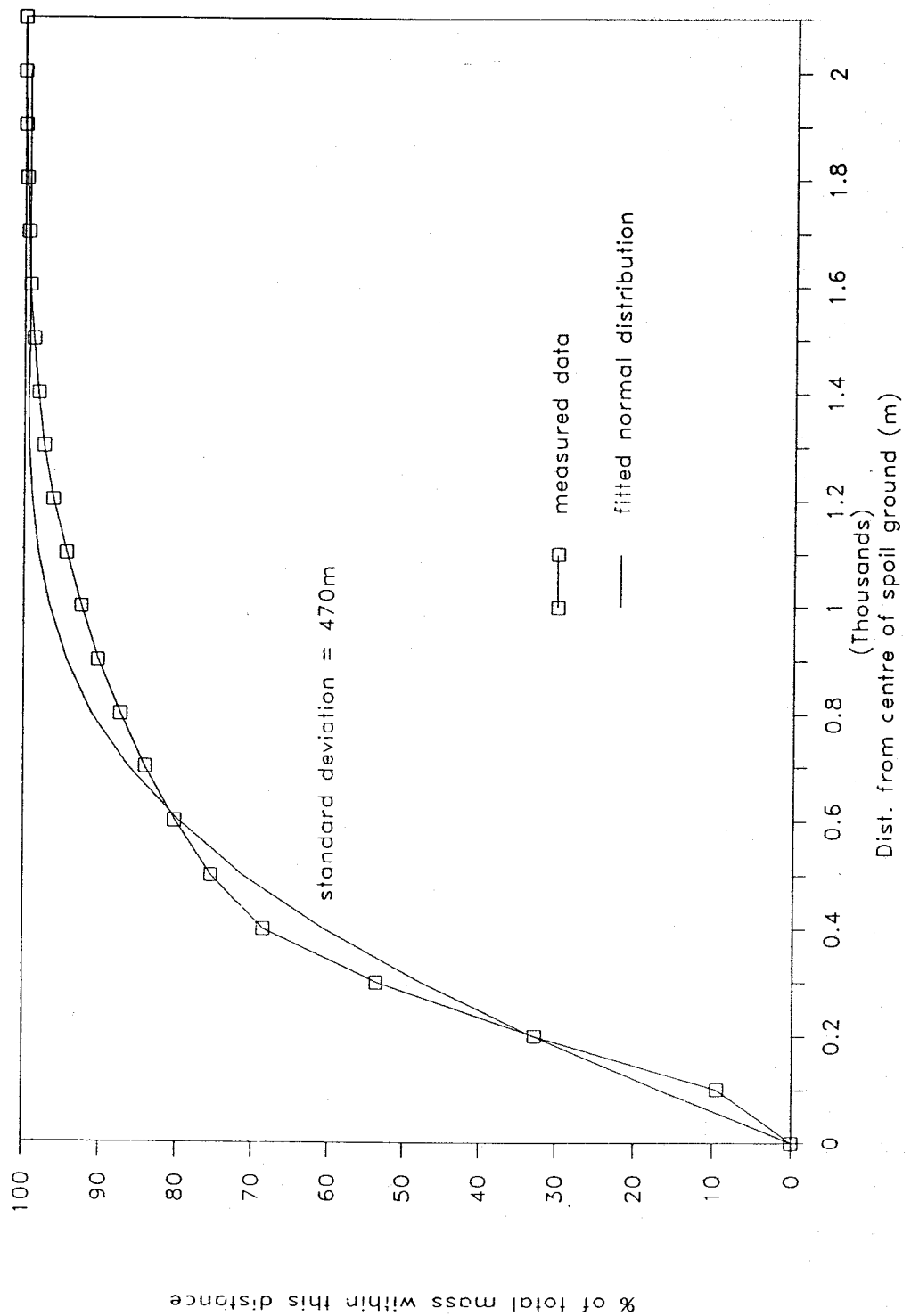

Fig 5 Cumulative mass against distance from centre of disposal site

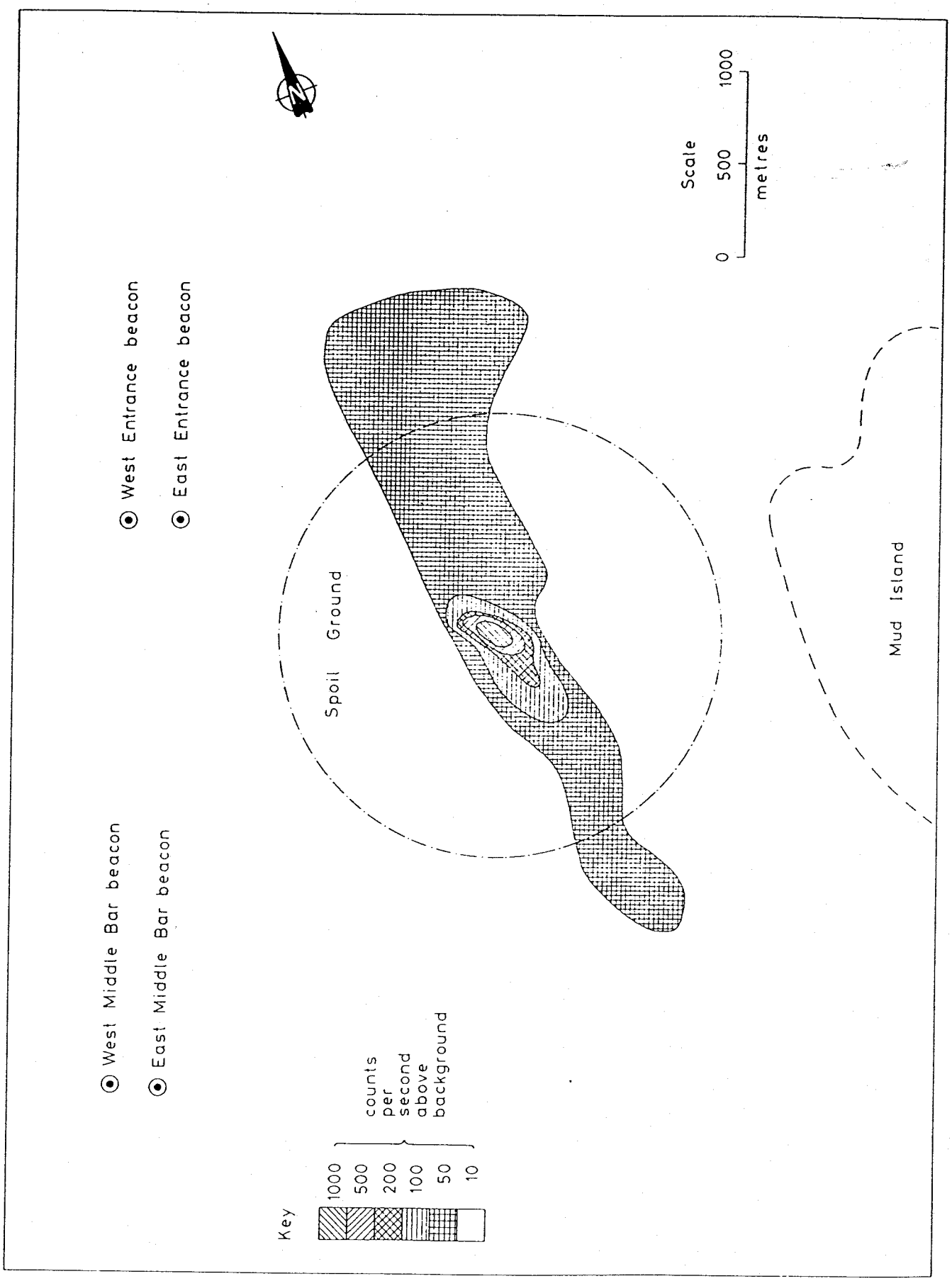

Fig 6 Mud Island: Distribution of tracer-injected sediment, 371 days after disposal

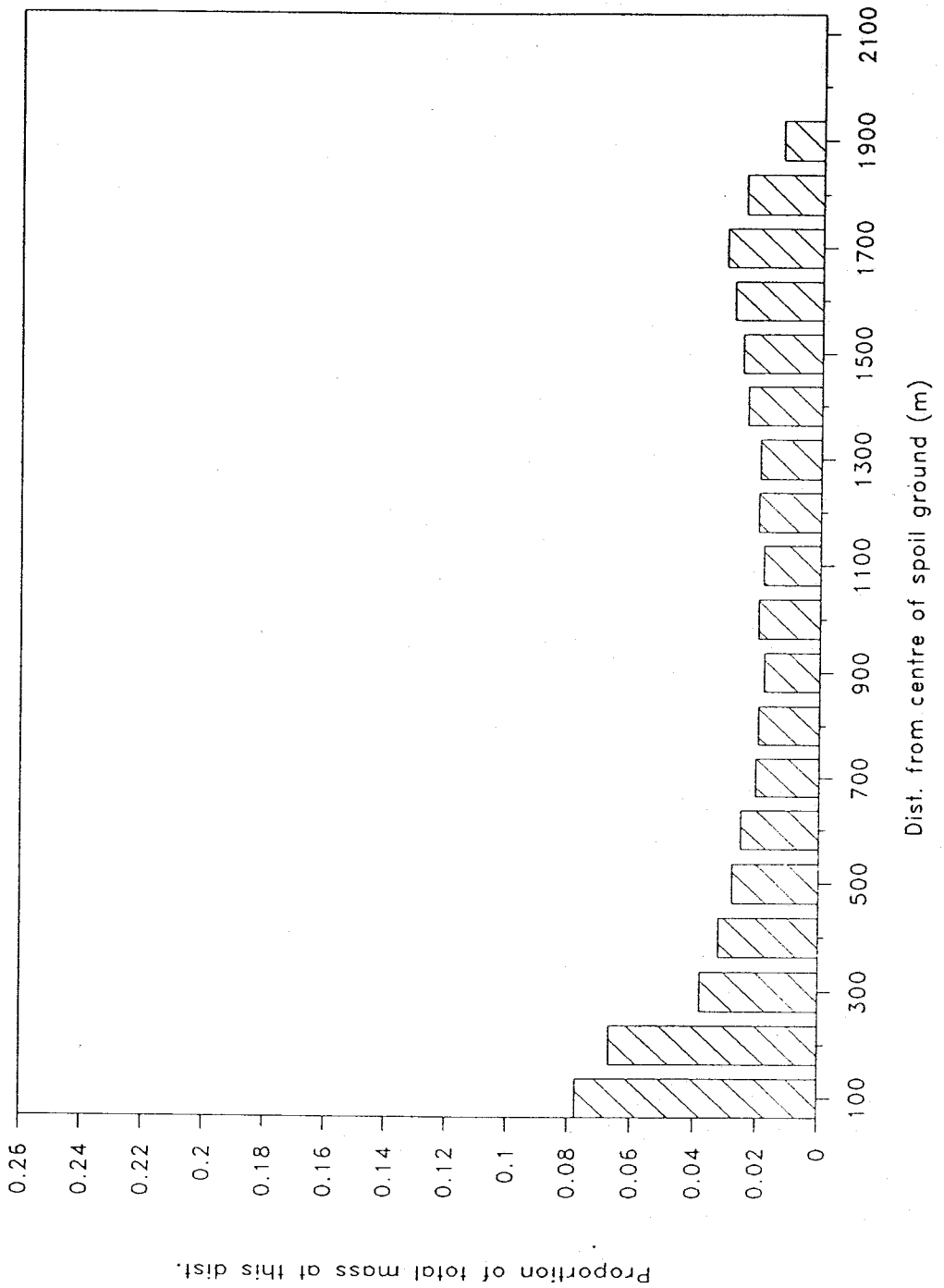

Fig 7 Distribution of sediment mass relative to distance from centre of disposal site, 371 days after disposal

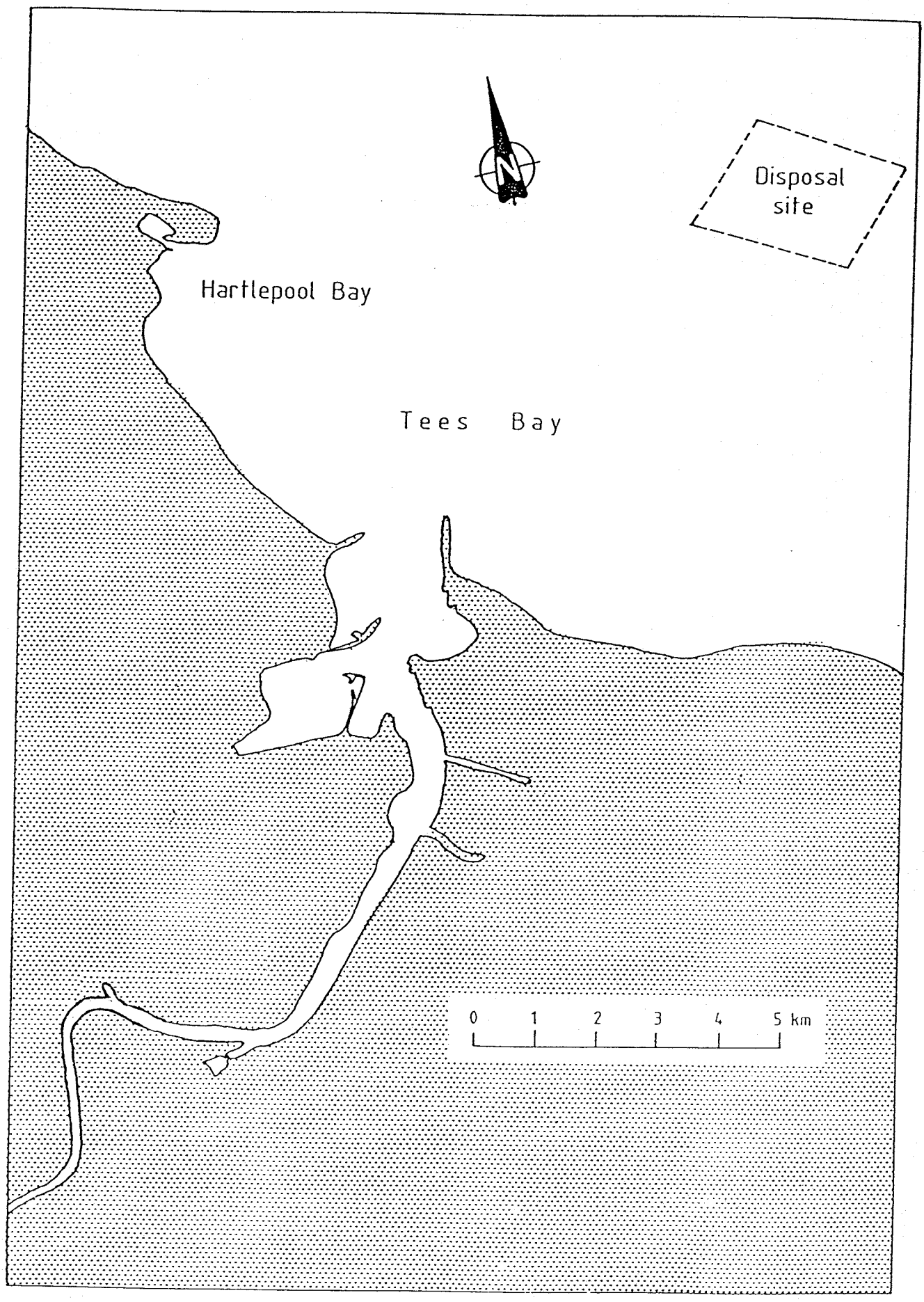

Fig 8 Location map of Tees Inner Disposal Site

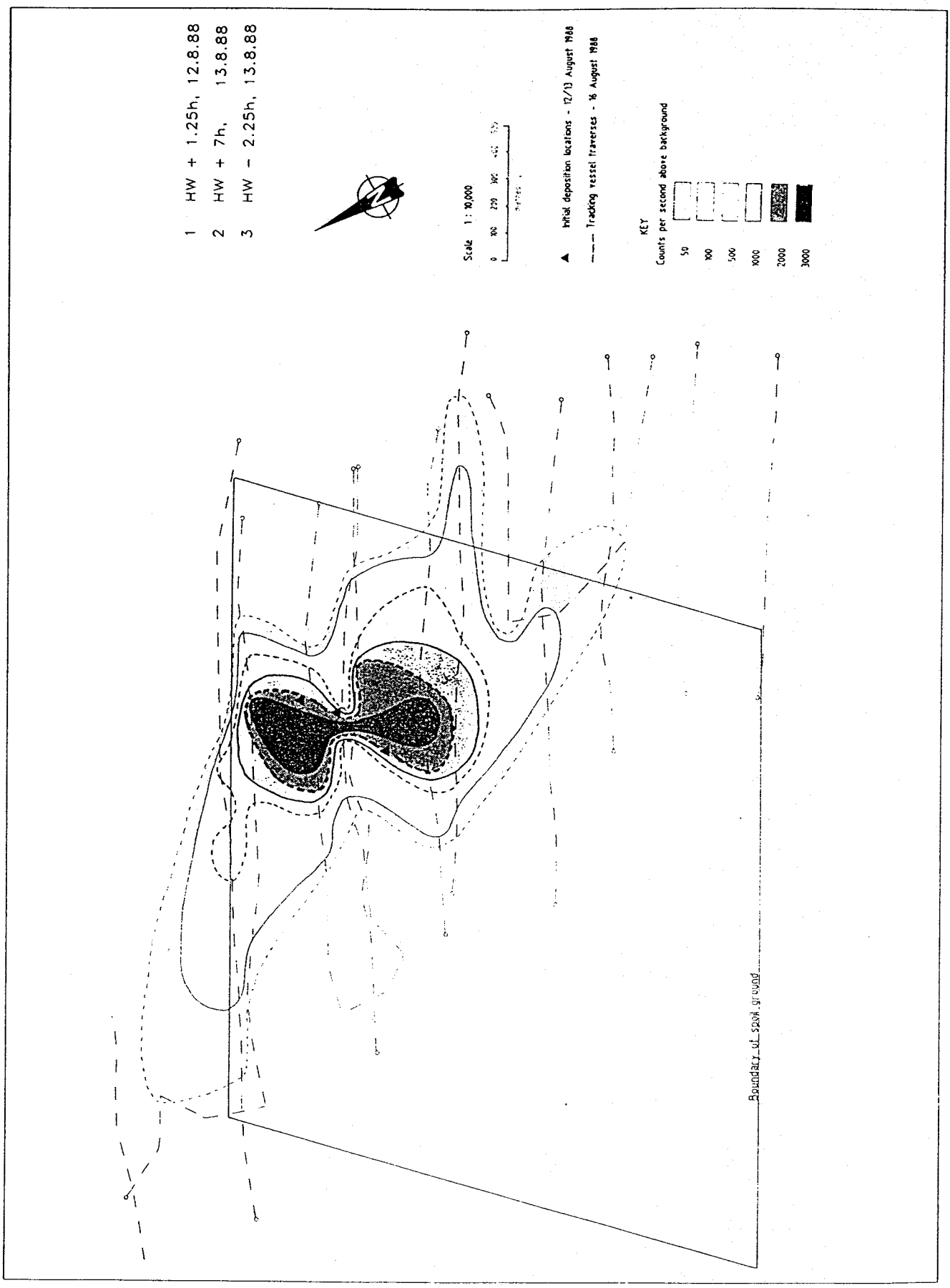

Fig 9 Tees: Distribution of tracer–injected sediment, 3 to 4 days after disposal

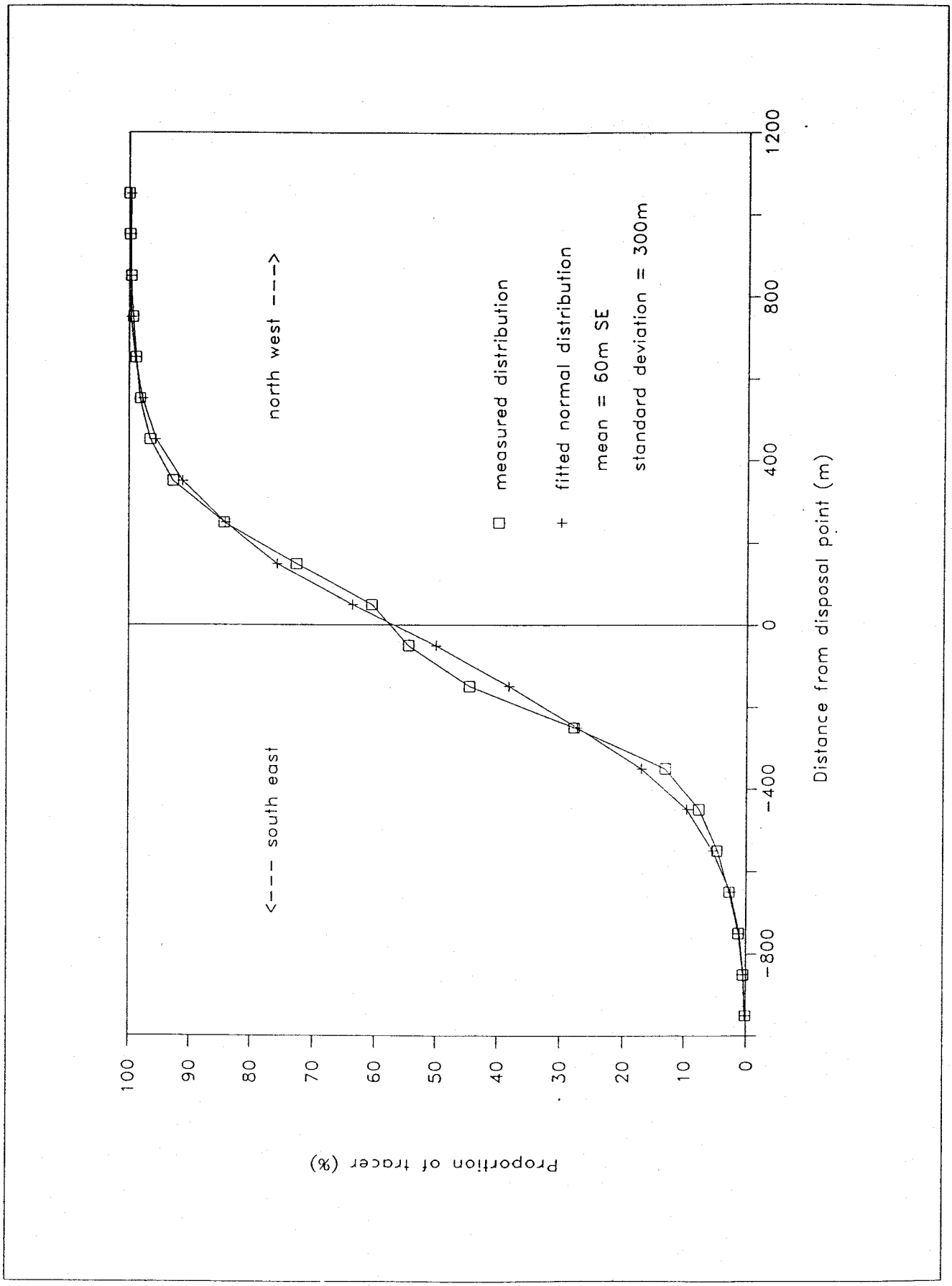

Fig 10 Initial distribution of tracer; cumulative mass against distance from disposal point

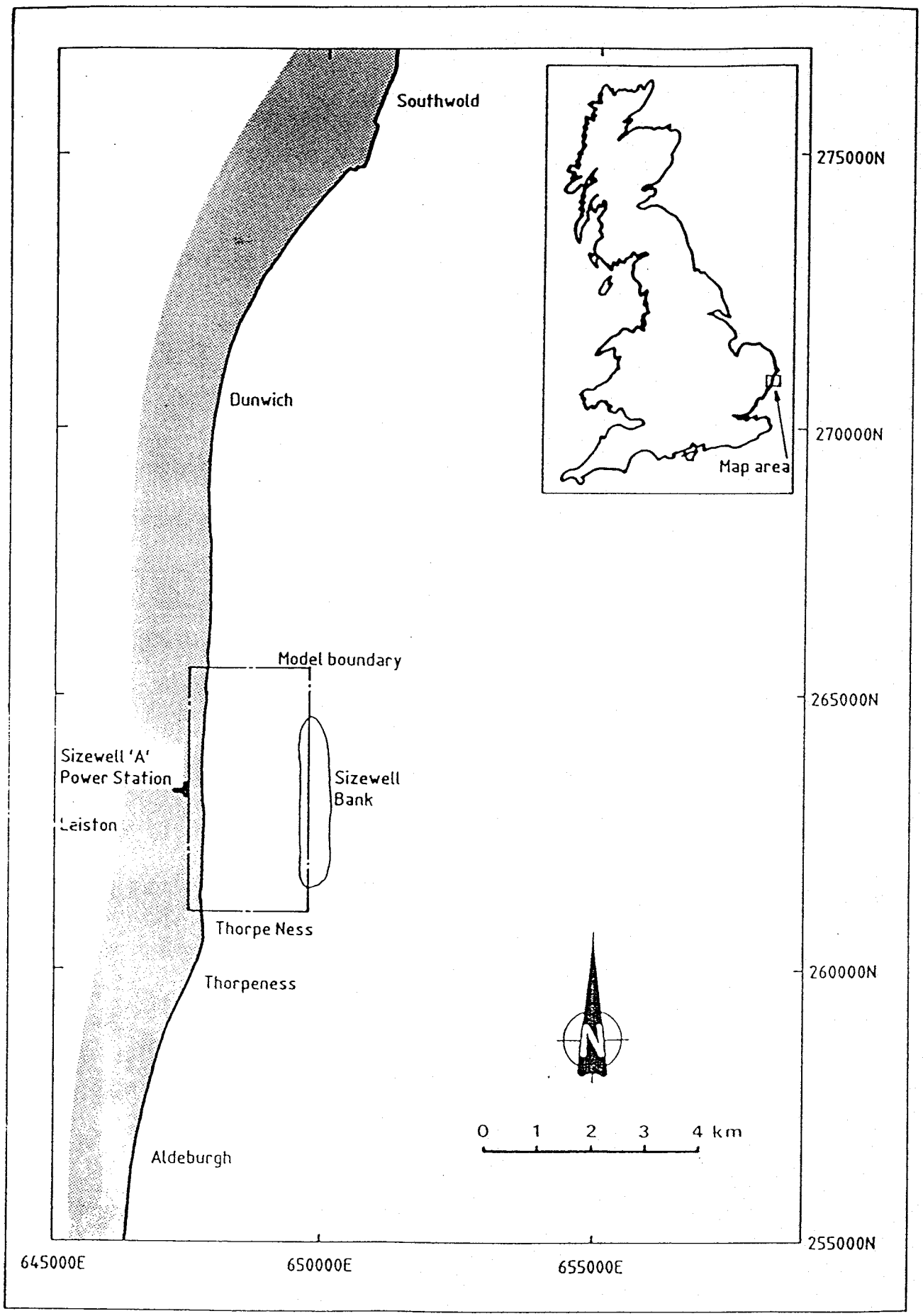

Fig 11 Location map of Sizewell flow and sediment transport models

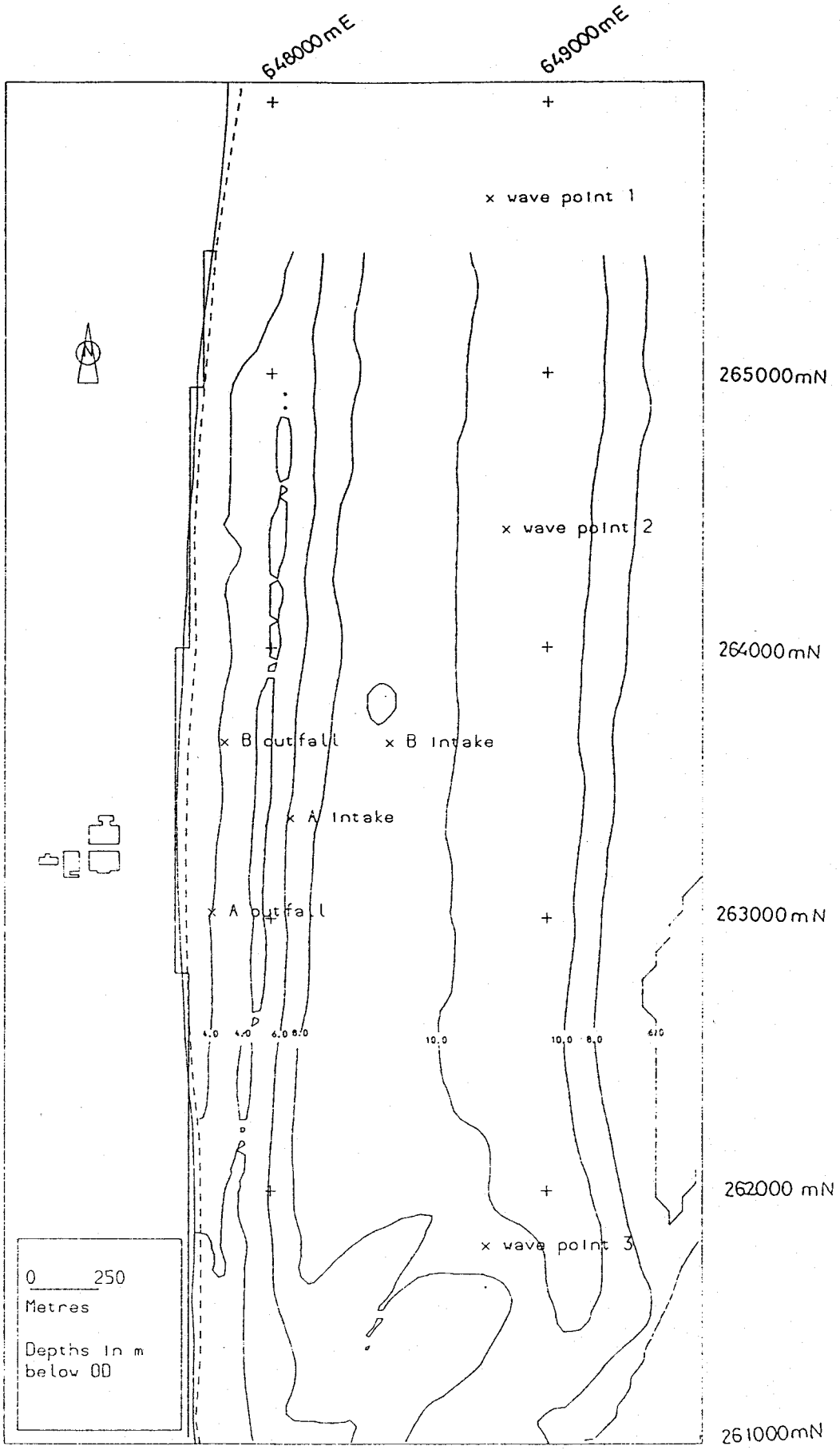

Fig 12 Sizewell model bathymetry

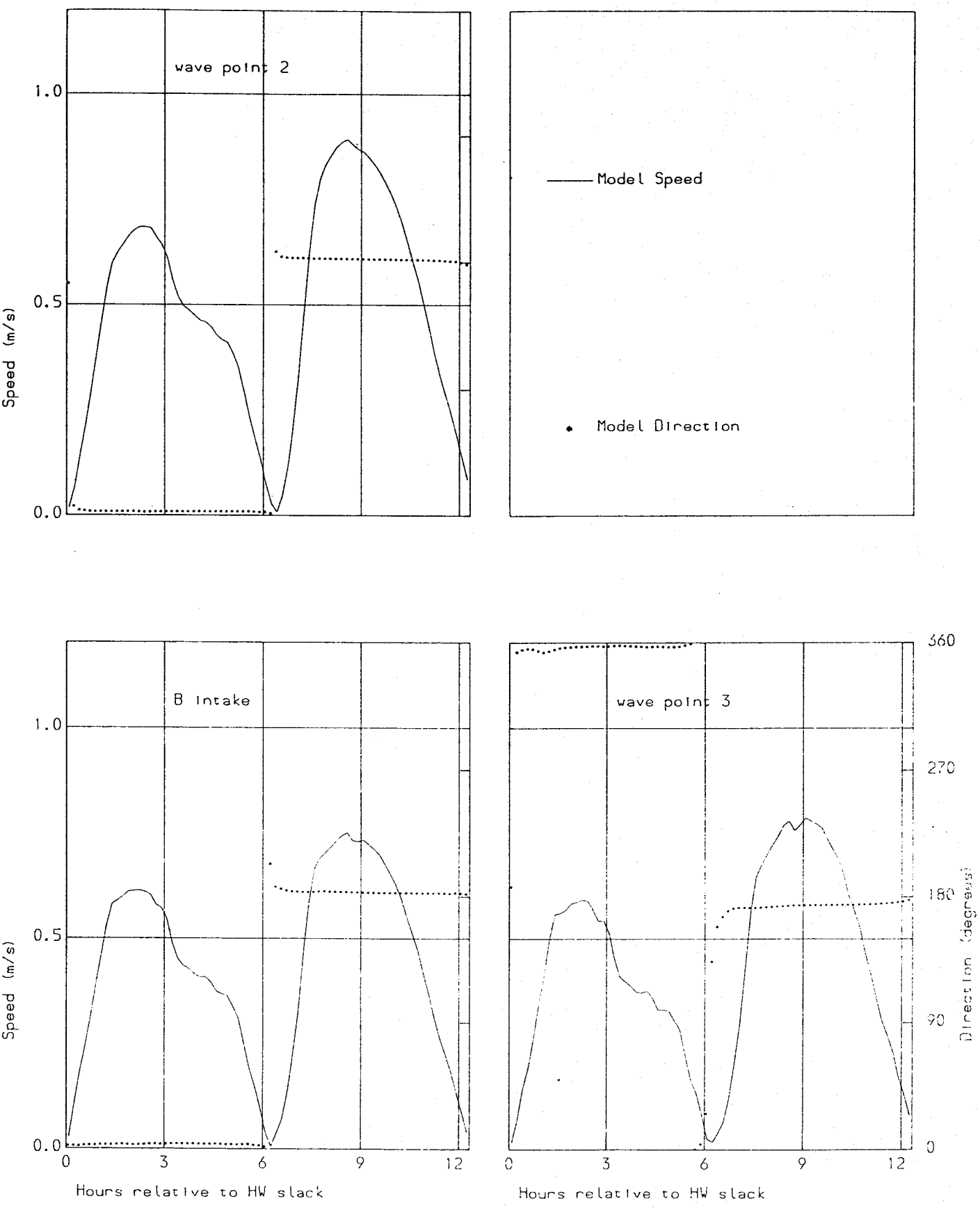

Fig 13 Spring tide currents

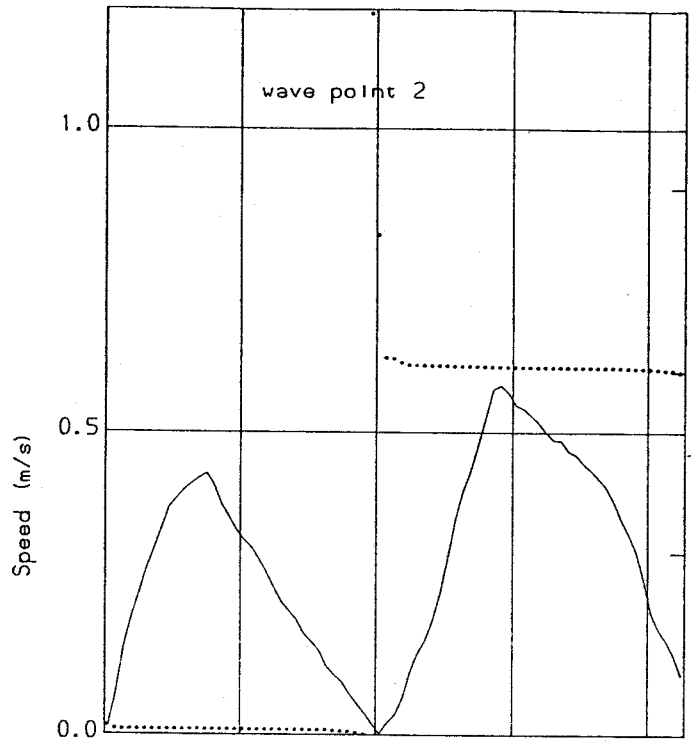

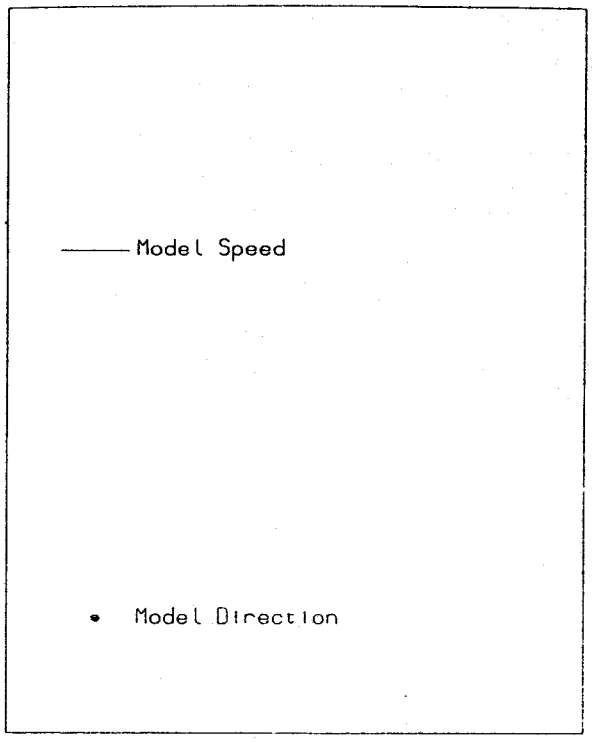

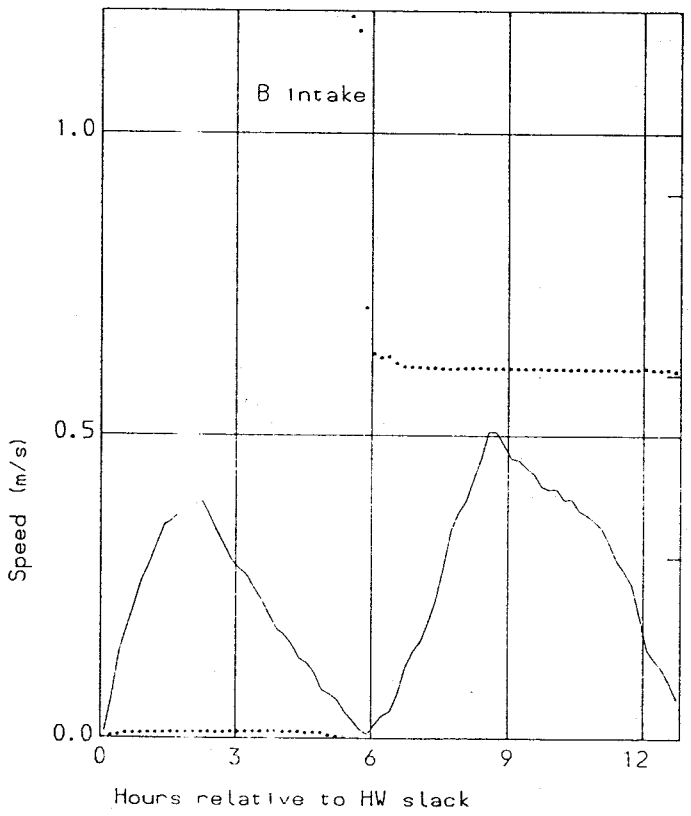

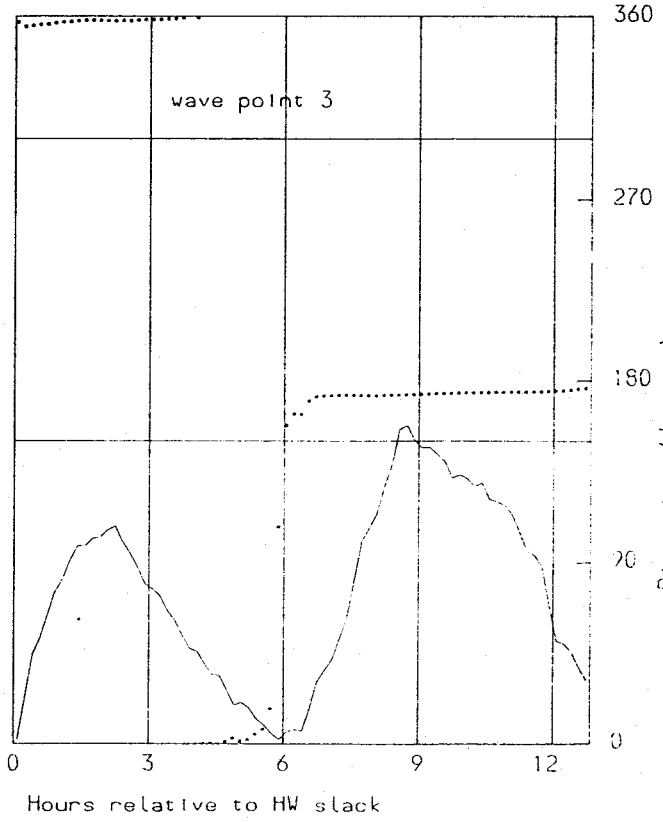

Fig 14 Neap tide currents

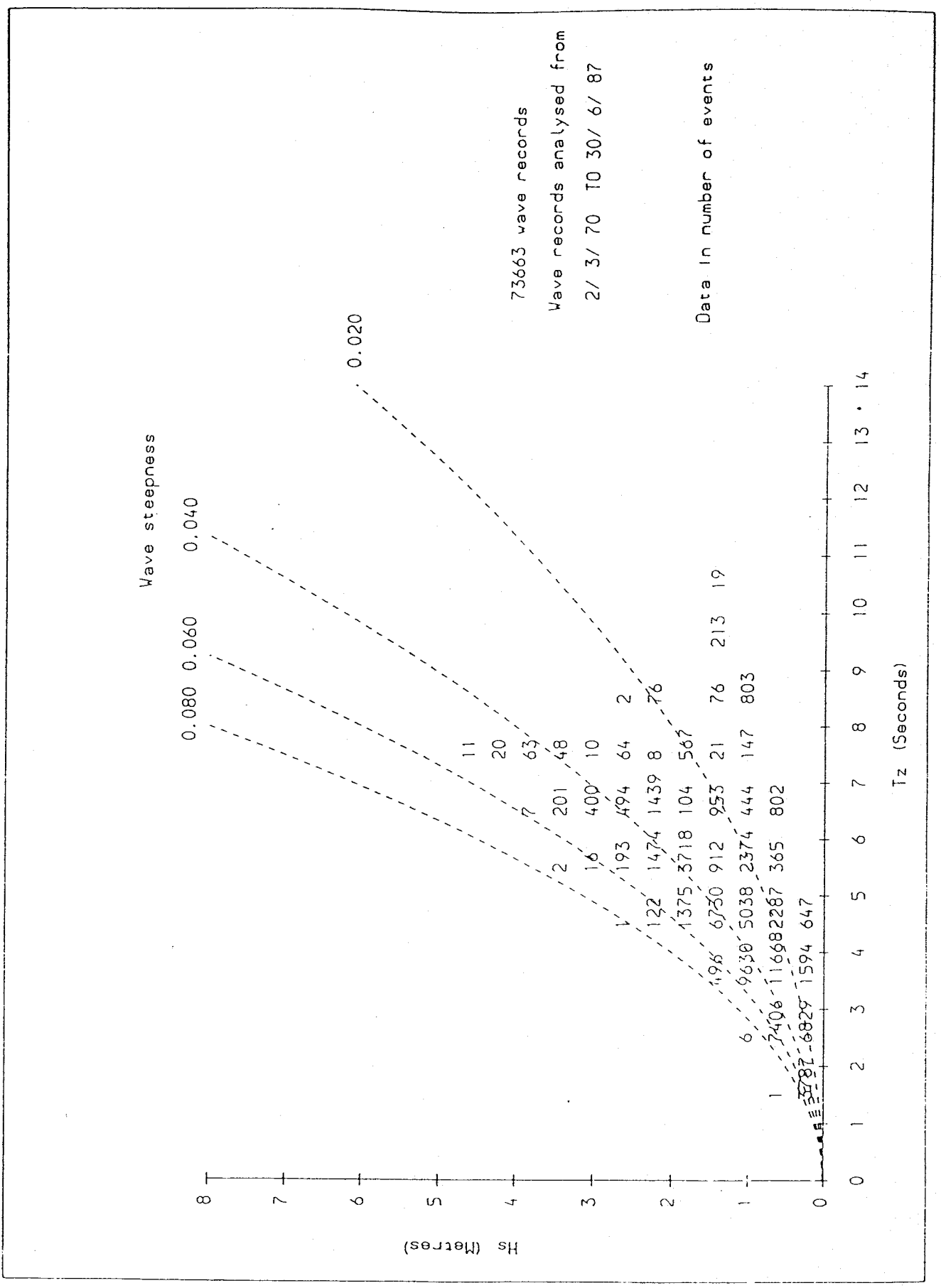

Fig 15 HsTz scatter plot for wave point 3

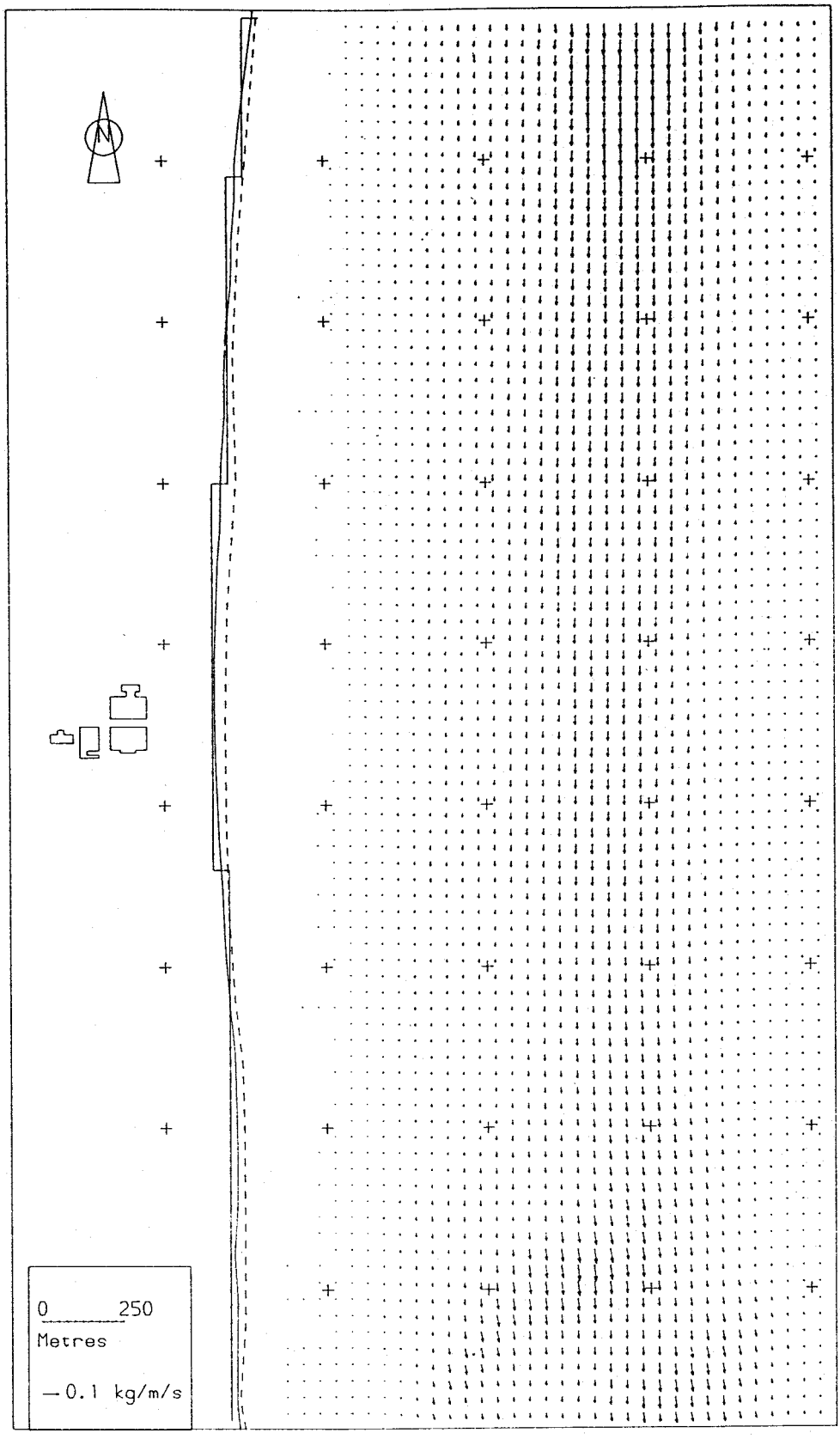

Fig 16 LTDISP net sediment transport vectors for a spring tide, no waves and Eqn 2 (van Rijn)

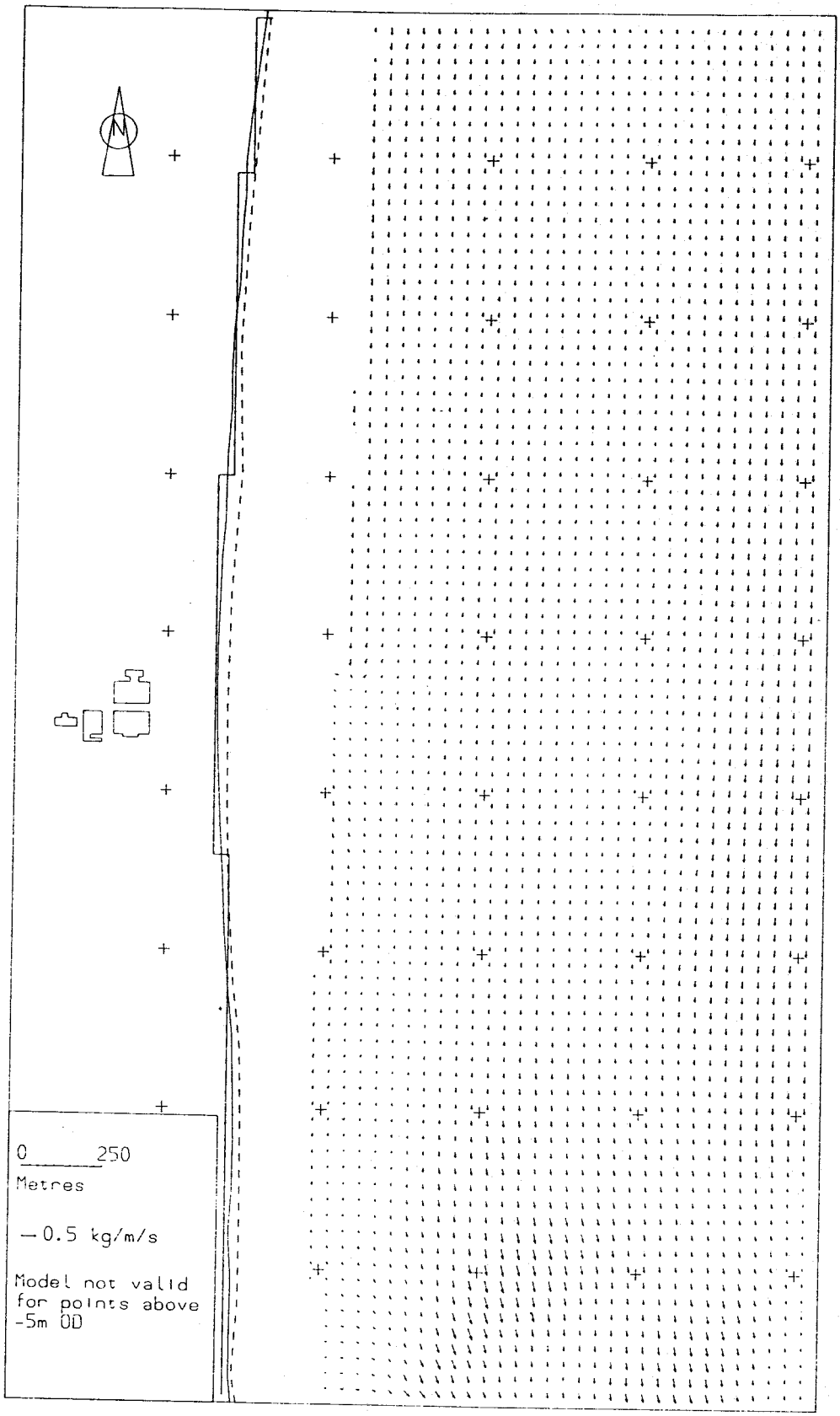

Fig 17 LTDISP net average tide sediment transport vectors for tides and waves and Eqn 3 (modified van Rijn)

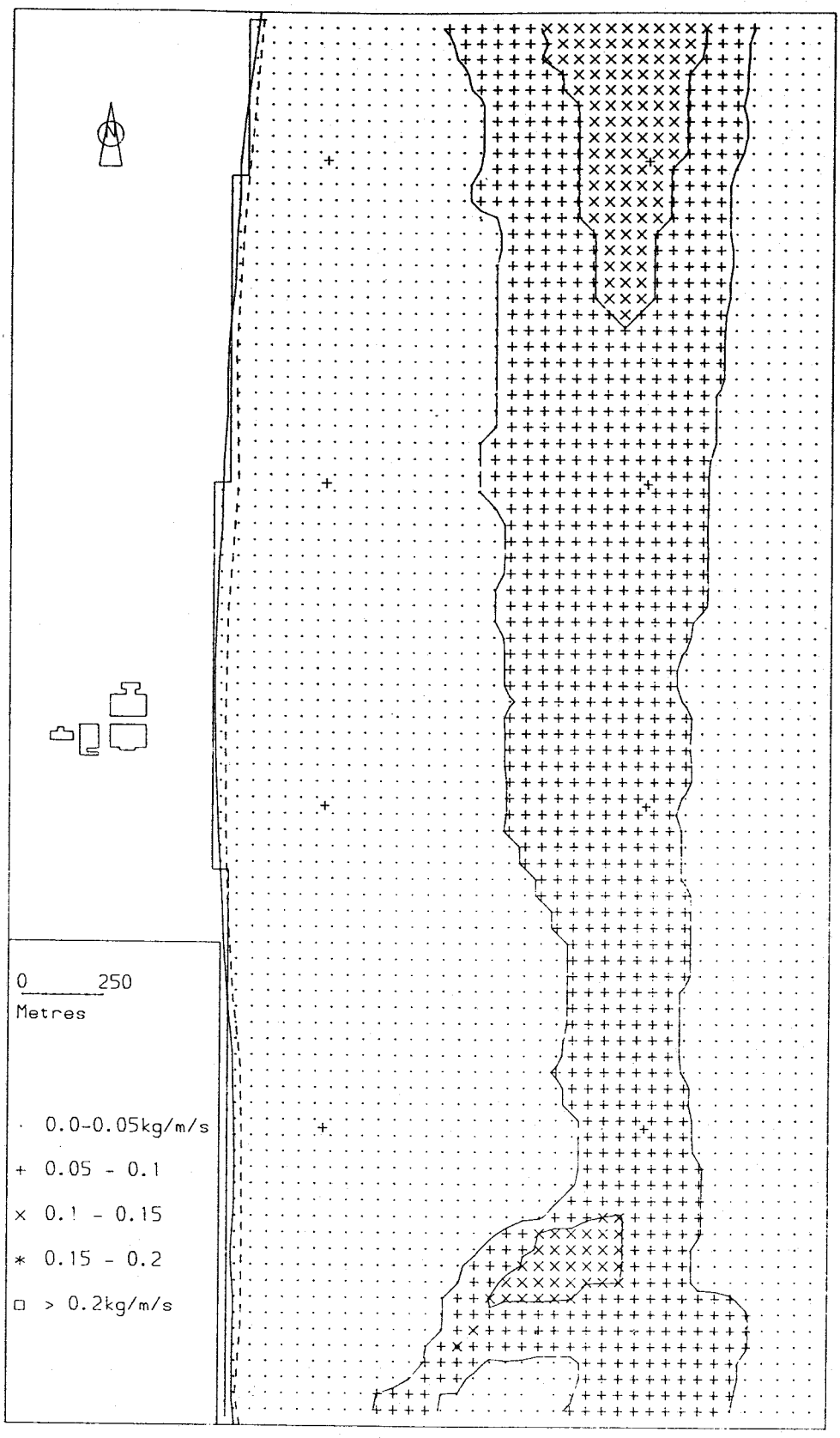

Fig 18 LTDISP average magnitude of hourly sediment transport vectors for a spring tide and Eqn 2 (van Rijn)

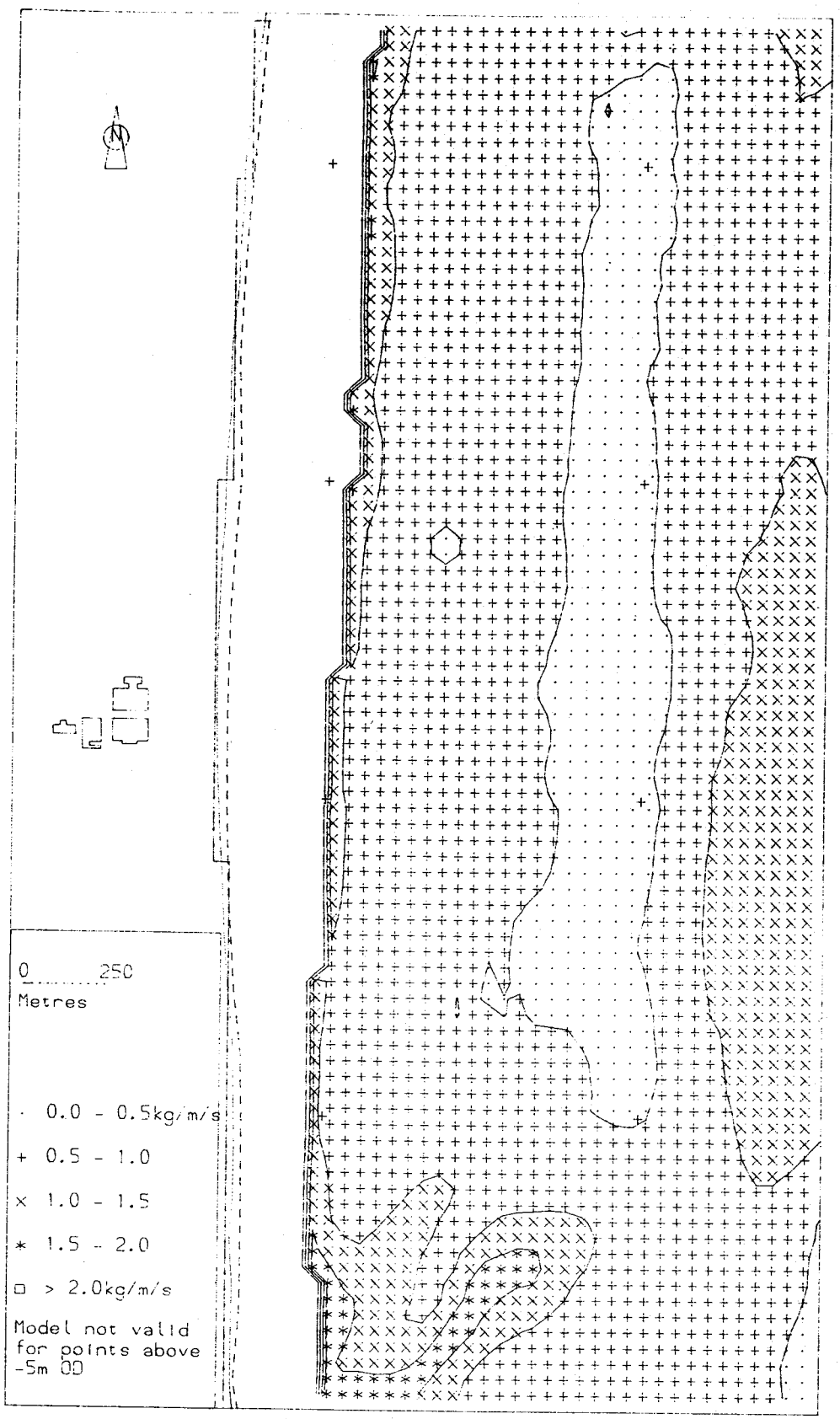

Fig 19 LTDISP average magnitude of hourly sediment transport vectors for tides and waves and Eqn 3 (modified van Rijn)

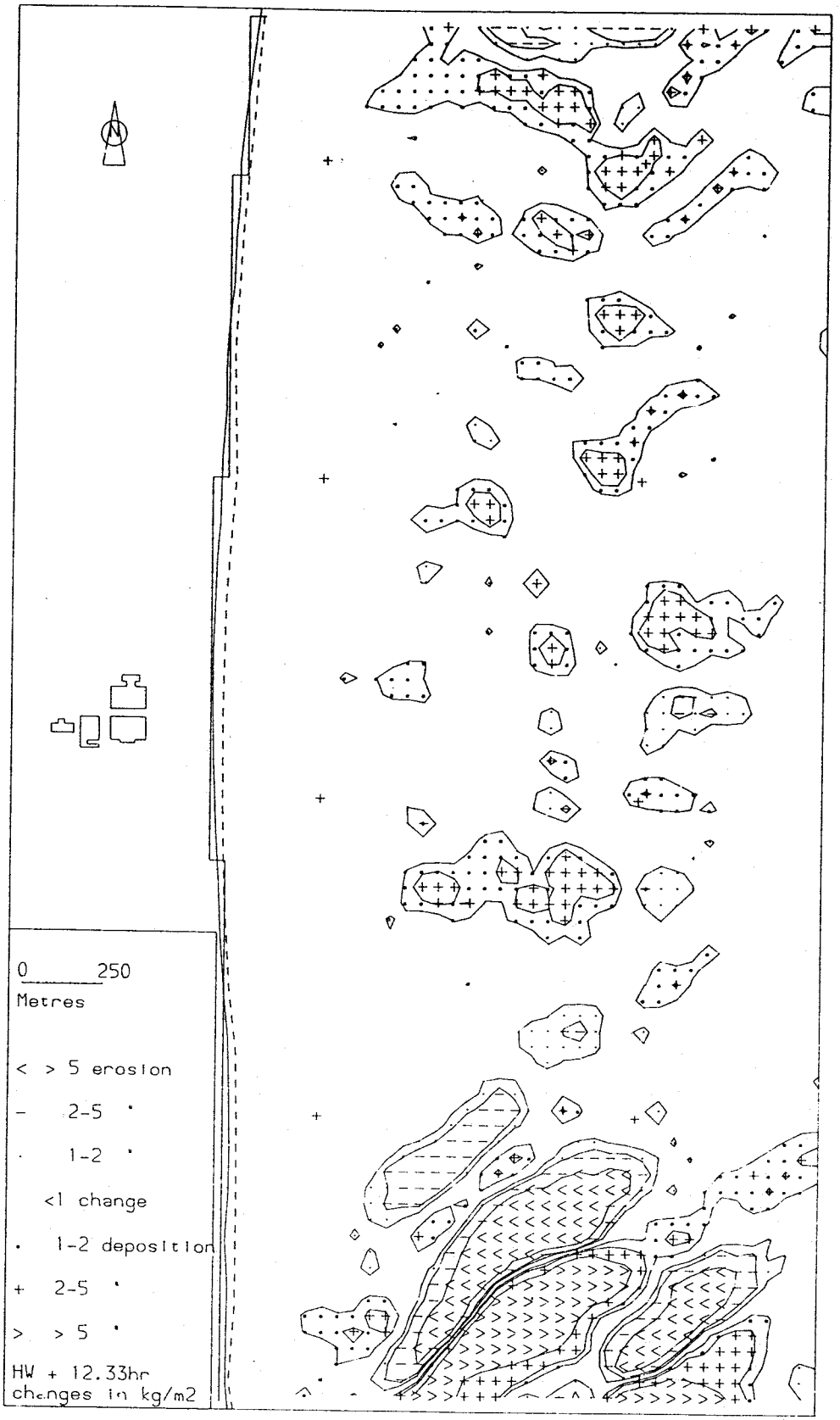

Fig 20 LTDISP changes in bed mass after one spring tide, no waves and Eqn 2 (van Rijn)

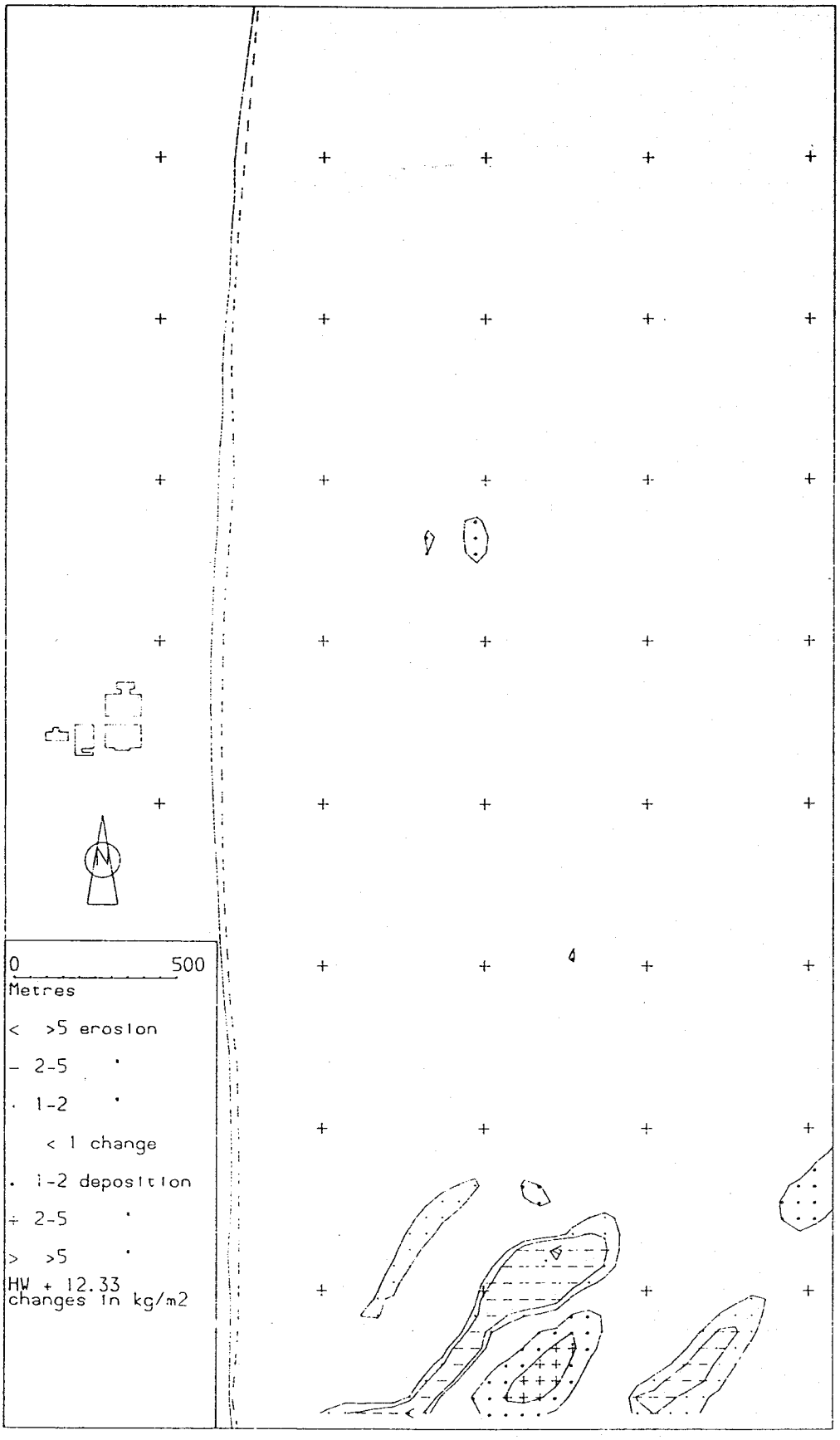

Fig 21 SANDFLOW changes in bed mass after one spring tide, no waves and Eqn 2 (van Rijn)

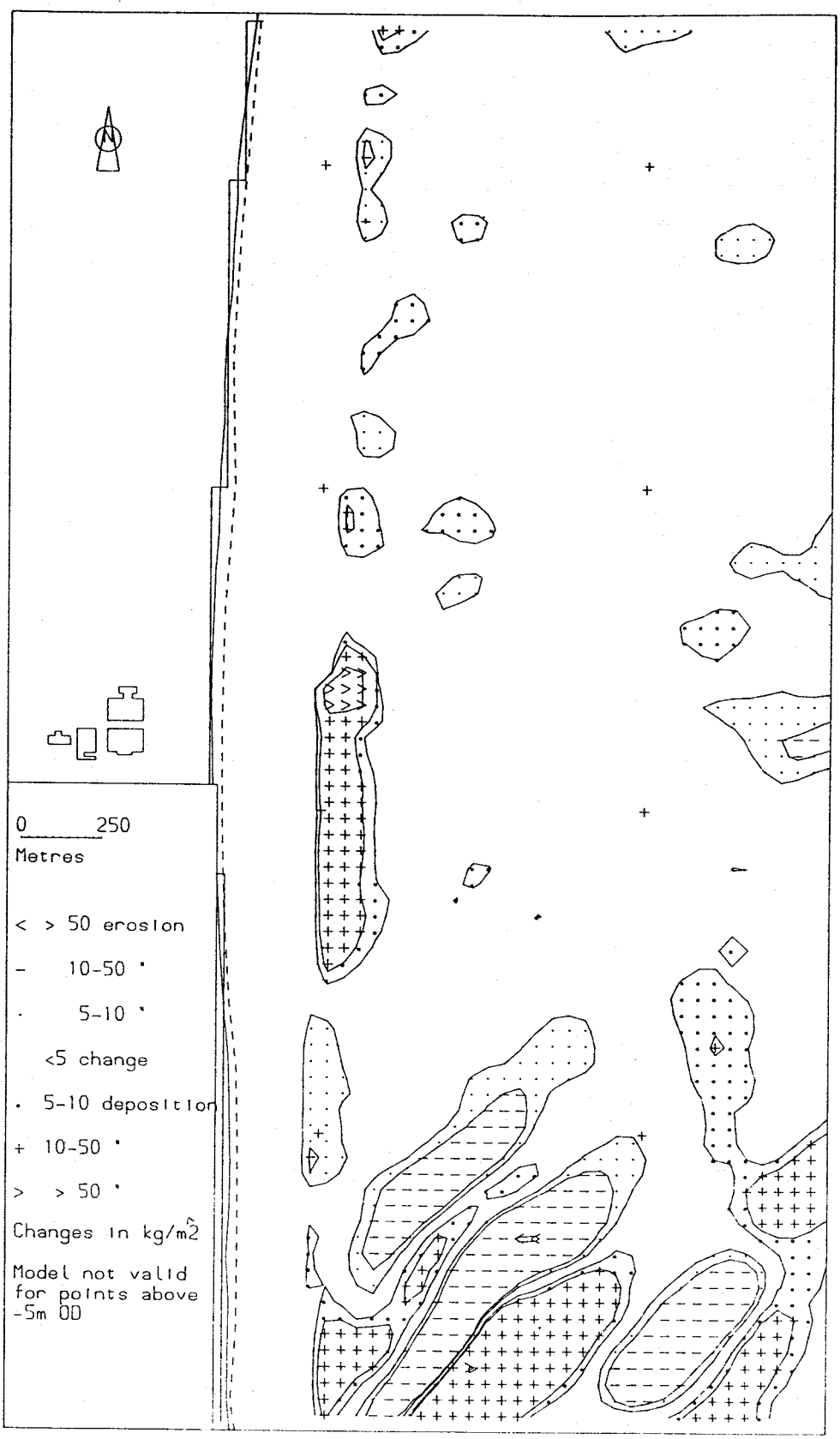

Fig 22 LTDISP net average tide changes in bed mass for tides and waves and Eqn 3 (modified van Rijn)

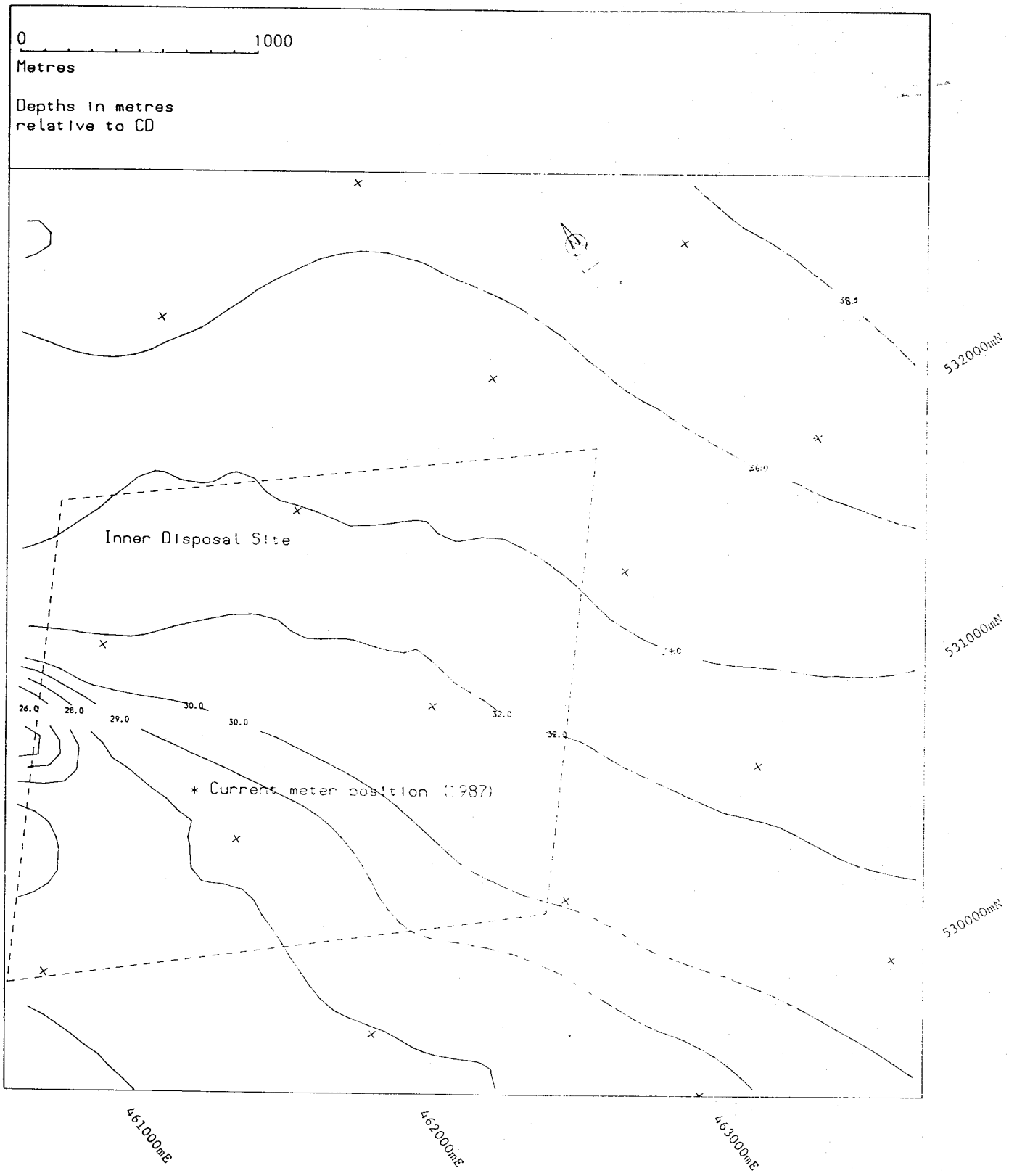

Fig 23 Bathymetry at the Tees Inner Disposal Site

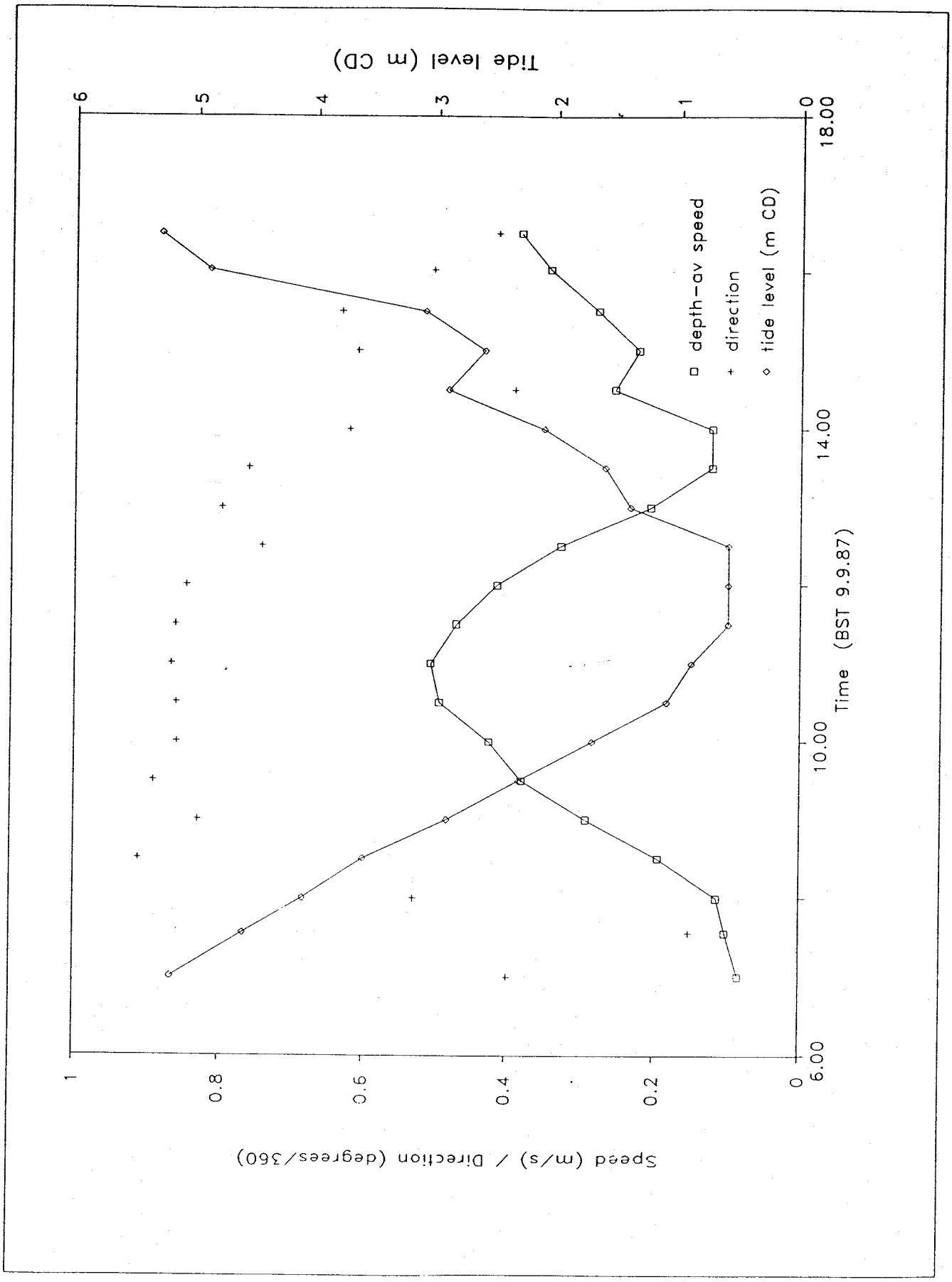

Fig 24 Field measurements of velocity and water level at the Tees Inner Disposal Site

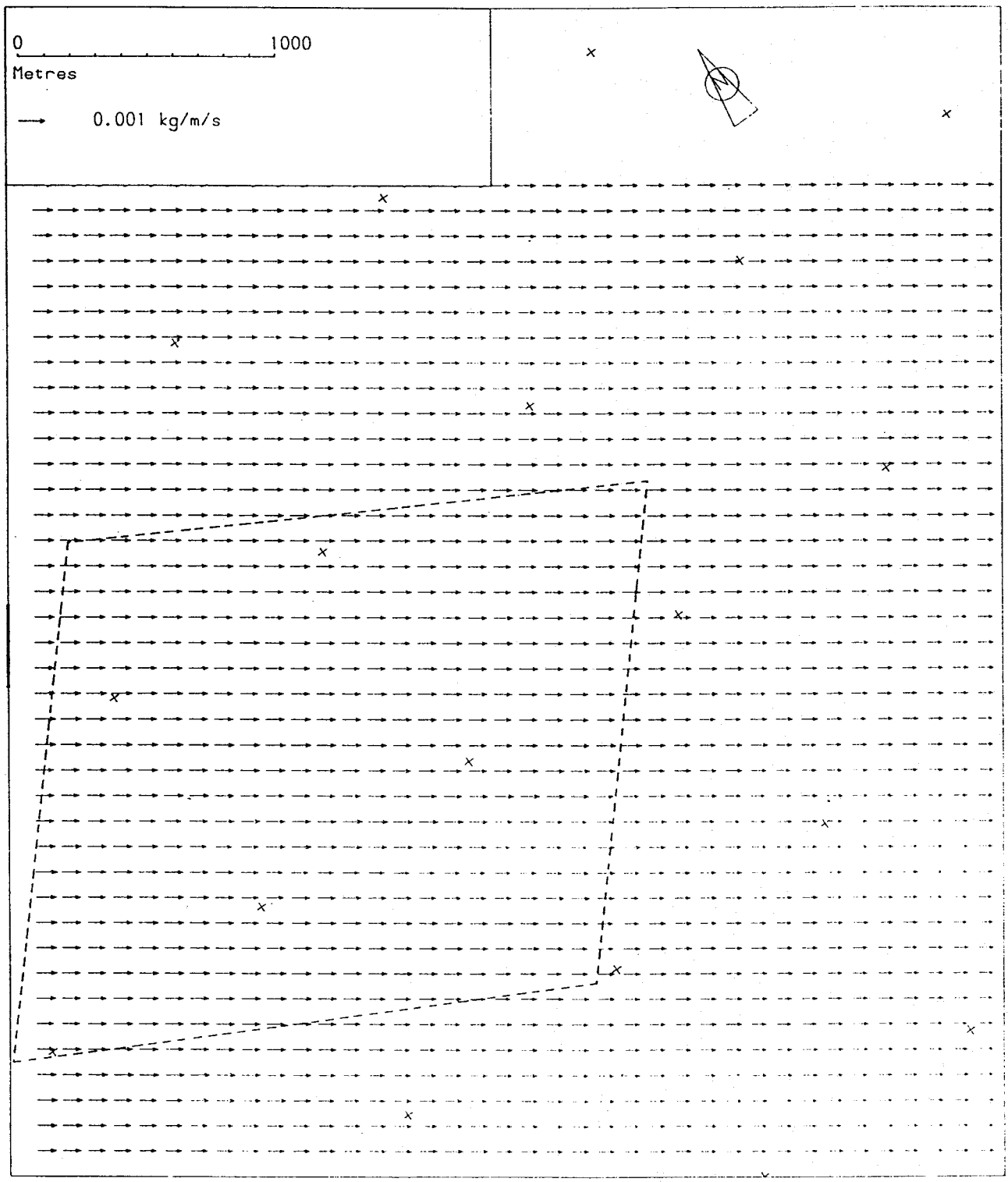

Fig 25 Tees: net sediment transport vectors from LTDISP

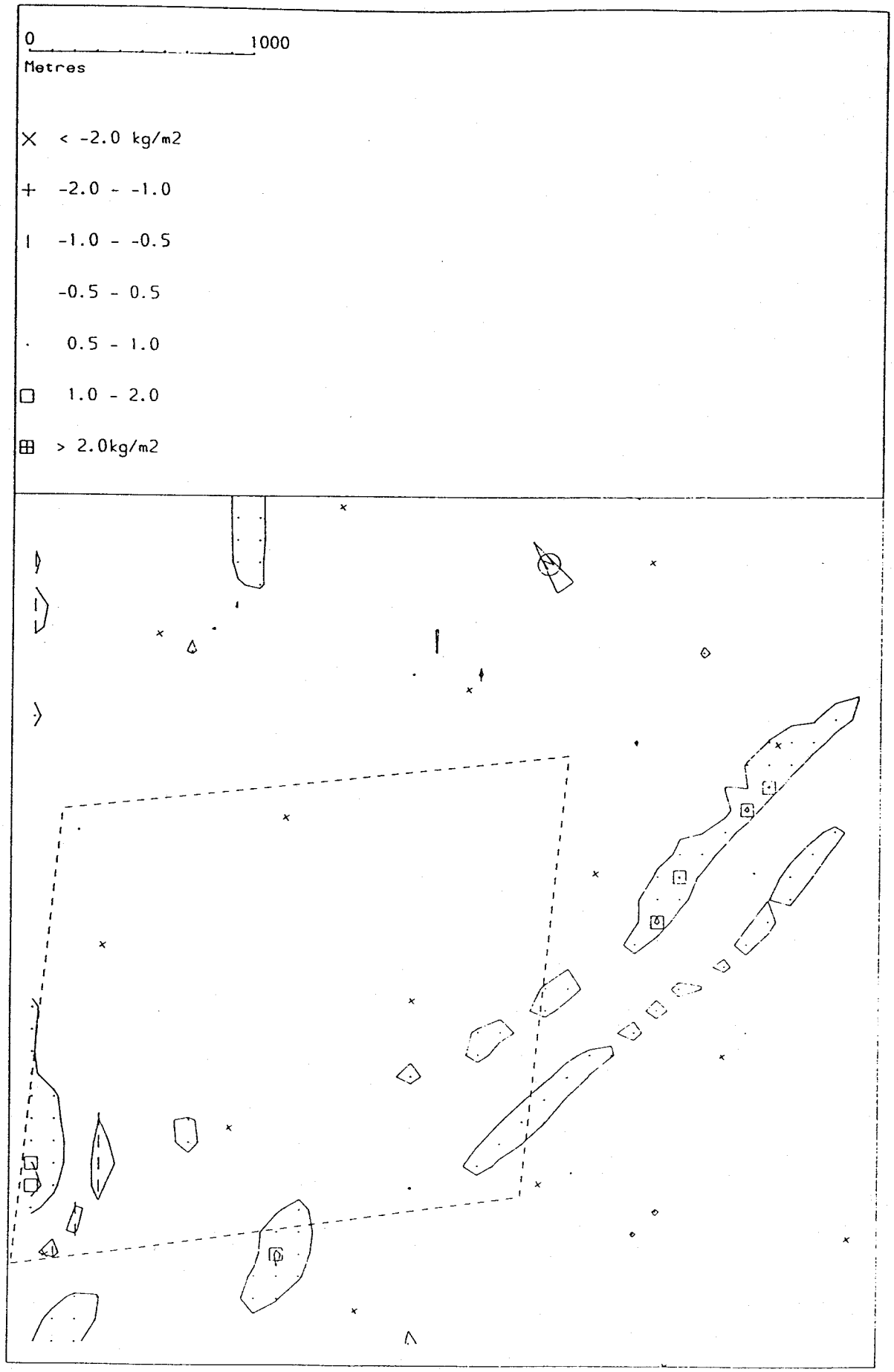

Fig 26 Tees: sand mass changes after four weeks

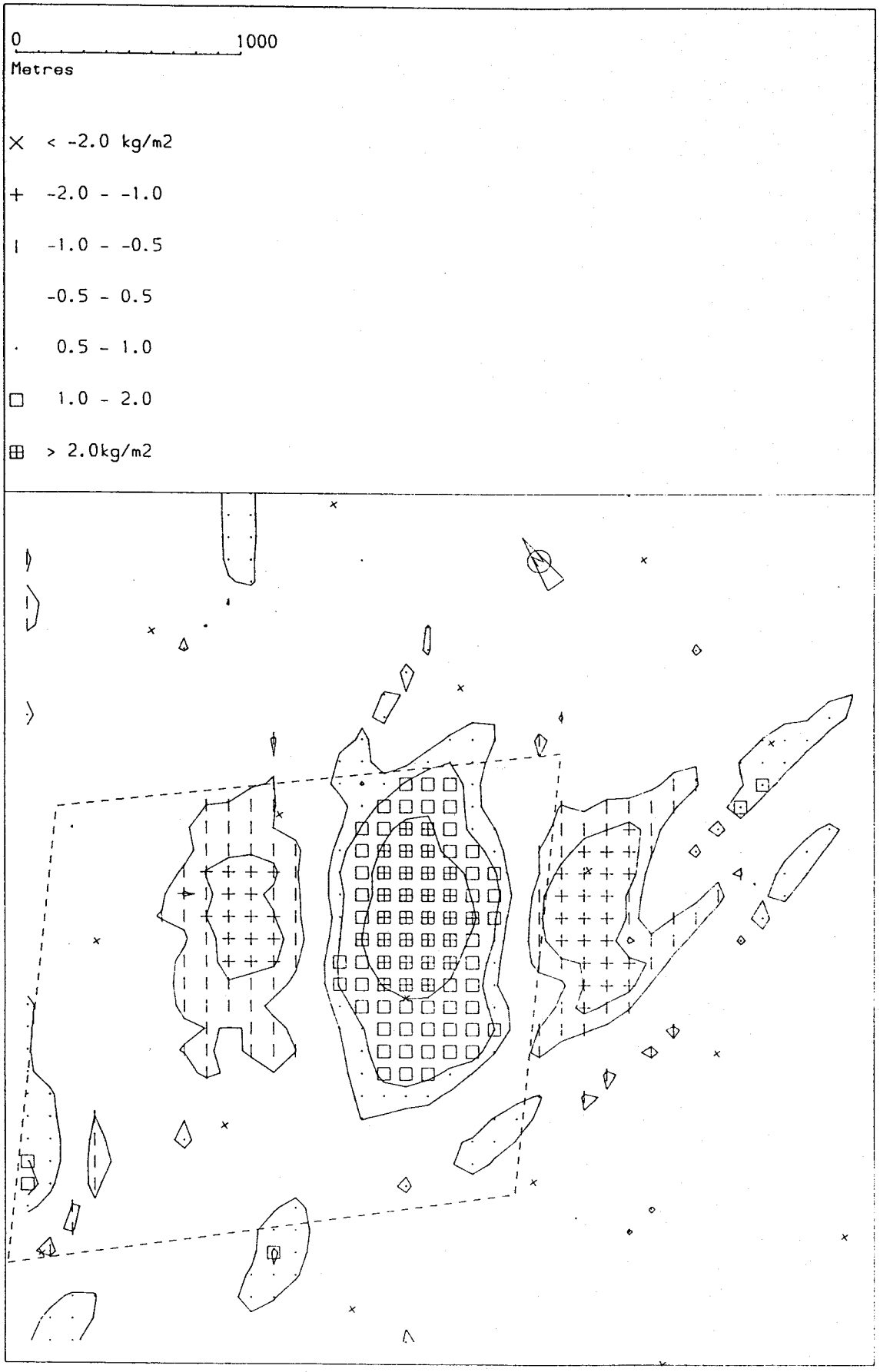

Fig 27 Tees: sand mass changes after four weeks, with continuous mud dumping

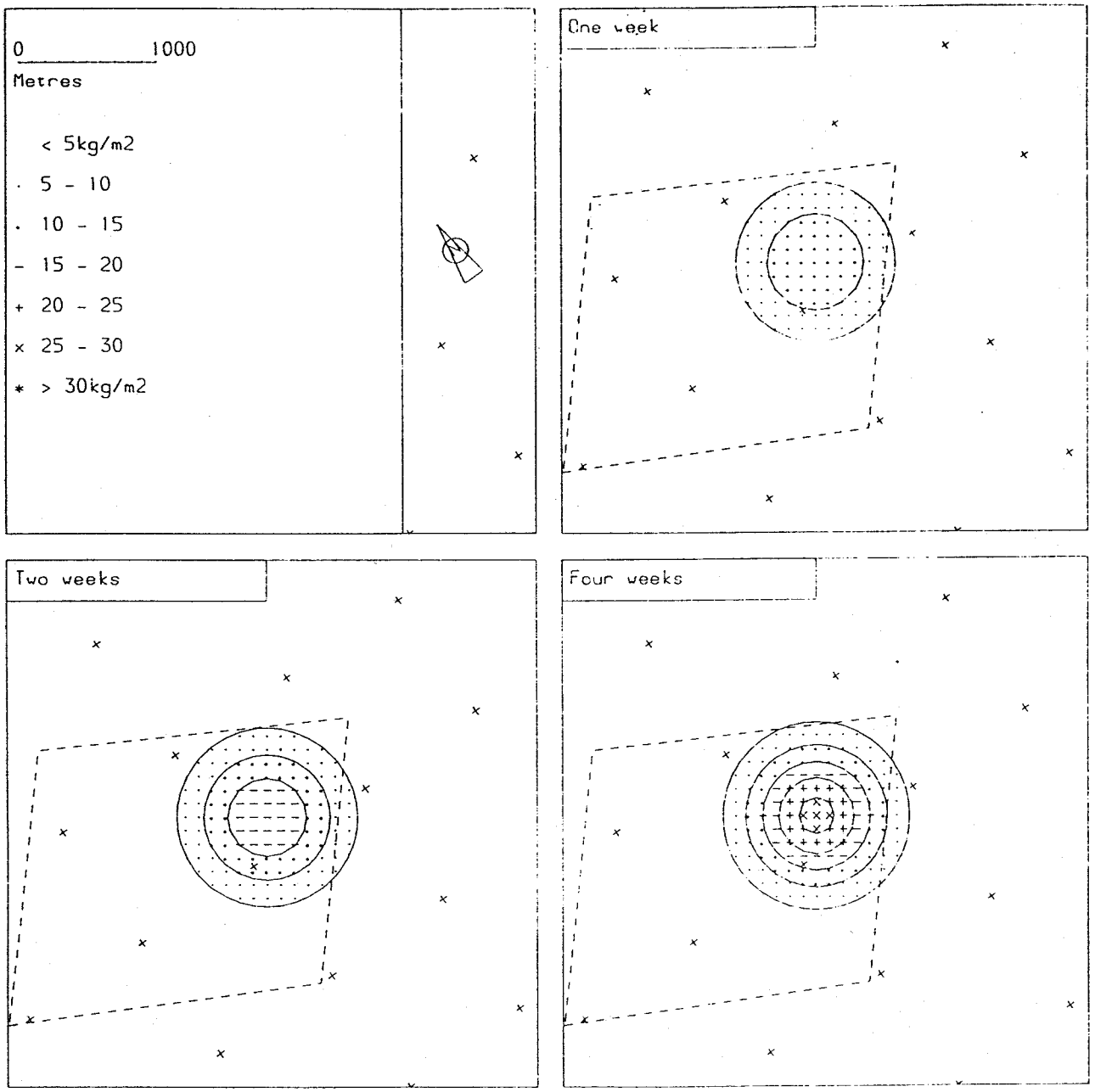

Fig 28 Tees: mud mass distribution during the first 4 weeks

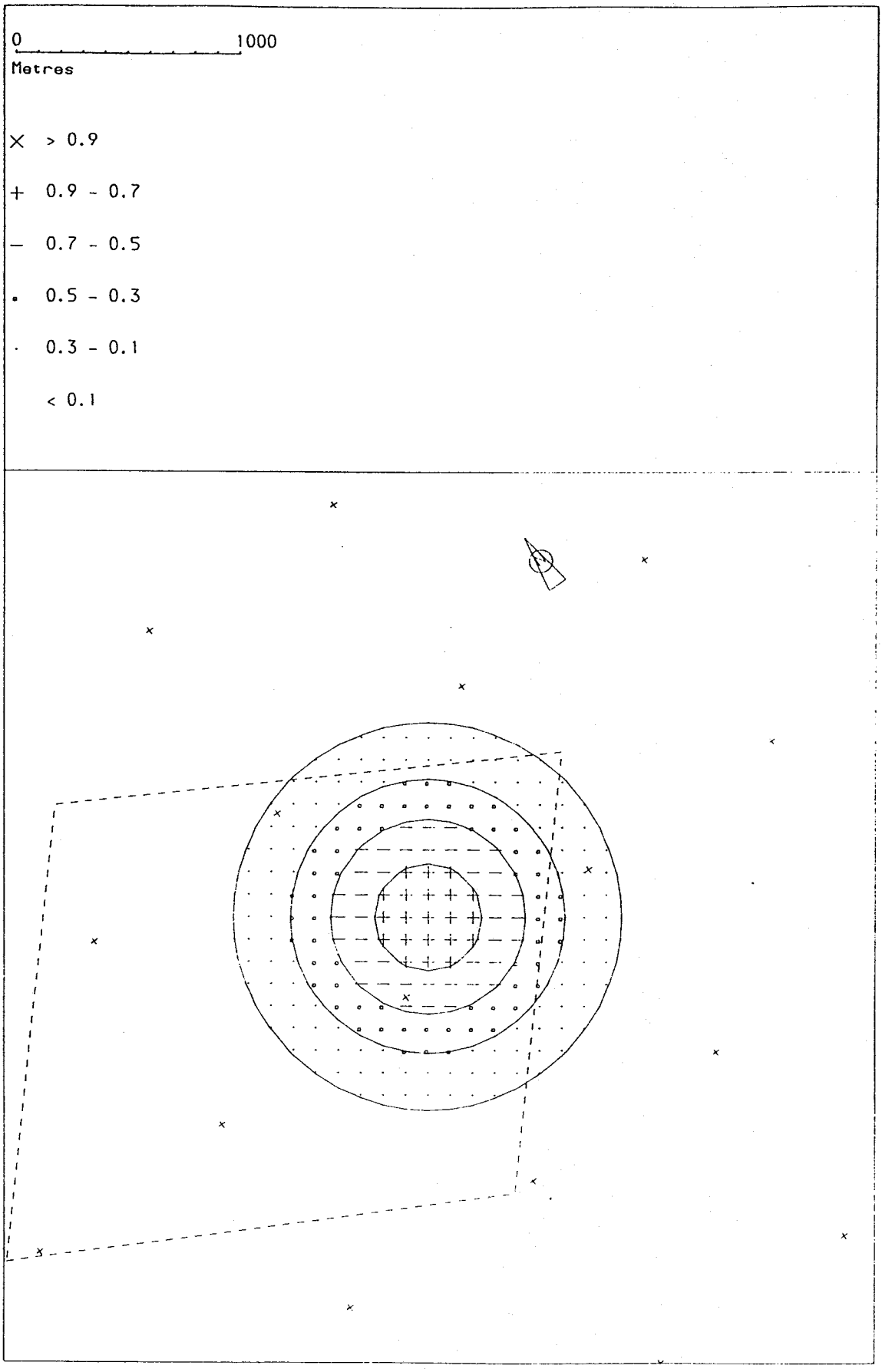

Fig 29 Tees: proportion of mud in the surface layer

APPENDICES

APPENDIX 1

Hydraulics Research
Wallingford

THE DEPOSITION OF DREDGED SPOIL AT THE TEES INNER DISPOSAL SITE

A study using a radioactive tracer

January 1989

Registered Office: Hydraulics Research Limited,
Wallingford, Oxfordshire OX10 8BA.
Telephone: 0491 35381. Telex: 848552

CONTENTS

scandium. The glass was ground and sieved in the laboratory to produce a tracer material in the silt and fine sand size ranges. A size analysis of the tracer material is shown in Fig. 2. This size distribution was fairly representative of the dredged material taken from the middle reaches of the Tees navigation channel. The behaviour of sediment in this size range is largely determined by the size of the flocculated groups of particles which are formed, rather than by the individual particle sizes. Mixing the tracer material in a large volume of the natural material ensures that the tracer particles become part of the natural flocculation process and therefore behave as the natural material.

Irradiation of the tracer was carried out in the Amersham International reactor at Harwell. The irradiation was designed to provide a total of 592 G Bq (16 Curies)* of the radioisotope Sc46 on 31 May 1988.

*Note. The Becquerel (Bq) is the SI unit of radioactivity. The Becquerel has superseded the previously used unit of radioactivity the Curie (CI).

1 Ci = 3.7×10^{10} Bq

3 FIELD EQUIPMENT

(a) Towed radiation detector

The HR survey vessel "Sir Claude Inglis" was used for all the bed tracking operations.

Two scintillation detectors were contained in a 1m long by 15cm diameter stainless steel tubular housing (Plate 1). The detector assembly was towed by a 100m long electro-mechanical cable which contained the

power and signal leads to the detectors. Because of the relatively deep water at the Tees disposal site, additional weight was required to ensure that the detector housing remained on the sea-bed at the normal towing speed of 1 to 2 m/s. This additional weight was provided by three 25cm diameter stainless steel wheels, each weighing 50 Kg. The total weight of the towed detector assembly was approximately 200 Kg.

The radiation detector assembly was towed from the stern of the "Sir Claude Inglis" and incorporated a safety release system. The release system was so designed that if the detector assembly became snagged on a sea-bed obstruction a "weak-link" on the towing vessel would break and allow the towing cable to run freely over the stern of the vessel. A watertight junction box at the upper end of the towing cable had a marker buoy permanently attached and this was used in detector recovery operations.

Two radiation detectors were incorporated in the underwater housing, one a high-sensitivity device for measurements outside the injection "hot spot", and the other a low-sensitivity unit which enabled measurements to be made in the immediate injection area without overloading the recording instrumentation. The outputs from the two radiation detectors were fed into a dual-channel digital counter/timer unit on board the survey vessel. The outputs from the two counter units were recorded on a digital printer unit. Also displayed on the printer roll was a manual fix number which was updated at regular intervals and related to simultaneous measurements of the vessel's position.

(b) Position Fixing

The tracking vessel's position was determined using a Motorola Miniranger III range-range position fixing system. Use was made of the THPA permanent Motorola chain which gave good coverage in the survey area.

4 BED BACKGROUND SURVEY

Prior to the introduction of the radioactive tracer material it was necessary to carry out a comprehensive background survey of the sea-bed in the experimental area. The tracer injection and initial survey were originally planned for June 1988. The background measurements were due to be completed in May 1988.

The initial background measurements were carried out on 23 and 24 May 1988. During the course of these measurements numerous snags were encountered on the sea-bed and the safety release system operated on many occasions. The subsequent recovery operations inevitably prolonged the background survey. In addition, the detector system suffered considerable damage. Water leakage into the detector housing curtailed measurements on 23 May. A spare detector system was utilised on 24 May. The cable on this spare system was damaged before completion of the background survey. Because of these initial problems it was necessary to return to Wallingford to carry out repairs to the detector systems.

Further background measurements were made on 6 and 7 June 1988. Again progress was slow because of numerous snags and further damage was suffered by the two detector systems. Adequate background coverage was completed on 7 June. By this time both detector systems were badly damaged and inoperative. Because of the extent of the equipment damage it was

necessary to postpone the injection of the tracer material until August 1988 in order that repairs could be made.

Background measurements obtained were generally between 50 and 100 counts per second and remained fairly uniform over large areas of the sea-bed. It was found that most of the detector snagging occurred around the nearshore limit of the spoil ground where it was assumed that there was a rock outcrop. It was decided therefore to inject the radioactive tracer at or near the offshore limit of the spoil ground in the hope that subsequent movement of the tracer would obviate the need to track in the rocky area.

5 DETECTOR CALIBRATION

In order to quantify the field tracer measurements it was necessary to calibrate the field detectors using a standardised radioactive source. A calibration source was made by mixing a standardised quantity of scandium glass tracer material with a fine sand. This tracer/sand mixture was spread in a 1cm thick layer using a plywood mould. The calibration source was then overlain by a 3mm thick perspex sheet which was screwed to the plywood base forming a sealed source of area 1.6m by 0.7m.

The initial source activity was approximately 1.85 M Bq (50 Ci)* per m^2. The detector was placed on the surface of the calibration source under 50cm of water.

The detector response to an "infinite" layer of 1cm thickness was found to be 4,700 pulses per second from a source of 1 MBq/m^2 or 174 pulses per second per μ Ci/m^2.

6 INJECTION AND INITIAL DEPOSITION OF TRACER

All tracer injections were carried out from the THPA suction dredger "Hoertnesse". To eliminate tidal bias on the initial tracer dispersion, three separate tracer injections were performed. The three seeded spoil cargoes were deposited at the spoil ground at various tidal states during the spring tide period 12-13 August 1988. The three deposits were made at mid-tide in ebb and flood directions and at low water slack. The locations of the three deposits are shown in Fig.3. The actual times of deposit are given in Table 1.

The hopper material for each tracer injection was taken from the middle reaches of the Tees navigation channel during routine dredging operations.

The tracer seeding operations were carried out with the vessel at the deposit site; this procedure eliminated the risk of tracer material leaking from the hopper during passage to the deposit site. The tracer material was irradiated in 20 standard aluminium 'A' cans. Each 'A' can contained 40g of the scandium glass tracer. The irradiation produced a total of 592 GBq (16 Ci) on 31 May 1988. As previously mentioned the tracer injection was delayed until 12/13 August 1988. The tracer had by that time decayed to 320 GBq (8.6 Ci). Each 'A' can therefore contained 16 GBq of scandium 46 tracer.

To seed each of the three hopper loads of spoil the following procedure was adopted: 4m long p.v.c. tubes, each sealed at the lower end with a rubber bung, were lowered into the hopper so that the lower end was at about mid-depth in the spoil. The upper end of each p.v.c. tube was attached to the guard rail

around the hopper. Seven similar tubes were distributed around the hopper. Individual 'A' cans were dropped into the p.v.c. tubes and rested on the rubber bung at the bottom of the tube. The combined effect of distance and absorption by the surrounding spoil reduced the dose level at deck level to just above the normal background. About one hour before the required injection time 500ml of a 75% hydrochloric acid solution was poured into each p.v.c. tube in order to dissolve the aluminium 'A' can. The scandium glass released into the base of the tube was unaffected by the acid. In order to dispense the scandium glass tracer from each p.v.c. tube a water pump was connected at the top end. The pressure generated in the tube forced the bung from the lower end and water was flushed through the tube to eject the tracer into the spoil and to flush the residue from the tube. As soon as all tracer was seeded into the spoil the dredger opened the bottom doors of the hopper to discharge the cargo. The individual deposition sites are shown in Fig. 3.

Weather conditions throughout the two day injection period were good with light winds and a calm sea.

7 INITIAL TRACER SURVEY AND RESULTS

Immediately after the tracer injection, the wind strength increased and a moderate swell built up which prevented tracking operations on the following two days, 14 and 15 August. Sea conditions had moderated by 16 August and the initial bed survey was carried out on that day. Although tracking operations were slowed down by a number of snags, the initial survey was completed in the one day.

A plot showing the initial tracer distribution is shown in Fig. 3. Iso-activity contours have been drawn on this figure to show the areal spread of the tracer (and hence the discharged spoil).

Planimetric determination of the contoured areas showed the tracer spread over an area of approximately $1.7 \times 10^6 m^2$. The major axis of the deposit, which was aligned with the current direction, was approximately 2.5km long and the maximum width of the deposit was about 1km.

The areas bounded by the individual contours were measured and a computation carried out to determine the quantity of tracer within each contoured area. Assuming that the tracer was spread as a thin surface layer, the total quantity of tracer detected was 305 GBq (8.2 Ci). This quantity represented about 95% of the initial 320 GBq (8.6 Ci).

Further analysis was carried out on the tracer results to determine the longitudinal distribution of the tracer deposit. The quantities of tracer within 100m-wide bands, drawn normal to the dominant current direction, were determined. The results are shown as a histogram in Fig.4 where the distribution indicates the flood direction and ebb direction movements from the approximate location of the initial deposits.

The longitudinal distribution is shown also as a cumulative recovery plot in Fig.5, with zero taken as the north-western extent of the tracer deposit and the cumulative tracer recovery plotted in 100m intervals as far as the limits of detection to the south-east. The initial tracer deposit shows no evidence of any tidal direction bias.

During the course of this initial survey major damage was suffered by one of the towed detection systems. The rear tubular watertight housing, containing two radiation detectors, was torn from the probe and lost - leaving only the nosecone assembly and towing cable. The survey was completed using the spare detection system.

8 SURVEY MEASUREMENTS AFTER ONE WEEK

There was insufficient time to obtain spares and carry out the major repairs on the damaged equipment before the next planned bed survey, one week after tracer injection. Measurements were attempted therefore using the spare detection system.

Bad weather delayed the start of this survey until 22 August i.e. some 10 days after injection.

Very little survey data was obtained before the detector again became snagged. On this occasion, the main towing cable became detached from the towing clamp/release system. This resulted in the detector and towing cable being released to the sea-bed with no surface marker buoy! Fortunately the position of the lost equipment was known precisely. Recovery operations, using divers, were successful. The divers reported, however, that the sea-bed in the area, which was near the northern boundary of the disposal ground, was littered with large boulders up to 2m in diameter! Upon recovery, the detector system was found to be inoperative and no further measurements were possible.

9 CONCLUSIONS

The unexpectedly rough sea-bed conditions in the general area of the Tees disposal ground led to severe operational problems throughout the field measurement period. As a consequence, the amount of field data collected was far less than had been hoped for. Clearly, the roughness of the sea-bed terrain precludes the use of the Tees disposal ground for further experiments of this nature.

The results obtained were limited to the period immediately after the initial spoil deposition. The analysis of these results does give useful information relating to the initial deposition process.

TABLE

TABLE 1 - TRACER DEPOSITION TIMES

DATE	TIME OF HIGH WATER (GMT)	TIME OF TRACER DEPOSITION (GMT)
12 August 1988	1555	1715
13 August 1988	0359	1056
13 August 1988	1627	1414

FIGURES

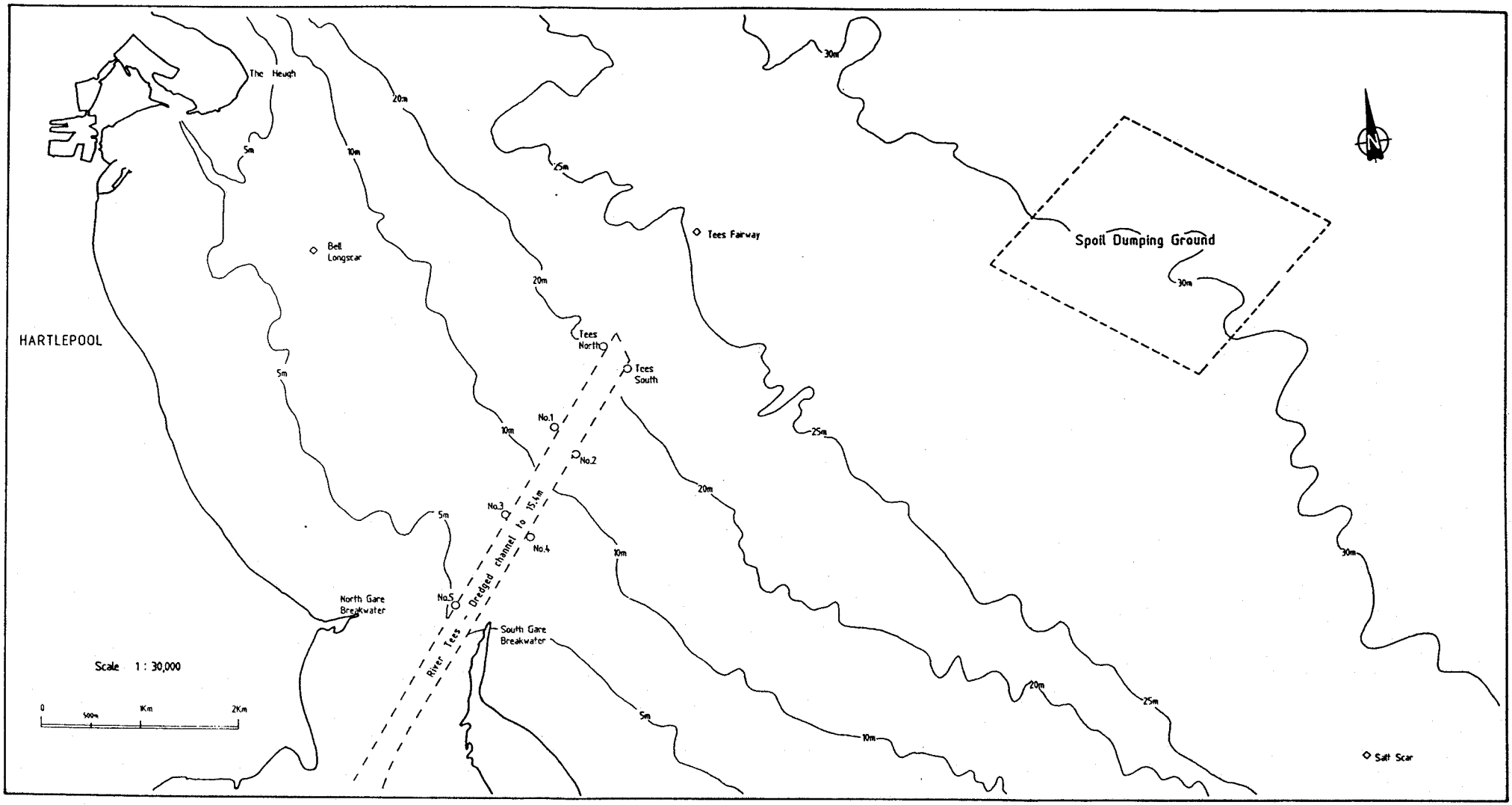

Spoil Ground Location

FIG. 1

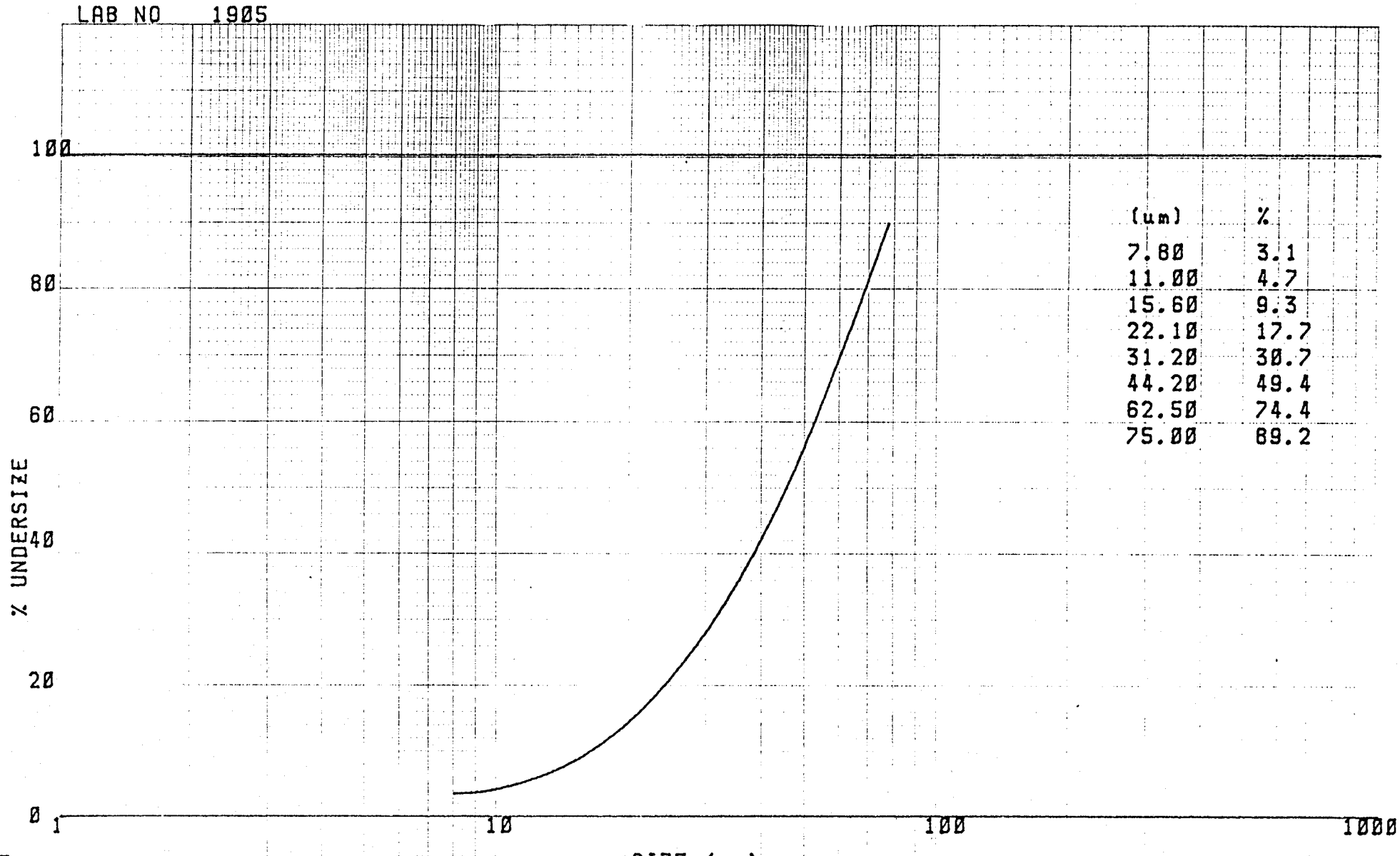

FIG. 2

SIZE DISTRIBUTION OF SCANDIUM GLASS TRACER

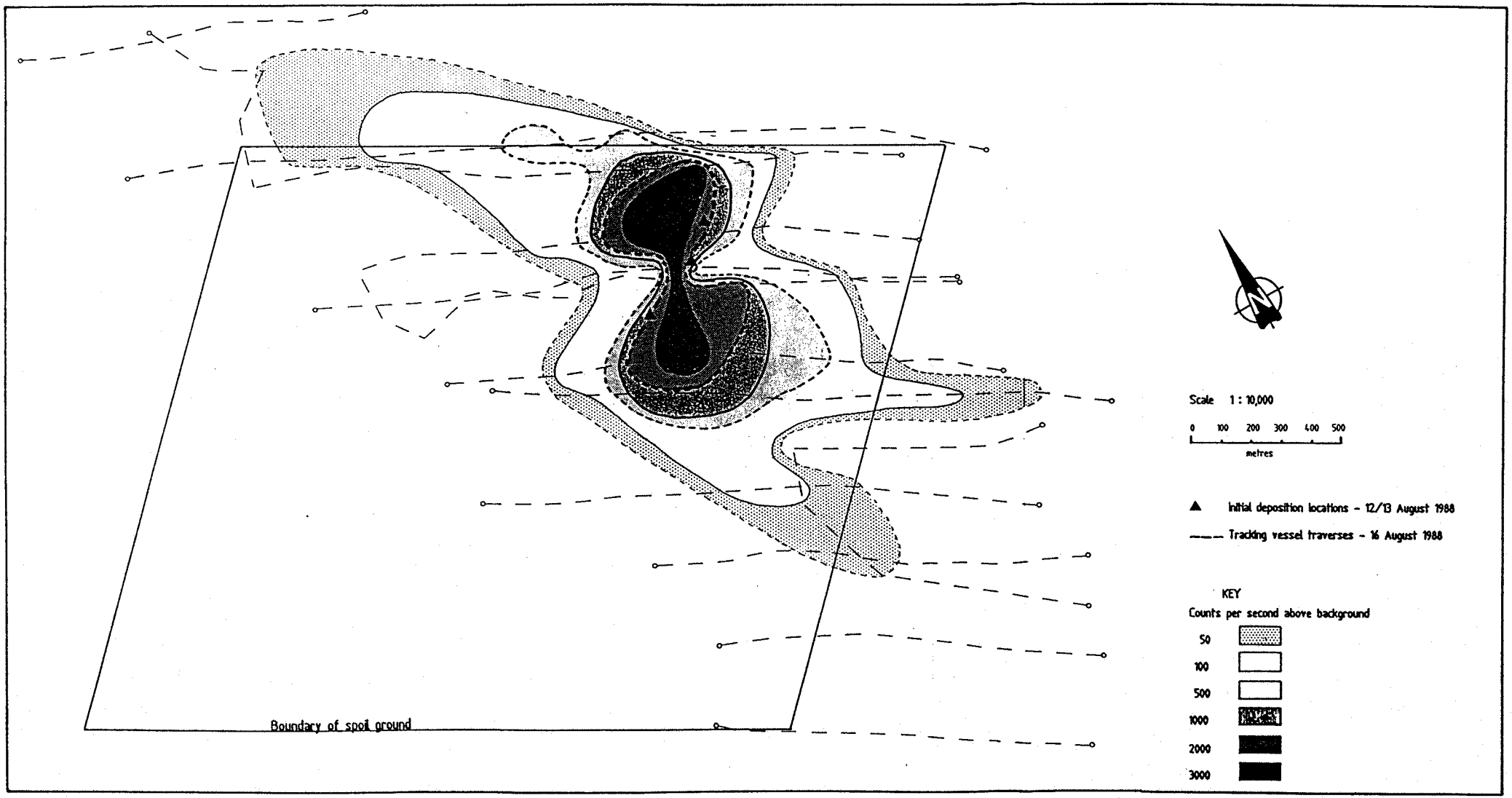

Tracer distribution 3/4 days after deposition FIG. 3

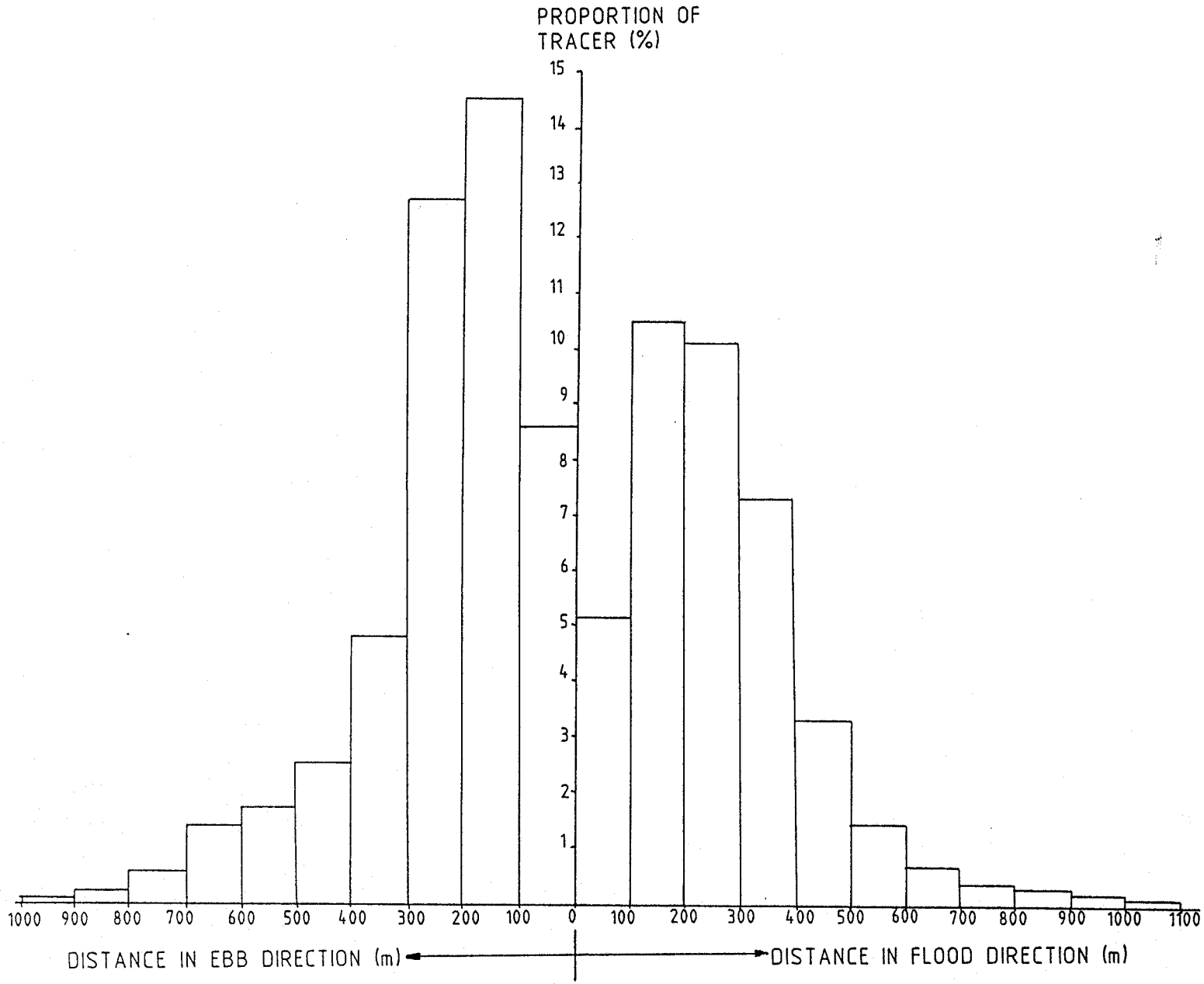

FIG. 4

INITIAL DISTRIBUTION OF TRACER IN FLOOD AND EBB TIDE DIRECTIONS

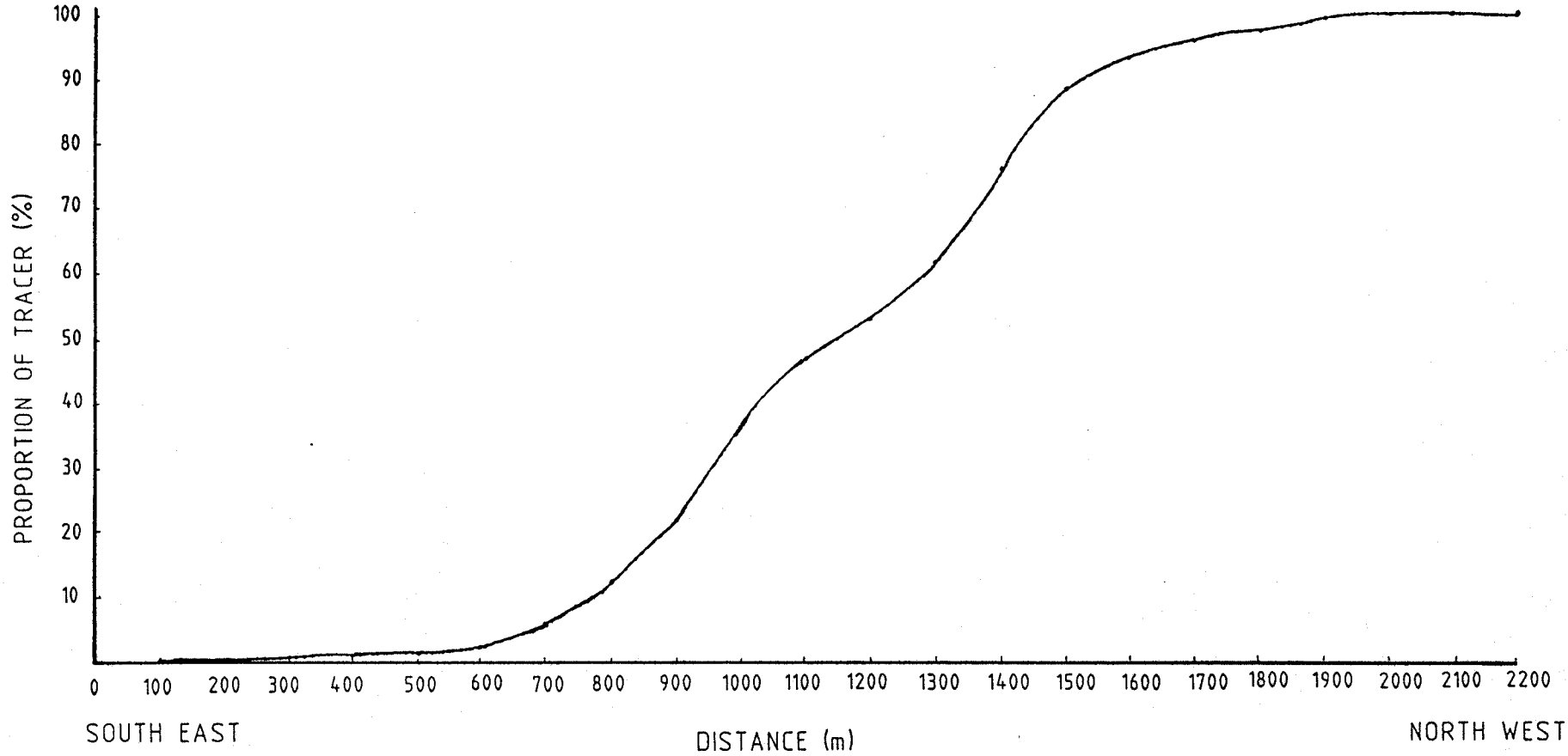

FIG. 5

INITIAL LONGITUDINAL DISTRIBUTION OF TRACER

PLATE

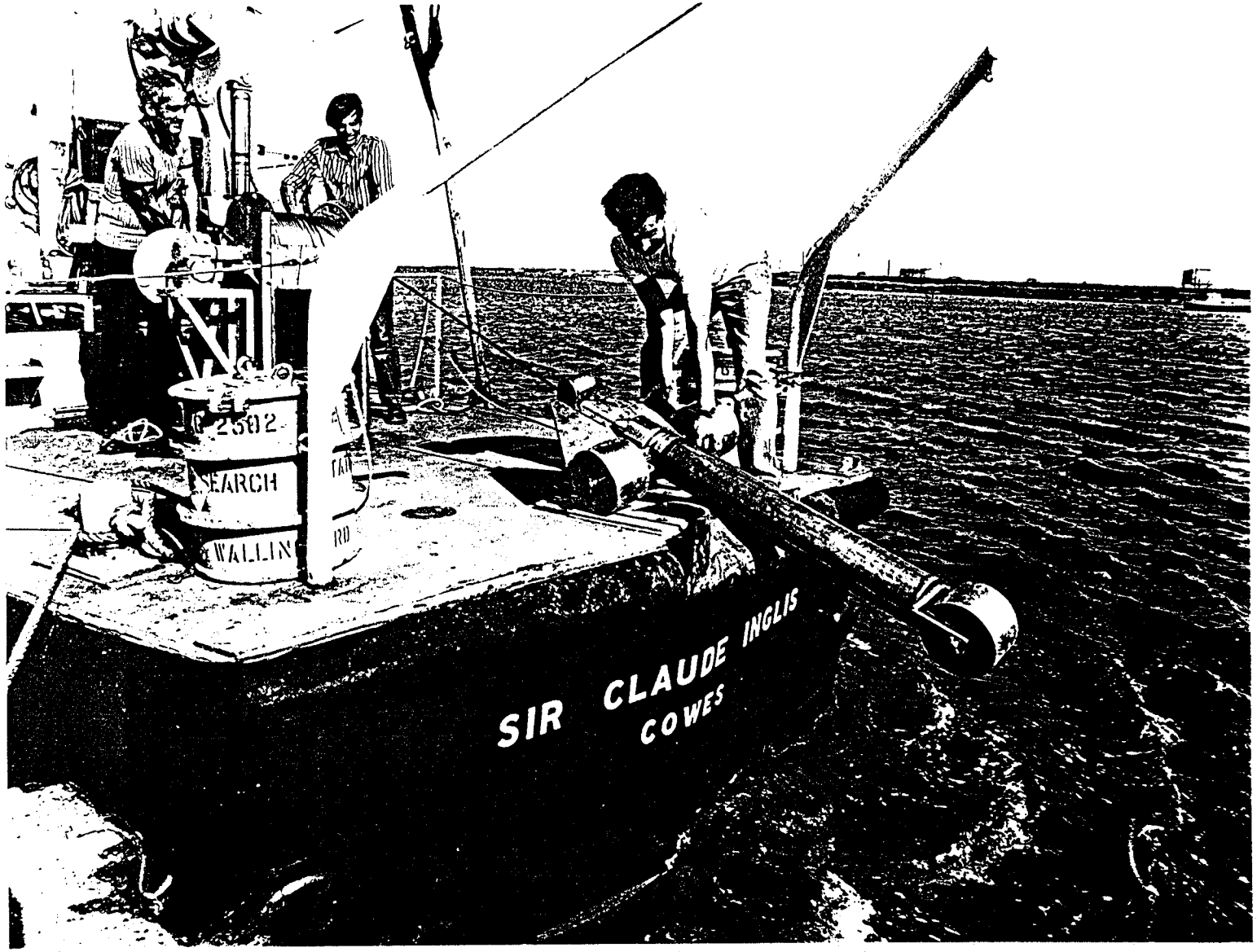

THE UNDERWATER RADIATION DETECTOR ASSEMBLY
ON THE STERN OF "SIR CLAUDE INGLIS".

Plate 1

APPENDIX 2

TIDEFLOW-2D MODEL DETAILS

The HR TIDEFLOW-2D model is two-dimensional: the computed velocities being depth-averaged.

The model utilises finite difference techniques to solve the following equations which represent the physical concept of conservation of mass and Newton's Laws of Motion:

Conservation of mass:

$$\frac{\partial \zeta}{\partial t} + \frac{\partial}{\partial x}(ud) + \frac{\partial}{\partial y}(vd) = 0$$

Conservation of momentum:

$$\frac{\partial u}{\partial t} + u\frac{\partial u}{\partial x} + v\frac{\partial u}{\partial y} = -g\frac{\partial \zeta}{\partial x} + \Omega v - fuq/d + D\nabla^2 u + \tau_{sx}/\rho d$$

$$\frac{\partial v}{\partial t} + u\frac{\partial v}{\partial x} + v\frac{\partial v}{\partial y} = -g\frac{\partial \zeta}{\partial y} - \Omega u - fvq/d + D\nabla^2 v + \tau_{sy}/\rho d$$

where:

- ζ is the water surface elevation relative to mean sea level
- h is the bed level relative to the same datum (m)
- d is the total water depth ζ + h (m)
- u,v are the depth averaged velocity components (m/s) referred to Cartesian co-ordinates x and y
- t is time (sec)
- g is the acceleration due to gravity (m/s^2)
- f is the friction factor
- Ω is the Coriolis parameter (t^{-1})
- D is the horizontal eddy viscosity coefficient (m^2/s)

q is the water speed $(u^2 + v^2)^{\frac{1}{2}}$ (m/s)

∇^2 is $\partial^2/\partial x^2 + \partial^2/\partial y^2$ (m^{-2})

τ_{sx} and τ_{sy} are the x and y components of surface windstress

The equations incorporate the assumptions that the flow is incompressible and well mixed, that vertical accelerations are negligible (hydrostatic pressure assumption), and that a quadratic friction law is valid.

The friction factor f is defined using the rough channel law,

$$(8f)^{-\frac{1}{2}} = 2\log_{10} (14.8d/k_s)$$

The roughness length, k_s, is related to the size of the protuberances on the bed, either directly in the form of particle sizes (especially in the case of shingle and stones etc) or indirectly in the form of ripple lengths (in the case of fine particles, ripple lengths are about 1000 times median grain size (see for example Yalin[1])).

The formula for the eddy viscosity coefficient, D is not well determined: Fischer[2] discusses various formulae. Fortunately the solutions to the equations are not in general critically dependent on D and an initial estimate based on Fisher's discussion can be taken as:

$$D = 0(u_* d)$$

where u_* is a typical shear velocity.

The size of D does have an effect on the size of tidal eddies and so, by comparing model eddy sizes with

observations, the value of D used could be roughly confirmed as being reasonable.

Output from a model run consists of tide levels and the two components of the current for each model cell. These are stored in the computer at frequent intervals during the tide and subsequently processed to yield computer plots of model flow patterns and particle tracks and curves of tide level and current speed and directions during the tide.

The stored results are also available if required for use as input to other elements of the TIDEWAY system to study sediment transport and the dispersion of cooling water and pollution.

[1] Yalin, M.S. Mechanics of sediment transport Pergamon Press, Oxford 1972.

[2] Fischer, M.B. Mixing and dispersion in estuaries. Ann Rev Fluid Mech 8 pp 107-133. 1976.

APPENDIX 3

THE HINDWAVE WAVE HINDCASTING MODEL

The HINDWAVE model

The HINDWAVE model (Ref 1) has been developed at HR, for prediction of wave climate at coastal locations, based on wind records for the area. It has been used successfully on many projects at various sites around the British coast.

The computations are split into two main parts. The first stage consists of production of a menu (or list) of about one thousand possible wave conditions, from a similar number of specific wind conditions. Fetch or open water rays are measured at 10° intervals around the wave prediction point for use as input to the first element of HINDWAVE, ie the JONSEY wave generation sub-model described in Section 2 of this Appendix. The second part consists of analysis of wind records. For each hour in the sequence, the wind/wave condition most closely corresponding to actual wind activity at that time is chosen from the menu. The analysis works with measured wind data collected at hourly intervals over a period of several years. The wave conditions at any time are estimated with regard to wind speeds during the preceding day or so.

It is first necessary to define a few standard terms used in wave prediction and analysis. Significant wave height (H_s) is a parameter in common use among coastal engineers as a means of expressing wave severity. It equates to the average height of the highest one third of the waves in a sequence. Wave period is usually indicated by either mean zero-crossing period (T_z), or peak period (T_p) at

which the wave energy spectrum is densest. Direction can be expressed as either wind direction (θ), or the mean wave direction (θ_w) averaged over all frequency and direction components.

The JONSEY program is used to assign a particular H_s, T_p and θ_w to each member of a particular set of wind conditions. The set comprises all possible combinations of sufficient values of speed, direction and duration to cover the range of values expected at that location. The predicted heights, periods and directions are stored for use as a look-up table. The technique described here is to break down the measured wind data into discrete categories, and then to select the corresponding H_s, T_p and θ_w from the table.

The first stage in the procedure is to select which wind conditions could occur and to divide them into discrete bands in terms of wind speed, direction and duration. The corresponding predicted H_s, T_p and θ_w values are calculated and retained.

If the wind speed remains steady over a long period, a twenty-four hour or even longer generation time is likely to be appropriate for exposed sites. However, if the wind speed or direction is rapidly varying, a shorter duration will be used as input to the wave prediction equations. The method of selecting the duration, wind speed and wind direction for each hour, is explained below.

Hourly wind speeds and directions are obtained from the Meteorological Office in the form of a computer data file. For each hour in turn, the method determines, for the chosen group of durations, the dominant set of wind conditions at the prediction location, with reference to the H_s table. This is achieved by vectorially averaging the wind velocities

over the various chosen durations leading up to that time in order to obtain an average speed and direction for each. The largest value is then selected from the corresponding set of H_s levels. This figure is retained together with the appropriate peak period and wave direction, in order to build up a probability distribution for each month.

A further option is automatic extrapolation to extreme wave heights, for different direction sectors, based on the overall predicted distribution of H_s. This is done by fitting a three-parameter Weibull distribution to the data in each direction sector in turn, after which the results are tabulated for various return periods.

The JONSWAP/SEYMOUR wave prediction model

It is observed that wind-generated waves show some directional spreading about their mean direction of transmits energy to the water in directions on either side of its own direction, which may fluctuate during the period of wave generation.

To incorporate this effect in the model, components of the total wave directional spectrum are calculated for various directions either side of the mean, and then a weighted average is taken using a standard spreading function. The significant wave height, period and direction are then calculated at the target point, by numerical integration of the spectrum.

The component directions (i = 1 to n) are spaced at regular intervals ($\Delta\theta$) in the range ±90° from the mean (θ_o). For each one (θ_i), the mean JONSWAP equation (Ref 2), representing a growing wind sea, is used to define the spectrum (E_i), given as a function of frequency (f):

$$E_i(f) = \alpha g^2 (2\pi)^{-4} f^{-5} \exp\{-1.25 (f/f_m)^{-4}\} \gamma^{\eta} \quad (1)$$

where:

$$\alpha = 0.032 (f_m U/g)^{2/3}$$

$$\gamma = 3.3$$

$$\eta = \exp\left\{\frac{-(f - f_m)^2}{2 f_m^2 \sigma^2}\right\}$$

$$\sigma = 0.07 \text{ for } f \leq f_m$$
$$0.09 \text{ for } f \geq f_m$$

f_m = the peak frequency (Hz)
$= 2.84 g^{0.7} F^{-0.3} U^{-0.4}$

U = the windspeed (ms^{-1})

F = the fetch (m) (fetch-limited conditions)
$= 0.008515 t^{1.298} g^{0.298} U^{0.702}$ (duration-limited)

g = the acceleration due to gravity (ms^{-2})

t = the duration (s)

The summation of the component spectra is then performed using the Seymour equation (Ref 3), which includes the cosine-squared directional spreading function for a directional wave spectrum ($E(f,\Theta)$). It is applied in the range ±90° from the principle wind direction. If the fetches are measured at say 10° intervals ($\Delta\Theta$), then the effective wave spectrum (E) for a particular direction (Θ_0) is calculated as the weighted average for seventeen component spectra ($E_i(\Theta_i)$, Θ_i = -80°, -70°, ..., 80° for i = 1, 17), as indicated in equation (2).

$$E = (2\Delta\theta/\pi) \sum_{i=1}^{17} E_i \cos^2(\theta_i - \theta_0) \qquad (2)$$

Although it is not part of the original theory, experience at HR indicates that cosine-sixth is sometimes a better spreading function to use. This is particularly true when the wave generation area is unusually narrow or the peak period is unusually long. In order to use this modification, the cosine term in equation (2) is raised to the power six rather than two, and the coefficient $2/\pi$ is increased to $3.2/\pi$.

The significant wave height (H_s) is the average height of the largest one third of the waves. The mean zero-upcrossing period (T_z) is the period measure most frequently used in engineering, this being the average time between successive upcrossings of the mean level by the water surface. The mean wave direction (θ_w) is taken as the average of the spectral components over all frequencies and directions. They are all approximated by numerical integration of equation (2).

$$H_s = 4m_0^{1/2} \qquad (3)$$

$$T_z = (m_0/m_2)^{1/2} \qquad (4)$$

$$\theta_w = \theta_0 + \frac{\int\int E(f,\theta)(\theta - \theta_0)\,df\,d\theta}{\int\int E(f,\theta)\,df\,d\theta} \qquad (5)$$

where $$m_n = \int E(f)\, f^n df$$

In order to use this method, fetch lengths must be known over a range of at least 180° around a point. It is convenient to use discrete frequencies in equations (1) and (2) which should also be specified.

For each application of the method, a duration and a fetch are given, although only one or other of these will produce the limiting condition used in equation (1). A complete directional spectrum is calculated, from which is obtained the one-dimensional spectrum as well as H_s, T_z and Θ_w.

The directional spread of the predicted wave spectrum will generally be frequency dependent. The cosine-squared function is applied to component spectra, which are generated over different fetch lengths, and which will consequently have different total energies and different peak frequencies. This has the following realistic effect upon the calculated directional spread of energy. If the wind direction corresponds to one of the long fetch directions, then the spreading of energy at the peak will be lower than average, whilst more spreading will be observed at the highest frequencies. If the wind is blowing along one of the shorter fetches, then the spread will tend to be more even across different frequencies, and in an extreme case, may produce greater than average spreading at lower frequencies.

Appendix References

1. Hawkes P J. A wave hindcasting method. Conference on modelling the offshore environment, Society for Underwater Technology, April 1987.

2. Hasselmann K et al. Measurements of wind wave growth, swell and decay during the Joint North Sea Wave Project (JONSWAP). Deutsches Hydrographisches Institute, Hamburg, 1973.

3. Seymour R J. Estimating wave generation on restricted fetches. Proc ASCE, Vol 103, No WW2, May 1977.

APPENDIX 4

THE OUTRAY BACK-TRACKING REFRACTION MODEL

Waves on the surface of the sea are constantly changing under the influence of a variety of external and internal forces which act simultaneously and independently. If the water is deep compared to the wavelength, the most important forces are usually the stresses resulting from wind action and internal viscosity. On the other hand, when the water becomes shallower, the effects of the seabed become increasingly important. For example, as the waves travel towards the shore they lose energy by viscous dissipation at the bed and by partial reflection, and as the water depth beneath them decreases, the waves also change direction, always tending to align their crests more nearly parallel to the contours.

This last mentioned process is known as refraction, and is similar to the refraction of light through media of different densities. The analogy can be extended further since some parts of a seabed will cause focussing of waves, whilst others will cause scattering, just as optical lenses do.

It is clear, therefore, that an accurate method of predicting wave refraction is a useful design aid when carrying out engineering studies in or beside the sea. The usual application of such a method is in predicting wave conditions at a site in shallow water, either directly or in comparison with another site. Similarly it may be used to examine changes at a site that would result from altering the seabed, for example, by dredging a channel.

In this Appendix, the Hydraulics Research method for calculating wave refraction is described.

Since the mathematical theory of wave propagation over an irregular bathymetry is far from complete, it is necessary to make simplifying assumptions and use approximate methods. Two such assumptions are made: (1) that the waves are linear, and (2) that a wave in water of local depth, d, will behave similarly to a wave in water of constant depth, d. With these restrictions it can be shown that waves progressing over a parallel contoured seabed, change their direction according to Snell's Law, i.e:

$C/\sin\alpha$ = constant

where α is the angle between the wave crests and the contours and where C is the wave phase speed, a function of the wave frequency, f, and the local water depth. Since the frequency of a wave remains constant, the wave direction changes only with changing depth.

The method described, like many others, relies on the concept of wave 'rays', which are lines everywhere perpendicular to the wave crests.

In order to use Snell's Law for waves proceeding over an irregular seabed, the following method is used. A lattice of triangular cells is laid over a chart of the area of interest and depth values are read off at each intersection. In each cell the seabed is then assumed to be planar, and linear interpolation is used to define the depth at any point within the triangle. Although there is no need for the cells to be of any particular shape it is usually more convenient to choose right angled triangles which, taken in pairs, give a rectangular element.

With this representation of the seabed the depth is continuous across any grid line although the slope is

usually discontinuous. It is also possible to apply Snell's Law in each cell and to follow a wave ray across it from some given entry point and direction. As the ray leaves one cell, its position and direction become the entry conditions for its journey across the next.

The time taken to calculate the ray's path across a cell can be reduced by making a further simplifying approximation. Provided the size of each cell is small and the slope of the seabed not too steep, the wave phase speed, C, at any point inside the cell can be closely approximated by linear interpolation of the exact phase speeds at the cell vertices. The ray path, under such an assumption, is part of the arc of a circle, and the path and its direction are continuous across each grid line although the curvature of the path is usually discontinuous. Because of the simplicity of the method, there are marked advantages in cost over methods which need, for example, iterative improvements at each step or more complicated representations of the seabed topography. Rounding errors can also be expected to be smaller in the described method.

The value of a wave refraction simulation, of course, lies not in the rapidity and accuracy of calculating ray paths but in the interpretation of the information they contain. Any method based on linear theory and using the concept of wave rays cannot be expected to reproduce non-linear wave effects. In areas where the bottom topography causes strong focussing of wave rays, a situation known as a caustic, the use of linear wave theory is woefully inadequate and errors from its use will inevitably accrue. However, the method of calculating wave conditions adopted here does reduce the importance of such phenomena as caustics, and gives realistic results.

First it is assumed that in the study area a wave energy distribution $S(\Theta, f, r)$ exists, where Θ is the wave direction, f the wave frequency and r a position vector. In a typical open sea situation in deep water the wave energy will depend only weakly on r. On the outer boundary of the area being considered, it is thus assumed that a homogeneous sea state exists and is described by $S_o(\Theta, f)$, the wave energy being considered to depend solely on direction and frequency. (The subscript o is used to denote quantities at the offshore boundary).

The purpose of the wave refraction method is to provide information on the wave conditions, or energy distribution at some point P close to the shore $S_p(\Theta, f)$, for a variety of offshore conditions, ie, different values of $S_o(\Theta,f)$.

Suppose a ray path exists which starts from the outer boundary of the area with direction Θ_o and frequency f_n and reaches the point P with direction Θ_p and frequency f_n. The functions S_o and S_p can then be linked by using a result of Longuet-Higgins (Appendix Ref 1), who showed that, when expressed as a function of two perpendicular wave numbers, k_1, and k_2, the directional spectrum $S_o(k_1,k_2)$ remains constant along a ray. So using the hypothetical ray mentioned above it can be shown that

$$S_p(\Theta_p,f_n) = \mu(f_n)S_o(\Theta_o, f_n) \qquad (1)$$

where:

$$\mu(f_n) = (C\ C_g)_o/(C\ C_g)_p \qquad (2)$$

because $S(\Theta, f)df\ d\Theta = S(k_1,k_2)dk_1dk_2$

and $dk_1\ dk_2 = k\ dk\ d\theta = \dfrac{f}{C\ C_g}\ df\ d\theta$

where $C = \dfrac{f}{k}$ the phase speed

and $C_g = \dfrac{df}{dk}$ the group velocity of waves.

Thus we have $C\ C_g\ S(\theta, f)$ is a constant along a wave ray, from which equation 1 follows. Provided that enough rays can be found linking the outer boundary with the point P, equation 1 can be used repeatedly to build up a picture of $S_p(\theta, f)$ for any function $S_o(\theta, f)$. All that would then be necessary are the depths at the outer boundary and the point, which would allow evaluation of C, C_g and thus $\mu(f)$.

To find such rays would be rather daunting if it were necessary to start at the outer boundary. Fortunately, however, the paths of the rays, like those in light, are completely reversible and this makes the task very simple.

Firstly a variety of wave frequencies are chosen. For a typical study these would lie in the range 0.05Hz - 0.30Hz, and about ten would be selected. Then, for each frequency a 'fan' of rays is sent out from the point of interest. Each ray is initially separated from its neighbour by a small angular increment, $\Delta\theta_p$; for reasons of economy the smallest separation chosen is set at $\Delta\theta_p = 0.25°$, but experience has shown that larger separations can be used for the higher frequencies without affecting the results.

Each ray is 'followed', using the method described above, until it runs ashore or reaches the outer boundary. The results from this stage of the

operation take the form of a list of those rays which connect the point to the boundary, with for each ray its frequency, f_n, its direction on leaving the point, Θ_p, and its direction at the outer boundary, Θ_o. Typically this list would contain information about several thousand rays.

For convenience this list is converted to three matrices which are called 'transfer functions', because they contain all the information necessary to evaluate the transfer of energy from the outer boundary to the point. Although it would be interesting to evaluate $S_p(\Theta, f)$, the energy distribution at the point, completely, in most cases all that is required is an idea of the mean direction and directional spread of the waves together with the distribution of energy over frequency which will allow the derivation of a significant wave height and a significant wave period.

To obtain the energy for each frequency component, f_j, in $S_p(\Theta, f)$ the angular dependence is integrated out. Equation 1 thus gives

$$S_p(f_j) = \int S_p(\Theta_p, f_j)d\Theta_p = \mu(f_j) \int S_o(\Theta_o, f_j)d\Theta_p \qquad (3)$$

The second integral is now replaced by a summation over all those rays followed for this frequency, and so

$$S_p(f_j) = \mu(f_j) \sum S_o(\Theta_o, f_j)\Delta\Theta_p \qquad (4)$$

where $\Delta\Theta_p$ is the angular separation used at the inshore point. This summation is now simplified as follows. It is assumed that the function $S_p(\Theta_o, f_j)$, is constant over angular sectors $(\ell - 1)\Delta\Theta_o$ to $\ell\Delta\Theta_o$, $\ell = 1, 2, \ldots, m$, with area $A_\ell(f_j)$ in each sector.

Equation 4 becomes:

$$S_p(f_j) = \mu(f_j)(\Delta\theta_p/\Delta\theta_o) \sum_{\ell=1}^{m} A_\ell(f_j) \cdot N_\ell$$

where N_ℓ is the number of rays with offshore direction between $(\ell-1)\Delta\theta_o$ and $\ell\Delta\theta_o$.

With the energy thus evaluated for all frequencies considered, ie f_j, $j = 1, 2, \ldots\ldots n$, the complete energy spectrum $S_p(f)$ has been approximated. Then, the significant wave height is defined as $4(\int S_p(f)df)^{\frac{1}{2}}$ and the zero-crossing period as $(\int S_p(f).df/\int S_p(f).f^2.df)^{\frac{1}{2}}$.

To obtain a mean direction and angular spread for $S_p(\theta, f)$ further investigation is necessary. We define a mean vector V at the point by

$$V(f_j) = \int S_p(\theta_p, f_j)\exp(i\theta_p)d\theta_p / \int S_p(\theta_p, f_j)d\theta_p \qquad (5)$$

The mean direction θ is then given by

$\theta(f_j) = ph(V(f_j))$, the phase of V_j

and the variance, or spread, $\sigma^2(f_j)$, by

$$\sigma^2(f_j) = 1 - \left|V(f_j)\right|^2$$

Following the same approximations as before, equation 5 is written

$$V(f_j) = \sum_{\ell=1}^{m} \frac{A_\ell}{\Delta\theta_o} \mu(f_j) \int \exp(i\theta_p)\, d\theta_p /$$

$$\sum_{\ell=1}^{m} \frac{A_\ell}{\Delta\theta_o} \mu(f_j) \int d\theta_p$$

which leads to

$$V(f_j) = \sum_{\ell=1}^{m} A_\ell (U_\ell + iV_\ell) / \sum_{\ell=1}^{m} A_\ell T_\ell$$

where $U_\ell + iV_\ell = \mu(f_j) \frac{\Delta\theta_p}{\Delta\theta_o} \sum \exp(i\theta_p)$

where this summation is over all the rays with offshore angle in the range $(\ell - 1)\ \Delta\theta_o$ to $\ell\Delta\theta_o$.

The transfer functions are thus

$$\begin{matrix} T_\ell & & 1 \\ U_\ell & = \mu(f_j) \frac{\Delta\theta_p}{\Delta\theta_o} \sum & \cos\theta_p \\ V_\ell & & \sin\theta_p \end{matrix} \qquad (6)$$

where the summation is over all the rays with offshore bearings in the range $(\ell - 1)\Delta\theta_o$ to $\ell\Delta\theta_o$.

We then have

$$S(f_p, f_j) = \sum_{\ell=1}^{m} A_\ell T_\ell \qquad (7)$$

the mean direction

$$\theta(f_j) = \tan^{-1} \left(\sum_{\ell=1}^{m} A_\ell V_\ell / \sum_{\ell=1}^{m} A_\ell U_\ell \right) \qquad (8)$$

and the variance

$$\sigma^2(f_j) = 1 - [(\sum A_\ell V_\ell)^2 + (\sum A_\ell U_\ell)^2]/(\sum A_\ell T_\ell)^2 \quad (9)$$

As can be seen from equation 6, the functions T, U and V can be calculated simply, using information about the ray paths. It is only for substitution into equations 7, 8 and 9 that it is necessary to calculate the offshore spectrum S_o at each frequency f_j and angular sector $(\ell-1)\Theta_o$ to $\Delta\Theta_o$ to give A_ℓ.

Thus for one set of wave rays, and consequently one set of transfer functions, wave conditions at the inshore point can be calculated for a large variety of functions $S_o(\Theta, f)$. The only restrictions on the offshore spectra that can be used are that they vary sufficiently slowly with Θ_o that they can be assumed constant over angular sectors of width $\Delta\Theta_o$ and that the frequencies f_j enable an accurate representation of the energy distribution over frequency. In practice, of course, the offshore spectra are chosen first and the quantities $\Delta\Theta_o$ and f_j are then chosen to satisfy these restrictions.

Appendix References

1. LONGUET-HIGGINS M S. The transformation of a continuous spectrum by refraction. Proc. Camb. Phil Soc, No 1, 1957, pp226 - 229.

APPENDIX 5

MODEL FOR TRANSPORT OF SANDY BACKGROUND MATERIAL, LTDISP: INPUT DETAILS AND FILE FORMATS

The model LTDISP consists of two stages: the first stage is to use the results from TIDEFLOW-2D velocity files, combined with a wave climate for each point to compute an Eulerian residual sediment transport vector for each point. The second stage is to use these vectors to calculate the change in bed mass at each point over a specified time period.

All file names used here are for illustration purposes only and may be changed by the user. All variables are in standard SI units unless stated.

Stage 1

The input files (names to be specified by the user) required for stage 1 are:

uspring	u-component of velocities for an average spring tide, from TIDEFLOW
vspring	v-component of velocities for an average spring tide, from TIDEFLOW
uneap	u-component of velocities for an average neap tide, from TIDEFLOW
vneap	v-component of velocities for an average neap tide, from TIDEFLOW
md	model bed data file (contains bathymetry) from TIDEFLOW
tide.in	low water and high water tide levels at the site for the whole period
hstz.in	HsTz scatter diagram information (wave conditions)
ltst.in	information about sediment transport formula and to control screen output

Stage 1 produces the following output files (names to be specified by the user):

vecu	u-component of net sediment transport vectors
vecv	v-component of net sediment transport vectors
vecl	average magnitude of sediment transport vector.

File formats for stage 1

The velocities files and the sediment transport vectors files are in standard Tideway results file format, ie direct access. The header of the file consists of two records of information. This is followed by one record for each storage interval, which contains the velocities at each active cell at that time. The header of each file may be viewed with program "insight". The vectors file contains two records of header information, followed by only one record of vector components for each active cell. It is better to generate the velocity files from a TIDEFLOW discharges file via an intermediate conversion program than to use instantaneous velocities (an option when running TIDEFLOW) because this gives smoother time averaged results.

The model bed data file is in Tideway format. This is a serial file, as documented in the Tideway manual.

The file 'tide.in' contains a string of low and high water values for the period of interest, which should either be measured or copied from the Admiralty Tide Tables. The file has the following format :

NTIDES - no of tides to be read in
LW HW LW HW LW HW LW HW LW HW LW HW LW HW LW HW
LW HW LW HW LW HW LW HW LW HW LW HW LW HW LW HW
LW HW LW HW LW HW LW HW LW HW LW HW LW HW LW HW
.
.
etc

The lines of low and high water values have the FORTRAN format: 16(F4.1,1X)

The file 'hstz.in' contains information about the wave climate, with a scatter diagram of significant wave height (Hs) against zero crossing period (Tz). This scatter diagram is applied as the wave climate at each point of the model. The file has the following format (all the data is read in free format, ie *):

HSINT, TZINT - Hs Interval, Tz Interval
NEVENT, NHSROWS, NTZCOL - No of recorded events,
No of rows (Hs),
No of columns (Tz)
IHSTZ - Array of integers representing the scatter diagram, with the first element being the lowest Hs and Tz category. Negative integers represent actual occurrences and positive integers represent parts per thousand. Put calms in the lowest Hs and Tz category.

The file 'ltst.in' contains general information about the sediment transport formula and screen output. This contains the following (all read in free format *):

GRSA, GRSB, GRSN, UCRIT - Grass constants a, b and n and critical velocity for movement of the background material

MHWS, MLWS, MHWN, MLWN - Tidal ranges from Tide tables (mean high water springs, etc)

ISWCH1, ISWCH2, ISWCH3, ISWCH4 - Printing switches

BOVINT, NTTC, TINT - interval size for bottom orbital velocity distribution, no of intervals and size of intervals for tidal current distribution.

The printing switches are integers which are generally set to 0 for normal running of the program. If they are set to a value greater than zero, screen output will be as follows:

SWITCH NO	OUTPUT
1	Probability distribution of tidal currents
2	Hs-Tz scatter diagram and probability distribution of bottom orbital velocities
3	Tables of sediment transport rates for each direction
4	Long term sediment transport rate vectors

All output is to channel 6 (and can therefore be redirected in UNIX and DOS from the screen to a file).

Stage 2

In stage 2, the net sediment transport vectors are used to calculate the change in bed mass in each cell. The input files required are:

vecu	u-component of net sediment transport vectors (from stage 1)
vecv	v-component of net sediment transport vectors (from stage 1)

md	model bed data file
input.in	file of input data about file names, smoothing coefficients etc.

The output file produced is a standard tideway format file of mass of sediment on the bed at time intervals specified by the user.

File formats for stage 2

The vector files and output file of masses are standard tideway direct access files. The model bed data is a serial file. The formats of both these file types are described in the Tideway manual. The program prompts for a file of input data which contains the vector and model bed data filenames. The format of the input data file is:

u-component of sand transport file	(format A32)
v-component of sand transport file	(A32)
model bed data file	(A32)
length of tidal cycle (hours)	(format F8.0)
number of tides to be run	(F8.0)
time step (in tides)	(F8.0)
printing interval for writing file (tides)	(F8.0)
grid (cell) size, x-direction	(F8.0)
grid (cell) size, y-direction	(F8.0)
smoothing coefficient for 1*1 grid	(F8.0)
smoothing coefficient for 3*3 grid	(F8.0)
smoothing coefficient for 5*5 grid	(F8.0)

APPENDIX 6

MODEL FOR MIXING OF MUDDY DREDGED MATERIAL: INPUT DETAILS AND FILE FORMATS

LTD3 is a model which simulates mixing of a muddy dredged material with the background material. It is an extension of the background transport program LTDISP. The program uses the sand transport vectors, as calculated in LTDISP. At each cell, at each timestep, the model predicts the mass of sand, the mass of mud and the proportion of sand in a surface layer of chosen depth. The proportion of sand (or mud) in this surface layer affects the sand transport rates and the mud erosion rates.

All file names used here are for illustration purposes only and may be changed by the user. All variables are in standard SI units unless stated.

The input files required are:

vecu	u-component of net sediment transport vectors (from LTDISP)
vecv	v-component of net sediment transport vectors (from LTDISP)
vecl	average magnitude of hourly sediment transport vectors (from LTDISP)
md	model bed data file
input.in	file of input data about file names, smoothing coefficients etc.

The output files produced are:

msand	total mass of sand in each cell
mmud	total mass of mud in each cell
psand	proportion of sand in surface layer of each cell

File formats for LTD3

The input files vecu, vecv, vecl are standard Tideway direct access files. The bed data file is a Tideway format serial file. The output files msand, mmud, psand are also standard Tideway direct access files. The file of input data has the following format (free (n) means free format, expects n numbers):

format A32	u-component of sand transport file
A32	v-component of sand transport file
A32	average magnitude of vector file
A32	model bed data file
F8.0	length of tidal cycle (hours)
F8.0	number of tides to be run
free (2)	time step (in tides), printing interval for writing file (tides)
free (2)	grid (cell) size x-direction, y-dirn
free (3)	smoothing coefficient for 1*1 grid, smoothing coefficient for 3*3 grid, smoothing coefficient for 5*5 grid
free (1)	NDUMPS, number of mud dumps (the next line must appear NDUMPS times)
free (5)	total mass in dump, time step during which this dump is dropped, coordinates of dump centre IC, JC, standard deviation of dump
free (4)	weighting coefficients for contributions to sand transport from cells 1, 2, 3 and 4 cells away
free (1)	erosion rate for mud (kgm^{-2} per tide)
free (1)	depth of active surface layer
free (2)	dry density of sand, dry dens. of mud
A32	filename for output of sand masses
A32	filename for output of mud masses
A32	filename for output of sand proportion in active surface layer.

Subroutine for calculation of proportion of sand in LTD3

```
*
      SUBROUTINE SAVAILABLE
*     Calculates an availability of sand at some time after the start,
*     based on relative proportions of mud and sand in top layer of
*     DCRIT
*     This is a fairly crude calculation of the amounts of mud and sand
*     available, particularly when sand is eroded.  Once mud has fallen
*     below the depth DCRIT, it is not reached again
*
*     Variables:
*     AVAIL(I,J) = proportion of sand in cell (i,j)
*     DSAND      = depth of sand deposited or eroded during time step
*     DMUD       = depth of mud deposited during time step (if mud is
*                  eroded the proportion of sand is increased before
*                  entering this subroutine)
*     DCRIT      = depth of active surface layer (constant)
*     KCELL      = KARRAY value for cell i,j (to compress 2-D array
*                  into 1-D, see Tideway manual for more details)
*     MCH(KCELL) = sand mass change in cell KCELL during time step
*     MUDPLUS(KCELL) = mud mass added to cell KCELL during time step
*     DENSSAND   = dry density of sand
*     DENSMUD    = dry density of mud
*
*
      INCLUDE 'genblocks.h'
      INCLUDE 'ltdphase3.h'
      INCLUDE 'inputphase3.h'
*
      REAL    DSAND, DMUD, DTOTAL

*     Calculate availability of sand at every cell of grid
      DO 200, J=1, N(NGRID)
        DO 100, I=1, M(NGRID)
          IJCELL = (J-1)*M(NGRID)+I
          KCELL = KARRAY(IJCELL)
          IF (KCELL.EQ.1) THEN
            AVAIL(I,J)=0.0
          ELSE
            DSAND=MCH(KCELL)/DENSSAND
            DMUD =MUDPLUS(KCELL)/DENSMUD
            DTOTAL=DSAND+DMUD

* If sand is deposited..
            IF (DSAND.GE.0.0) THEN

* If dtotal=0.0, no change to availability
              IF (DTOTAL.NE.0.0) THEN

* If total deposition is more than DCRIT
                IF (DTOTAL.GE.DCRIT) THEN
*    Availability is in proportion to sand/mud deposited
                  AVAIL(I,J)=DSAND/DTOTAL

                ELSE
```

```
*     Availability includes some of previous top layer
                    AVAIL(I,J)=(DSAND+(DCRIT-DTOTAL)*AVAIL(I,J))/DCRIT
                  ENDIF

               ENDIF

             ELSE
* (Sand is eroded)
* If dtotal is greater than zero, net deposition:  Availability is *
dependent on amount of mud deposited and what was previously in top *
layer
                  IF (DTOTAL.GE.0.0) THEN
                     AVAIL(I,J)= 1.0 - MIN(1.0,
     *                (DMUD+(1.0-AVAIL(I,J))*MAX(0.0,DCRIT-DTOTAL))/DCRIT)
                  ELSE
* (net erosion, but does not consider mud below previous top layer)
                     AVAIL(I,J)=1.0 - MIN(1.0,
     *                (DMUD+(1.0-AVAIL(I,J))*DCRIT)/DCRIT)
                  ENDIF
               ENDIF
            ENDIF
            SNDMUD(KCELL)=AVAIL(I,J)
  100    CONTINUE
  200 CONTINUE
*
      RETURN
      END
*
*************************************************************************
```

APPENDIX 7

MODEL FOR FLOW OF VISCOUS MUD LAYER DOWN A SLOPE: INPUT DETAILS AND FILE FORMATS

All file names used here are for illustration purposes only and may be changed by the user. All variables are in standard SI units unless stated.

The input files required are:

md	model bed data file
input.in	file of input data about file names, smoothing coefficients etc.

The output file produced is:

fmud	total depth of mud in each cell

File formats

The bed data file is a Tideway format serial file. The output file is a standard Tideway direct access file. The file of input data has the following format (free (n) means free format, expects to read n numbers):

format A80	title of project
A80	job number and/or other text info.
A16	location of study
A32	model bed data file
F8.0	length of tide (hours)
F8.0	number of tides to be run
free (2)	time step (in tides), printing interval for writing file (tides)
free (2)	grid (cell) size x-direction, y-dirn
free (3)	smoothing coefficient for 1*1 grid, smoothing coefficient for 3*3 grid, smoothing coefficient for 5*5 grid

free (4)	coordinates of dump centre IC, JC, thickness of mud dumped (m), radius of dump (m)
free (2)	bulk density of water (kgm^{-3}), bulk density of mud (kgm^{-3})
free (1)	Dynamic viscosity of mud layer (Nsm^{-2})
A32	filename for output of mud depths.

APPENDIX 8

EULERIAN AND LAGRANGIAN SEDIMENT TRANSPORTS

1. When calculating the transport of a water-borne substance, the mean transport velocity is given by the Lagrangian residual velocity U_L. This is given by the distance travelled by a water particle during some reference time, divided by the reference time. In the tidal context, the reference time is usually taken to be one tidal cycle. In the general case in which the velocity field varies spatially over the area of interest, the Lagrangian residual will be different from the Eulerian residual velocity U_E (the time-mean of the velocity at a fixed point), because the particle is constantly wandering into a new part of the area. Calculations of Lagrangian residuals are usually made in the context of substances which move with the water body, such as chemical contaminants, radioactive solutes, or fish eggs, but the same principles should apply to transport of sediment.

2. Although in areas with a complicated spatial distribution of velocity it is usual to obtain Lagrangian residuals by numerical particle tracking in a full computer model of the flow distribution, some important conclusions can be reached by considering a simple idealised flow field analytically.

   Consider a one-dimensional rectilinear tidal flow field (Fig. 1) in which the Eulerian residual velocity U_E is constant everywhere, but the amplitude $\hat{U}$ of the tidal velocity (assumed sinusoidal with frequency w) increases linearly

with x, so that the instantaneous flow velocity U(x,t) can be written

$$U(x,t) = U_E + \hat{U} \sin (wt + \emptyset) \qquad (1)$$

$$\text{with } \hat{U} = \frac{x}{L} . \hat{U}_1 \qquad (2)$$

The length-scale L is the distance over which the linearly varying amplitude $\hat{U}$ reduces to zero, and $\hat{U}_1$ is the value of $\hat{U}$ at the point of interest. A particle is released at time t = 0, when the phase in the tidal cycle is $\emptyset$.

Defining non-dimensional units $\xi = x/L$, $\tau = wt$, $b = U_E/(Lw)$, and $a = \hat{U}_1/(Lw)$, equations (1) and (2) can be written as a differential equation for the particle's subsequent position:

$$\frac{d\xi}{d\tau} = b + a\,\xi \sin (\tau + \emptyset) \qquad (3)$$

Solving this equation subject to the initial condition $\xi = 1$ at $\tau = 0$ gives the position of the particle after one tidal cycle as

$$\xi(\tau=2\pi) = 1+b\exp(-a\cos\emptyset)\int_0^{2\pi} \exp(a\cos(\tau'+\emptyset))d\tau' \qquad (4)$$

After re-dimensionalising, this shows that the ratio of the Lagrangian to the Eulerian residual velocity is given by

$$\frac{U_L}{U_E} = \exp(-a\cos\emptyset) \int_0^{2\pi} \exp(a\cos(\tau'+\emptyset))d\tau' \qquad (5)$$

The integral can be approximated to order a^3, for $a < 1$, to give the final expression

$$\frac{U_L}{U_E} = e^{-a\cos\phi}\left(1 + \frac{a^2}{4}\right) \qquad (6)$$

3. The problem was also tackled by means of a simple one-dimensional particle-tracking computer program for the flow field given by equation (1). The particle-tracking gave results which were identical with the full analytical expression equation (5). They were also within 1.5% of the approximate expression equation (6) for $a \leq 1$. Equation 6 is shown in Figure 2. The greatest difference between U_L and U_E occurs for $\phi = \pi$, when U_L is 3.4 times larger than U_E for $a = 1$. The phase $\phi = \pi$ corresponds to release of a particle at slack water just before the tide flows in the opposite direction to that in which $\hat{U}$ increases. At phase $\phi = 0$, U_L is reduced to only 0.45 U_E for $a = 1$. At phases $\pi/2$ and $3\pi/2$, corresponding to peak ebb and flood tides, U_L is approximately 25% larger than U_E, for $a = 1$.

4. In view of the dependence of the Lagrangian residual on the particle's trajectory, it seems possible that asymmetries in the tidal velocity cycle might markedly affect U_L. To test this, a second harmonic of amplitude $\epsilon\hat{U}$ and frequency 2w was added to the original sinusoid of amplitude $\hat{U}$ in the particle-tracking program. This will distort the periodic velocity, while maintaining a zero mean (apart from U_E). Although the resulting values of U_L now depend on the amplitude and phase of the second harmonic, it was found that they never exceeded the envelope

of values which would be given by a single sinusoid of frequency w and amplitude $(1 + \epsilon)\hat{U}$.

5. The following conclusions can be deduced directly from equation (6):

i) It is not possible to generate a non-zero Lagrangian residual unless the Eulerian residual is also non-zero.

ii) U_L is always in the same direction as U_E, and proportional to U_E by a factor which depends only on the tidal part of the velocity, and not on the size or direction of U_E.

iii) The proportionality factor depends primarily on $a = \hat{U}_1/Lw$. The local value of "a" can be calculated in a tidal model for a tide of period T by $a = \frac{2\pi}{T} \frac{d\hat{U}}{dx}$. Since "a" is the ratio of the tidal semi-excursion to the distance over which the tidal amplitude falls to zero, it will generally be no greater than one.

iv) U_L may be larger or smaller than U_E, depending on the phase in the tidal cycle when the particle is released.

v) Asymmetry of the tidal time variation produces a Lagrangian residual which does not exceed that of a sinusoidal variation whose amplitude is equal to the peak of the asymmetric velocities.

6. Practical implications for sediment transport are as follows:

i) Making an analogy between velocity and transport rate, the Lagrangian transport rate Q_L of

sediment will be in the same direction and of the same order of magnitude as the Eulerian transport rate Q_S.

ii) An estimate of the ratio Q_L/Q_S can be made by calculating $a = \frac{2\pi}{T}\frac{d\hat{U}}{dx}$ from a tidal numerical model, and applying equation (6). Bounds on the ratio are given by taking $\emptyset = 0$ and π.

iii) The movement of a patch of marked sand could in principle be calculated by applying the transport equivalent of (6), with particles being released continuously, with the rate of release related to the instantaneous velocity (eg proportional to $U^2(x,t)$). The net movement is then calculated as the weighted mean of (6) over $0 \leq \emptyset < 2\pi$. However, this would require an assumption that a sand grain, once released, continues to move with the water. In practice, it would move in short hops, making exchanges with the bed material. This process should really be included. However, to a first approximation it can be seen that a heavy weighting occurs at the times of maximum flood and ebb tidal velocity, ie at $\emptyset = {}^{\pi}/_{2}$ and ${}^{3\pi}/_{2}$. The weighted average of equation (6) will thus be of order

$$\frac{U_L}{U_E} \approx 1 + \frac{a^2}{4} \qquad (7)$$

Making the above assumptions, the movement of the centroid of the sand patch will take place at the Lagrangian transport rate Q_L, but this will be no more than about 25% larger than Q_S.

iv) For the Sizewell case, the velocity field changes only slowly in the North-South direction, so "a"

will be small, and the differences between Eulerian and Lagrangian rates can be neglected compared with the uncertainties in calculating Q_s.

FIGURES.

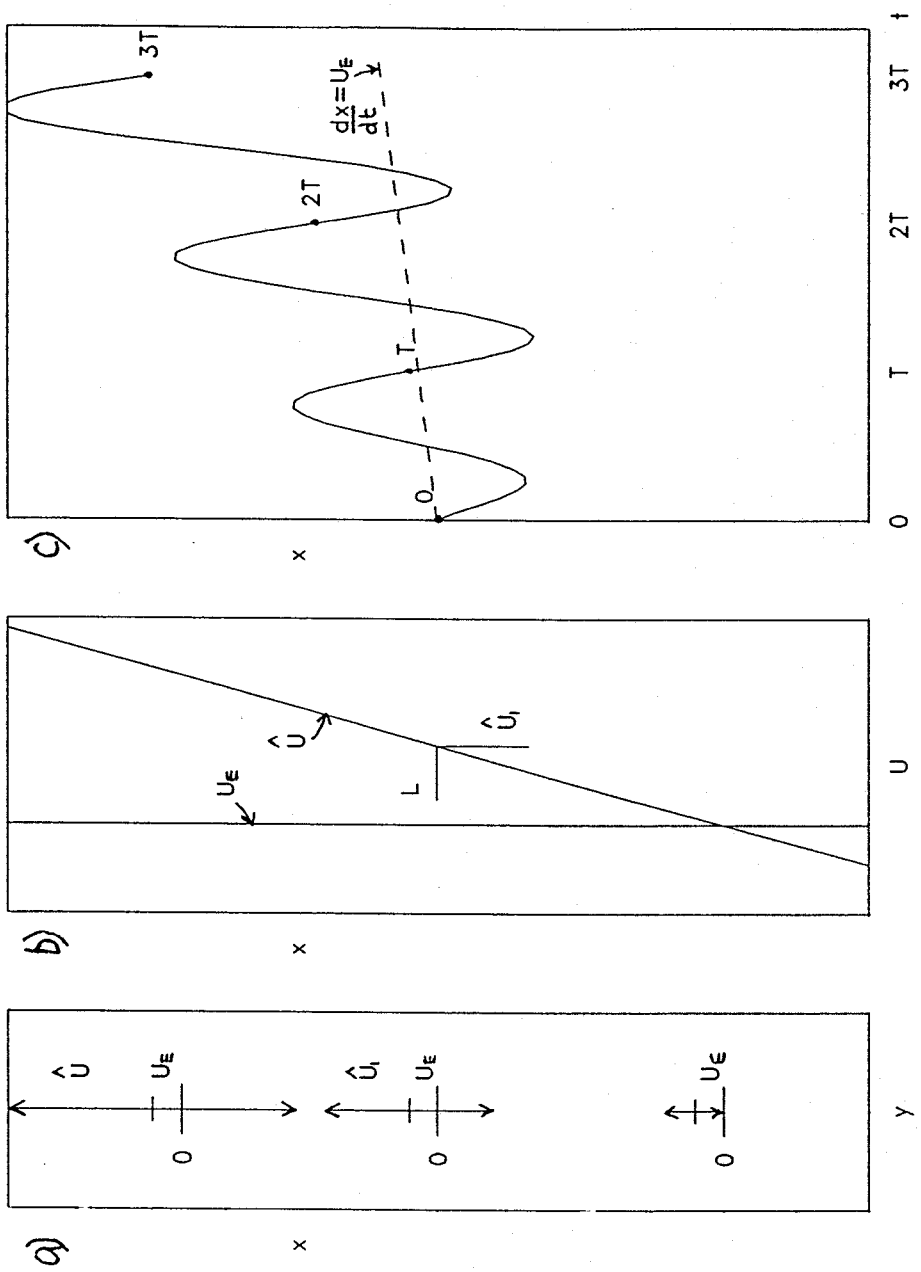

Fig A8.1 Idealised flow field: a) Velocity vectors, b) Constant U_E, linear variation in $\hat{U}$, c) Trajectory of particle with time, path taken if travelling at Eulerian velocity only

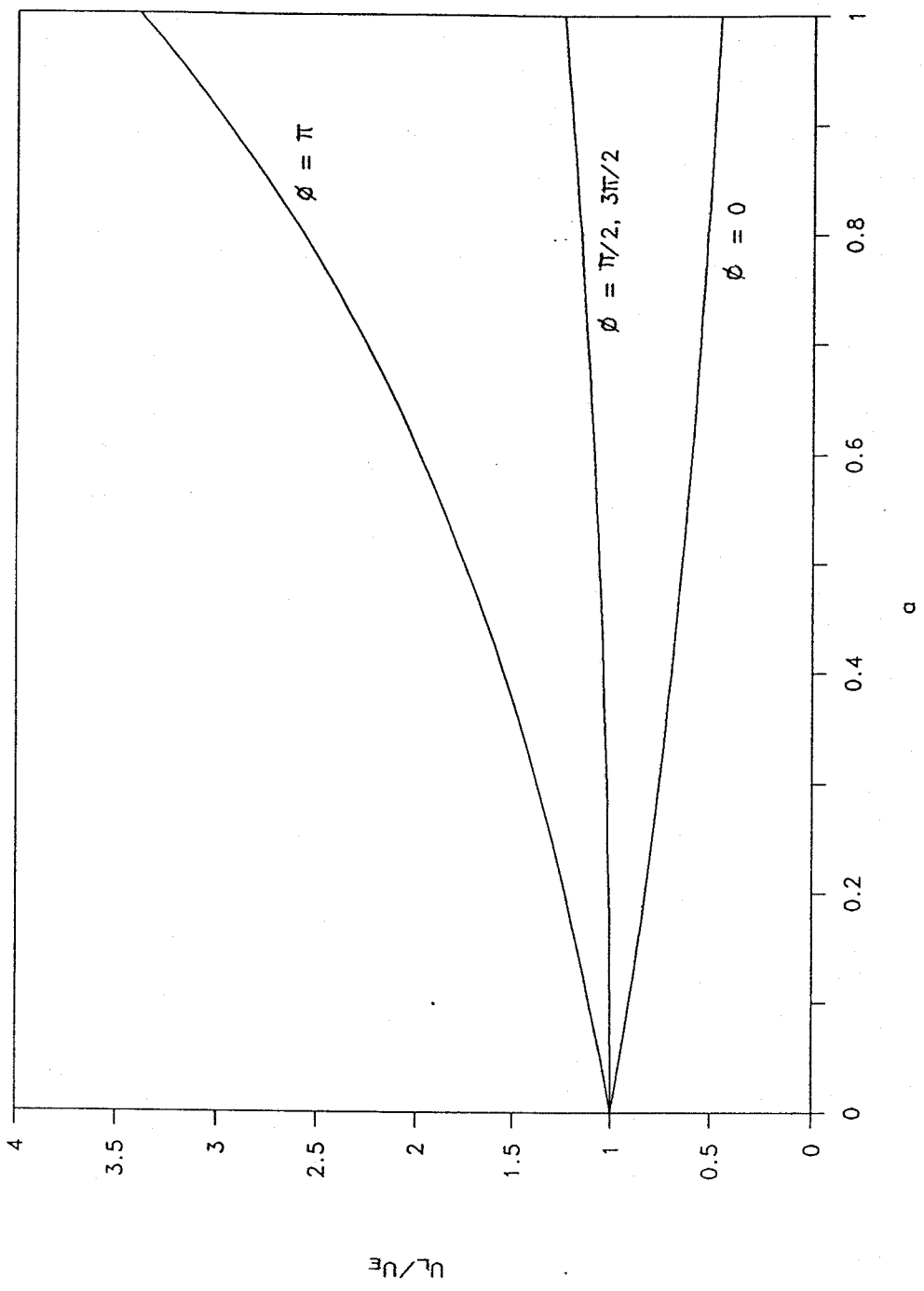

Fig A8.2 Ratio of Lagrangian to Eulerian residual velocity as a function of "a" and phase of release ϕ, from equation 6.